NOO RP-13

THEORY AND PRACTICE OF GEOPHYSICAL SURVEY DESIGN

THOMAS M. DAVIS

OCTOBER 1974

This thesis was submitted in partial fulfillment of the requirements for the Degree of Doctor of Philosophy–The Pennsylvania State University, Department of Geosciences.

NAVAL OCEANOGRAPHIC OFFICE
WASHINGTON, D.C. 20373

NOO RP-13

THEORY AND PRACTICE OF GEOPHYSICAL SURVEY DESIGN

THOMAS M. DAVIS

OCTOBER 1974

This thesis was submitted in partial fulfillment of the requirements for the Degree of Doctor of Philosophy–The Pennsylvania State University, Department of Geosciences.

NAVAL OCEANOGRAPHIC OFFICE
WASHINGTON, D.C. 20373

FOREWORD

The requirement for designing geophysical surveys in such a way that the true continuous field may be derived to a predetermined accuracy from digital samples is basic to any data collection operation. The time required in the collection and analysis of the reconnaissance data, which is necessary for the utilization of these survey design procedures, may be justified not only from a purely scientific standpoint but, with the escalating cost of shipboard operations, from an economic standpoint as well. Application of the theory and algorithms presented in this report is expected to result in a significant improvement in survey platform utilization.

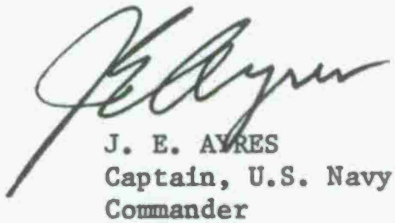

J. E. AYRES
Captain, U.S. Navy
Commander

ABSTRACT

A theory for designing parallel track-type geophysical surveys, as well as the necessary numerical algorithms for implementing this theory, has been developed which is easily applied to many different sampling problems. Within this context, survey design consists of defining the appropriate track spacing, track direction, and down-track sampling rate which will produce a set of discrete digital measurements describing the environment to a predetermined accuracy.

These procedures are based primarily upon the use of one and two-dimensional Fourier transforms applied to appropriate numerical models of the sampling process in order to estimate the variance or mean square error as well as the spectral content of the sampling error. Since these error estimates are computed in the spatial frequency domain, application of the convolution theorem is shown to produce a particularly efficient process for propagating the error estimates through a variety of linear operations performed upon the survey data.

Several practical applications are presented to illustrate the adaptability of the theory. These applications include the near real-time design of hydrographic surveys utilizing a small-scale computer, the design of gravity surveys from which estimates of vertical deflection and geoid undulation may be derived to a specified accuracy, and the design of oceanic sound speed surveys which illustrates the application of the theory to three-dimensional fields.

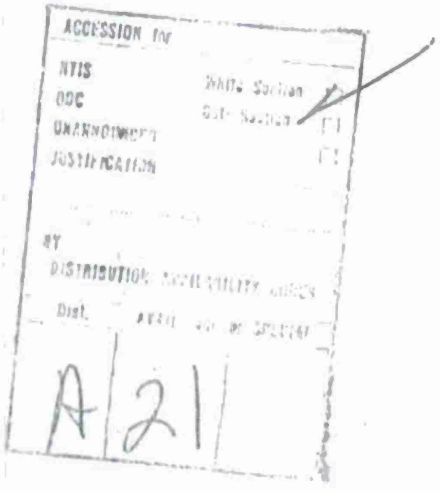

Price $3.00

ACKNOWLEDGEMENTS

The author wishes to thank Professor P. M. Lavin of the Department of Geosciences, The Pennsylvania State University, under whose guidance and encouragement this work was completed. Discussions with Dr. B. E. Olson, A. L. Kontis and J. G. Hankins of the U. S. Naval Oceanographic Office have been most helpful and stimulating.

Gravity data were supplied by the Gravity Division and oceanic sound speed data were provided by the Deep Ocean Surveys Division of the U. S. Naval Oceanographic Office.

TABLE OF CONTENTS

LIST OF TABLES

LIST OF FIGURES

LIST OF FIGURES - continued

LIST OF FIGURES - continued

LIST OF FIGURES - continued

INTRODUCTION

In any area of science which relies upon the utilization of discrete measurements of a spatially or temporally variable physical process as a primary source of information, it is highly desirable, if not critical, that estimates be made of the error which is introduced by discrete sampling. In many cases, a requirement exists for estimating not only this primary sampling error associated with the original measurements, but a secondary sampling error which is the result of propagating the primary error through a series of linear operations to produce quantities computed from the sampled data. Examples of this type of linear operation are upward and downward analytic continuation of potential fields, one and two-dimensional differentiation, and the calculation of vertical deflection components and geoidal undulations from measurements of the earth's gravity field.

Although the appropriate estimates of sampling error may be computed after the measurements are completed, by far the most efficient use of the theory and algorithms described in this report is made during the design phase of the data collection operation. The application of these procedures to geophysical processes falls under the general heading of geophysical survey design. Large scale geophysical surveys are presently conducted primarily by aircraft, ships, and satellites travelling along survey tracks laid out in some prescribed manner. Under these conditions, geophysical survey design consists of defining the appropriate track spacing, track direction, and down-track sampling rate which will produce a set of discrete measurements describing the environment to a predetermined accuracy.

Some preliminary theory for estimating sampling error has been developed by applying statistical methods based on one-dimensional covariance functions to physical geodesy. These methods were utilized by Rapp (1964) to estimate numerically the error of prediction or interpolation of gravity anomalies. Heiskanen and Moritz (1967) outlined the procedure for propagating this covariance estimate of sampling error through the calculation of spherical harmonics of the gravity field and the computation of geoidal undulations. The assumption of isotropy inherent in the application of one-dimensional covariance functions to two-dimensional fields, the practical problems of computing accurate local covariance estimates utilizing a finite amount of data from a process which is basically non-stationary with respect to spatial coordinates, and the numerical complexity of error propagation through linear operations severely limits the utility of these existing procedures for survey design.

In order to overcome these limitations, a theory of geophysical survey design, as well as the necessary numerical algorithm for implementing this theory, has been developed which is quite easily applied to many different sampling problems. This theory is particularly efficient for propagating the desired sampling error estimates through a variety of linear operations. These procedures are based primarily upon the use of one and two-dimensional Fourier transforms applied to numerical models of the sampling process in order to estimate the variance or mean square error as well as the spectral content of the sampling error. Since these error estimates are computed in the spatial frequency domain, straightforward application of the convolution theorem results in an efficient error propagation process.

Several practical applications are presented to demonstrate the

use of the theory and the relative ease with which it may be adapted to many different types of survey operations. Although in some cases, sampling error may be considered to have a minor impact upon the quality of the results obtained from an analysis of the data, this does not negate the requirement for designing an efficient survey plan, especially in light of the present cost of large scale survey operations.

THEORY OF SURVEY DESIGN

In order to develop a comprehensive theory which could form the basis for a practical procedure to design geophysical surveys, the following general criteria were used:

1. The theory should be easily adaptable to a wide variety of survey operations, with the emphasis being placed on the design of large scale track-type geophysical surveys.
2. Application of the theory should allow estimates to be made of the total variance or mean square error and the two-dimensional spectral content of the sampling error as a function of the survey pattern.
3. The error estimates should be in a form that would facilitate their propagation through a variety of linear operations.
4. The computational burden associated with the numerical implementation of the theory should be minimized to the extent that survey design could be performed in near real-time with small scale computers.

Utilizing these general criteria as guidelines, a procedure for designing track-type surveys has been developed which is based upon the use of mathematical models of the survey process, combined with classical sampling theory, to estimate the two-dimensional spectrum of the error associated with the discrete sampling of a continuous two- or three-dimensional function which is essentially non-stationary. The successful practical implementation of this theory involves the use of reconnaissance data to estimate the boundaries of statistically

homogeneous provinces, the design of appropriate models of the survey pattern, and the reliable estimation of both one- and two-dimensional Fourier transforms of geophysical data. In this section, the theory, and the numerical formulation developed for implementation will be presented in detail. Fortran IV computer programs are available from the author for each of the algorithms required for practical utilization of this theory.

Practical Problems in Spectral Estimation

Throughout this discussion, the following definitions will be used. The direct Fourier transform is defined by $G(\omega) = \int_{-\infty}^{\infty} g(x)e^{-i\omega x}dx$, and the inverse Fourier transform is defined by $g(x) = \frac{1}{2\pi}\int_{-\infty}^{\infty}G(\omega)\ e^{i\omega x}d\omega$.

The problems associated with estimating the one-dimensional autocorrelation function and power spectrum of a continuous function from a sample of finite length are presented in detail in the classical work by Blackman and Tukey (1958). More recently, Lacoss (1971) applied two new nonlinear spectral analysis techniques to the problem of resolving narrow spectral peaks in seismic data. These techniques (Maximum Likelihood Method developed by Capon (1969), and Maximum Entropy Method utilized by Burg (1967)), appear to yield results superior to those obtained by straightforward window modification applied to the estimated autocorrelation function.

In contrast, the problem of estimating the spectral content of a finite length of data from geophysical processes such as the earth's gravity or magnetic fields is generated not by prominent spectral peaks but by the large amount of energy contained in wavelengths considerably longer than the length of the available data record.

Processes which possess this type of spectral character have been termed "red noise" processes by Shapiro and Ward (1960). The generalization of a pure "red noise" spectrum as the power spectrum of a first-order linear Markov process has been developed by Gilman et al (1963). Alldredge, et al (1963) computed a one-dimensional spectrum of the earth's magnetic field which shows the large amount of energy in the field at the long wavelengths. In a statistical sense, this long wavelength energy may be considered as the non-stationary component of our finite length sample. Since the basis of survey design lies in estimating the Fourier transform of the error generated by sampling a locally stationary two- or three-dimensional function, two distinct problems must be addressed. These problems are outlined as follows:

1. A significant amount of the energy contained in the spectra of the earth's gravity and magnetic fields is located in wavelengths much longer than the extent of any particular survey operation. This long - wavelength energy causes $g(x,y)$ to appear to be non-stationary with regard to spatial coordinates, that is, the mean and autocorrelation function of $g(x,y)$ vary over the survey area.
2. Only in rare instances are closely spaced gridded values of $g(x,y)$ available for numerically computing a local two-dimensional spectrum which may be assumed to be free of sampling error.

In practice, the second problem is generally annoying in that it requires the collection of additional survey data, but the first problem is often fatal unless adequate precautions are taken. The first problem generates what is often referred to as spectral leakage (Tukey, 1967). In one-dimension, the collection of a finite length of

data ($-T/2 \leq x \leq T/2$) from a continuous function $g(x)$ consists essentially of multiplying $g(x)$ by a rectangular data window function $w(x)$ defined by

$$w(x) = \begin{cases} 1, & -T/2 \leq x \leq T/2 \\ 0, & \text{elsewhere} \end{cases}$$

It may be shown by straightforward integration that the Fourier transform of $w(x)$ is given by

$$W(\omega) = T \frac{\text{Sin } T\,\omega/2}{T\omega/2},$$

where T is the total length of the data window.

In the frequency domain, the effect of multiplying $g(x)$ by $w(x)$ to obtain a finite length of data is equivalent to convolving $G(\omega)$ with $W(\omega)$. Thus, the Fourier transform which is actually computed is not $G(\omega)$ but $G_c(\omega)$, which is given by

$$G_c(\omega) = \int_{-\infty}^{\infty} G(u)\, W(\omega-u)du.$$

Historically, many different data window functions have been proposed and used in an attempt to make $G_c(\omega)$ a better approximation of $G(\omega)$ (see e.g. Blackman and Tukey, 1958). Prior to the current trend of computing spectra through utilization of the FFT (Fast Fourier Transform) developed by Cooley and Tukey (1965), these data windows were applied to the sample autocorrelation function. With the development of the FFT as a standard analysis tool, the data windows must be applied directly to the sampled function. The design of these data window functions involves a compromise between the "sharpness" of the frequency cutoff of $W(\omega)$ and the magnitude of the side lobes. For

example, the window function consisting of a so called cosine taper defined as

$$w_t(x) = \begin{cases} 1/2(1+\cos \frac{2\pi x}{T}), & -T/2 \leq x \leq T/2 \\ 0, & \text{elsewhere} \end{cases}$$

is often used to reduce the magnitude of the side lobes at the expense of broadening the main lobe. The Fourier transform of the cosine taper window is given by

$$W_t(\omega) = \frac{T}{2} \frac{\text{Sin } T\omega/2}{T\omega/2} + \frac{T}{4} \left[\frac{\text{Sin } (\pi - T\omega/2)}{\pi - T\omega/2} + \frac{\text{Sin } (\pi + T\omega/2)}{\pi + T\omega/2} \right]$$

Figure 1 is a plot of $\frac{W(f)}{T}$ and $\frac{W_t(f)}{T}$ in which the substitution $\omega = 2\pi f$ has been made to more clearly indicate the relationships between the transforms of the window functions and their length (T). Note that the main lobe of $\frac{W_t(f)}{T}$ is much wider than that of $\frac{W(f)}{T}$, but the magnitude of the first side lobe has been decreased from approximately 0.21 to approximately 0.01. In practice, the use of $w_t(x)$ tends to reduce the oscillatory character of $G_c(\omega)$, but a significant amount of spectral leakage may still be present. As a consequence of the negative side lobe on the cosine taper window, negative power spectral estimates often occur when this window is applied to the autocorrelation function computed from processes exhibiting "red noise" character. Other windows, such as the Bartlett window (Blackman and Tukey, 1958), defined as

$$w_B(x) = \begin{cases} 1 - \frac{2|x|}{T}, & |x| < |T/2|, \\ 0, & \text{elsewhere} \end{cases}$$

may be used to eliminate the negative power estimates at the expense of increasing the magnitude of the side lobes.

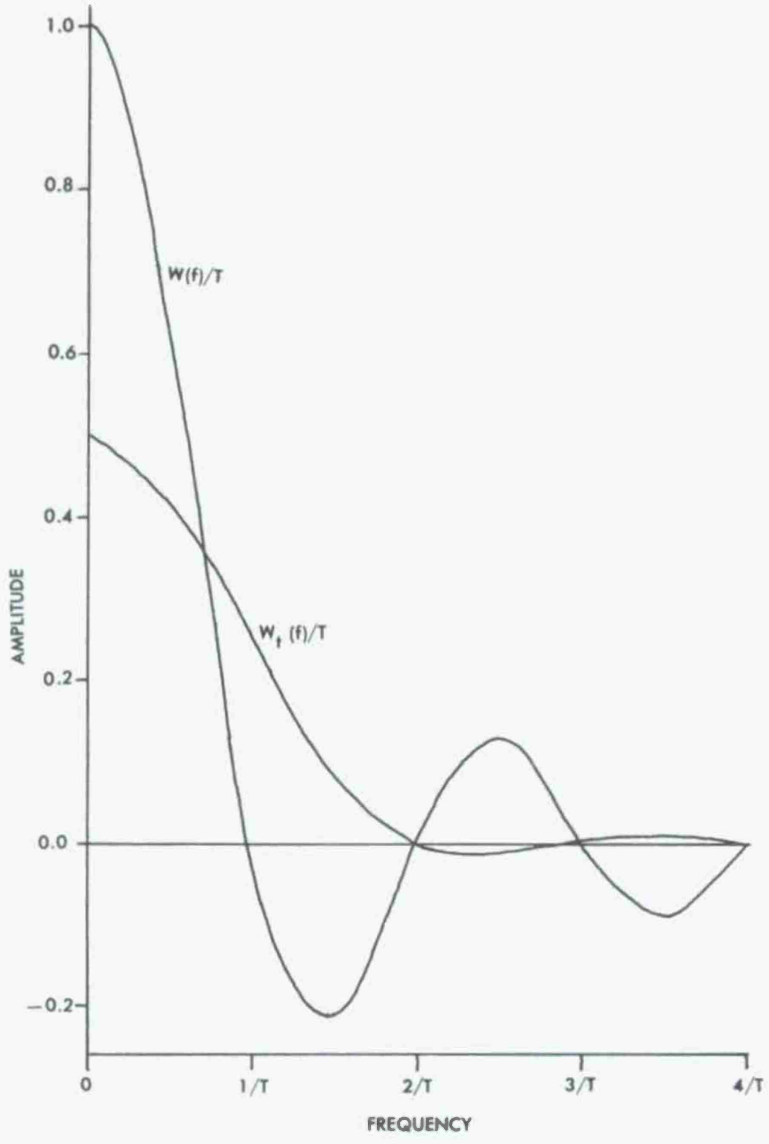

Figure 1. Fourier transform of cosine taper $(W_t(f)/T)$ and rectangular $(W(f)/T)$ data windows.

For a real, asymmetric g(x), the Fourier transform is a complex quantity of the form $G(\omega) = E(\omega) + iD(\omega)$ with an even real part ($E(\omega)$) and an odd imaginary part ($D(\omega)$). The amplitude spectrum of g(x) is defined as $|G(\omega)|$ and the power spectrum or energy spectrum is defined as $|G(\omega)|^2$ (Bracewell, 1965). The computed amplitude spectrum of g(x) multiplied by a data window is then given by

$$|G_c(\omega)| = ([E(\omega)*W(\omega)]^2 + [D(\omega)*W(\omega)]^2)^{1/2},$$

where * denotes the convolution operation. In the case of gravity and magnetic fields, this leakage of the long wavelength energy through the side lobes of the window function may easily become serious enough to distort the computed spectrum completely. In light of the ever increasing utilization of the FFT, the importance of this problem cannot be overemphasized.

As a quantitative illustration of this leakage effect, a comparison is made between the theoretical and numerical amplitude spectrum of the gravity anomaly generated by a deep-seated two-dimensional fault model shown in Figure 2. The gravity anomaly along a profile perpendicular to the strike of this body for a dip angle (A) of 90° is given by (Davis, 1971)

$$g(x) = \gamma\rho T + 2\gamma\rho\left\{(D+T)\tan^{-1}\left(\frac{x}{D+T}\right) - D\tan^{-1}\left(\frac{x}{D}\right) + \frac{x}{2}\ln\left\{\frac{(D+T)^2+x^2}{D^2+x^2}\right\}\right\},$$

where D, T, x, and ρ are defined as in Figure 2, and γ is the universal gravitational constant. Since g(x) is not absolutely integrable ($\int_{-\infty}^{\infty}|g(x)|dx$ is not finite), the Fourier transform of g(x) theoretically does not exist. Nevertheless, a representation of the transform which will be sufficient for our needs is given by

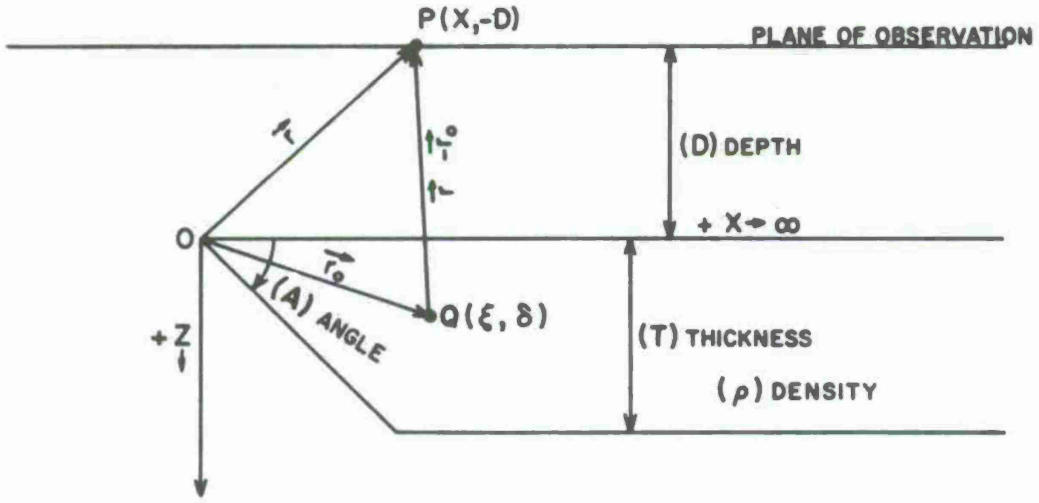

Figure 2. The two-dimensional gravity fault model.

$|G(\omega)| = 2\pi\gamma\rho\left\{(\pi T\delta(\omega))^2+\left[\frac{1}{\omega^2}[e^{-\omega D}-e^{-\omega(D+T)}]\right]^2\right\}^{1/2}$ (Davis, 1971), where $\delta(\omega)$ is the Dirac delta function. For $\omega \neq o$, this reduces to $|G(\omega)| = \frac{2\pi\gamma\rho}{\omega^2}\left|e^{-\omega D}-e^{-\omega(D+T)}\right|$. The curve denoted by the symbol (Δ) in Figure 3 is a plot of the theoretical amplitude spectrum of the gravity anomaly generated by a fault model for a depth of 1 km, a thickness of 10 km, and a density contrast of 1 g/cc. Digital data for computing a numerical FFT amplitude spectrum were generated by evaluating g(x) at a data interval (DI) of ΔX = 0.5 km for the range -64 km <x< 64 km. Note that all FFT spectra are computed and plotted at equal increments of normalized frequency with units of cycles per data interval (~/DI). The resulting numerical spectrum computed from this data set using the rectangular window function, w(x), is shown by the curve denoted by the symbol (□) in Figure 3. The effect, on the computed amplitude spectrum, of multiplying g(x) by w(x) with the resulting convolution in the frequency domain is readily apparent. The distortion of the numerical spectrum at the high frequency end is generated by leakage as the side lobes of $W(\omega)$ operate on those spectral components of $G(\omega)$ with wavelengths longer than 128 km. This distortion is typical of that obtained in practice from geophysical processes such as gravity or magnetic fields which possess a "red noise" type of spectrum.

In practice, an alternative procedure called prewhitening (Tukey, 1967) has been found to yield more consistently accurate spectral estimates than those generally obtainable by applying window modifications to this type of "red noise" process. In this application, prewhitening is considered to be a numerical process which operates on the original data set in such a way that the resulting amplitude spectrum is nearly

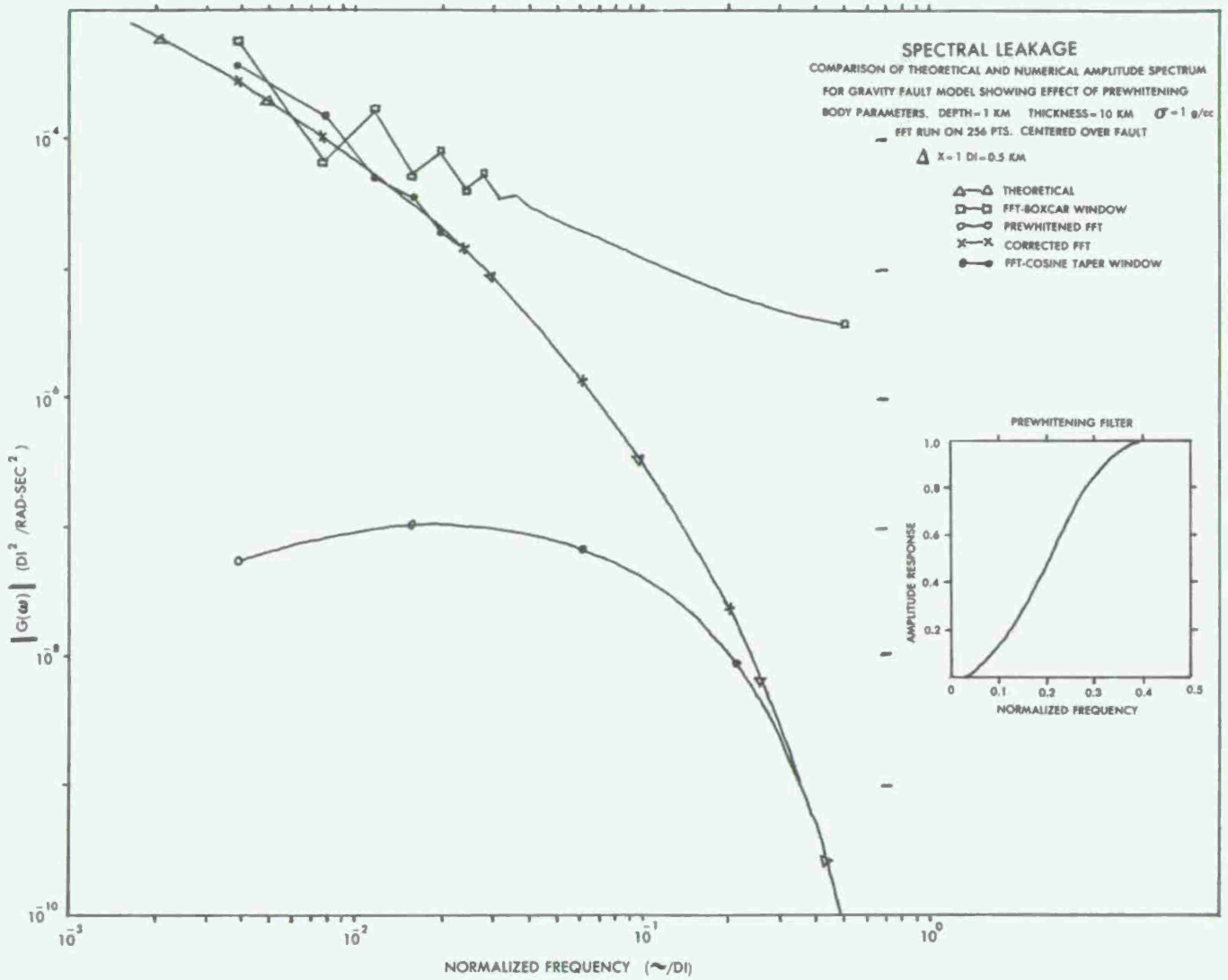

Figure 3. Numerical example of spectral leakage.

flat (within one or two orders of magnitude for gravity or magnetic data) over the frequency range of interest and nearly zero outside this range. The manner in which the prewhitening operation reduces the effect of applying a rectangular data window may be shown as follows:

Define a function g(x) which possesses a flat spectrum, i.e.,

$$g(x) = \delta(x), \text{ and } G(\omega) = 1.$$

With $\omega = 2\pi f$, $G(f) = 1$, and the Fourier transform of the rectangular data window is given by

$$W(f) = T \frac{\mathrm{Sin}\pi fT}{\pi fT} \quad .$$

The computed Fourier transform ($G_c(f)$) is the result of convolving G(f) with W(f), thus,

$$G_c(f) = \frac{2}{\pi} \int_0^\infty \frac{\mathrm{Sin}\pi\eta T}{\eta} \, d\eta$$

and (Gradshteyn and Ryzhik, 1965),

$$G_c(f) = G(f) = 1.$$

As is shown by this example, the application of the rectangular data window to a function possessing a flat spectrum has no adverse effect upon the computed spectrum.

Assuming that N equally spaced digital data values are available for analysis, this prewhitening process is most easily accomplished by applying an appropriately designed digital filter to these N data values. Since, as the example shown in Figure 3 indicates, a

realistic spectrum cannot generally be computed prior to prewhitening, the appropriate amplitude response of this filter can be obtained only through experience with a particular type of data. As a practical matter, a technique which has been found to be particularly effective in this regard is to compute the spectrum of a sample set of data using the cosine taper window $w_t(x)$ and then develop the appropriate response for the prewhitening filter from this first estimate. Another equally effective, though slightly more time consuming method, consists of applying a set of contiguous numerical band-pass filters to the data set, and integrating the output of each filter to produce an estimate of the energy contained within each frequency band. In addition, a priori knowledge of the expected form of the spectrum for the type of data being analyzed is sometimes available. In the case of two-dimensional gravity or magnetic fields, the fact that the amplitude spectrum is generally dominated by a term of the form $e^{-D\omega}$, where D is the depth to the disturbing body, is helpful.

A filter possessing an amplitude response as shown in Figure 3, which has been set to effectively remove normalized frequencies less than 1/N cycles per data interval has been found to work reasonably well for both gravity and magnetic data. Details concerning the design of this type of filter are presented in Appendix A. Figure 3 illustrates the improvement which was obtained by prewhitening the gravity fault model data in the space domain, computing the amplitude spectrum of these filtered data, then utilizing the convolution theorem to correct this spectrum for the effect of the filter over the frequency range 1/N to 0.5 cycles per data interval by dividing the computed FFT by the frequency response of the filter. The final corrected FFT

spectrum (denoted by the symbol (x) is nearly identical to the theoretical curve over the entire frequency range.

The FFT spectrum obtained through application of the cosine taper window ($w_t(x)$) is also presented for comparison. Note that there is essentially no residual oscillation in the low frequency components of the prewhitened and corrected FFT while the side lobes of the cosine taper window operating on the $\delta(\omega)$ component of $G(\omega)$ produced a significant ripple at these frequencies. As this example illustrates, the design of the prewhitening filter is not particularly critical (ie. the prewhitened spectrum does not need to be exactly white), but the employment of some form of prewhitening or window modification is imperative if accurate spectral estimates are to be expected from a finite length of data obtained from a "red noise" process.

One-Dimensional Sampling

As developed here, the underlying theory utilized in geophysical survey design consists of combining the Shannon sampling theorem (Shannon, 1949) with various models of one- and two-dimensional sampling functions and Parseval's relationship (Hamming, 1962) to estimate the variance or mean square error and the spectral content of the sampling error as a function of survey track direction and track spacing.

The proof of the one-dimensional Shannon sampling theorem is outlined in Papoulis (1962). Since this is the basis for practical survey design, the detailed proof is presented in Appendix B. This theorem states that, given equally spaced digital values f(mT) of a continuous function f(t) which is band-limited to the normalized frequency range

$-\pi \leq \omega \leq \pi$, and such that $\int_{-\pi}^{\pi} |F(\omega)| d\omega$ exists, f(t) may be represented by

$$f(t) = \sum_{m=-\infty}^{\infty} f(mT) \frac{\text{Sin } \pi(t-mT)}{\pi(t-mT)} \quad \text{for all } t.$$

In this formulation, T is the spacing between the digital samples of f(t). Thus, this discrete numerical convolution of the digital samples of f(t) with a Sinc function $(\frac{\text{Sin } t}{t})$ amounts to a perfect interpolation procedure.

Within the context of survey design, the ultimate aim is to estimate the variance and spectral content of the error generated by sampling a continuous function, which is band-limited for practical purposes, at a rate less than that required by the Shannon theorem. In order to generate this estimate of the so-called sampling error, consider that the equally spaced digital samples (f(mT)) of the continuous function (f(t)) are obtained by multiplying f(t) by an infinite sequence of unit impulses spaced a distance T apart. Bracewell (1965) called this sequence the shaw symbol and defines it as $\text{Ш}(t) = \sum_{m=-\infty}^{\infty} \delta(t-mT)$. Hsu (1970) shows, in a straightforward manner, that the Fourier transform of $\text{Ш}(t) = \frac{2\pi}{T} \sum_{m=-\infty}^{\infty} \delta(\omega - \frac{2\pi m}{T})$.

As a consequence of the convolution theorem for Fourier transforms (see e.g. Papoulis, 1962), the multiplication of f(t) by Ш(t) to produce the digital samples f(mT) in the time domain results in convolving the Fourier transform of Ш(t) with the Fourier transform of f(t). These relationships are shown in Figure 4. From this figure, it is clear that, as T increases, the spacing between the impulses of Ш(ω) becomes less. If T is allowed to increase to the point where $\frac{2\pi}{T} < 2A$, then the convolution operation replicates F(ω) in such a way

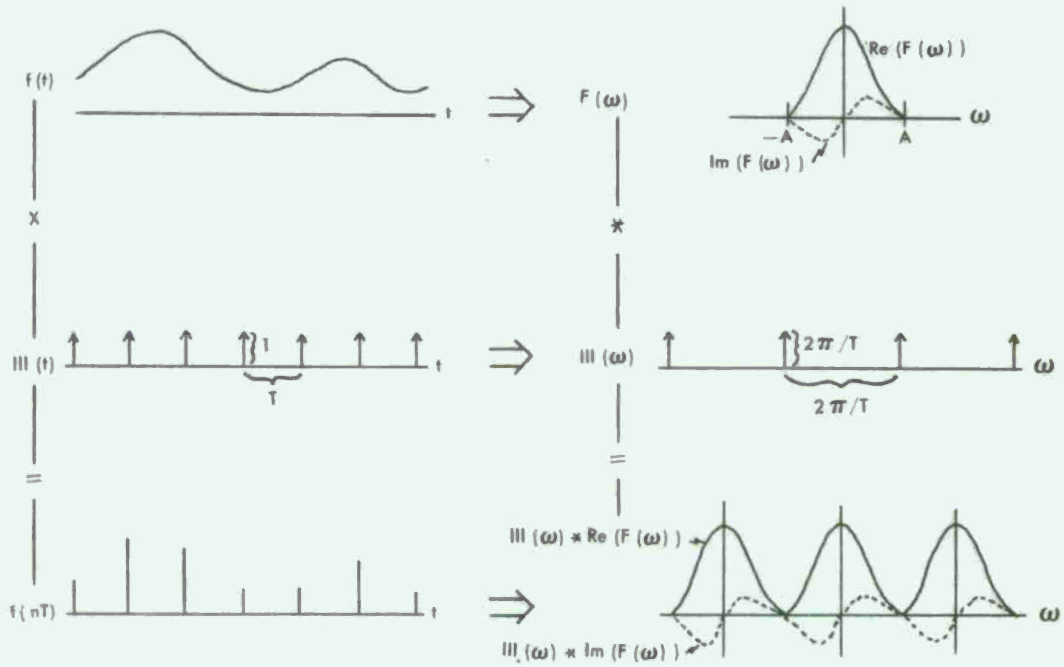

Figure 4. One-dimensional sampling.

that $F(\omega)$ overlaps itself at the folding frequency ($\pm\frac{\pi}{T}$) producing what is called sampling error.

The Fourier transform of this sampling error is composed of two parts. The first part may be considered to be the error of commission or the aliasing error. The Fourier transform of this error component is defined as the difference between $F(\omega)$ and $111(\omega) * F(\omega)$ up to the folding frequency. The amplitude spectrum of this error component is given by

$$|F_A(\omega)| = |\ 111(\omega) * F(\omega) - F(\omega)| \qquad (1)$$

The second part of the sampling error may be considered to be the error of omission since spectral components of $F(\omega)$ for $\frac{\pi}{T} < |\omega| \leq A$ are not recoverable from the sampled data. The amplitude spectrum of this error component is simply

$$|F_o(\omega)| = |F(\omega)| \quad \text{for } \frac{\pi}{T} < |\omega| \leq A.$$

These two error components combine to form the sampling error spectrum defined as

$$|F_S(\omega)| = |F_A(\omega)| + |F_o(\omega)| \qquad (2)$$

This error is shown in Figure 5 for the real part of $F(\omega)$.

For survey design operations, the interest lies not only in the spectrum of the sampling error but also in the mean square error or RMS of the error as a function of sample spacing. This mean square error estimate is readily available through the application of Parseval's formula (Papoulis, 1962). This formula states that energy is conserved when transformations are made between the time or space domain and the frequency domain and is given by

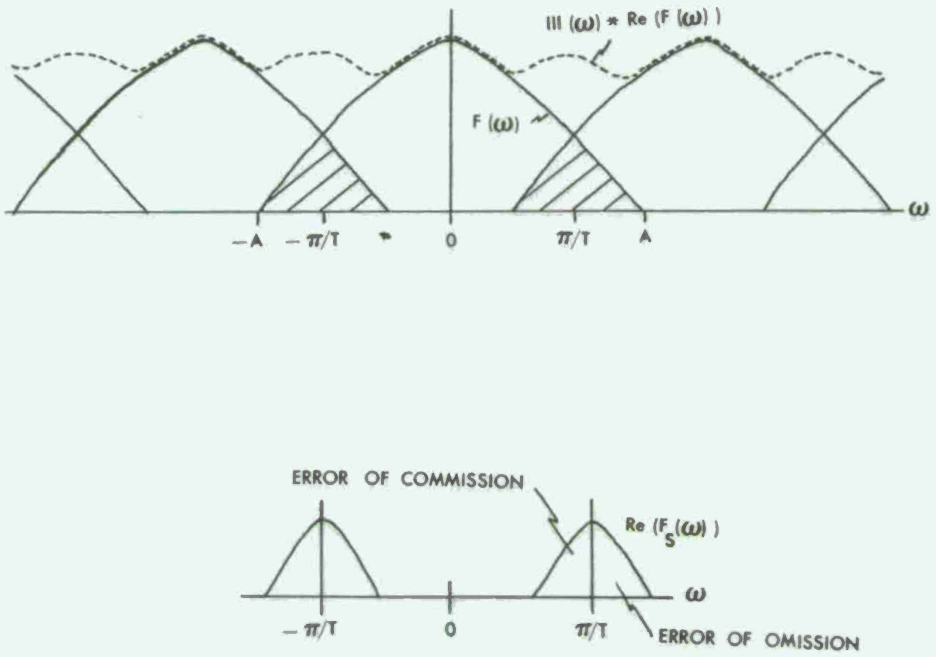

Figure 5. The two components of one-dimensional sampling error.

$$\int_{-\infty}^{\infty} |g(t)|^2 dt = \frac{1}{2\pi} \int_{-\infty}^{\infty} |G(\omega)|^2 d\omega = \int_{-A}^{A} |G(f)|^2 df \text{ for } \omega = 2\pi f \text{ and}$$

g(t) bandlimited to ±A. In practice, G(f) is computed numerically utilizing the Fast Fourier transform which produces discrete estimates of G(f) at a normalized frequency spacing of $\frac{1}{N}$ cycles per data interval for N digital values (g_m) of g(t). A numerical estimate of the mean square sampling error using Parseval's formula is then given by

$$\frac{1}{N} \sum_{m=o}^{N-1} g_m^2 = \frac{1}{N^2} \left| |G_S(o)|^2 + |G_S(\tfrac{1}{2})|^2 + 2 \sum_{K=1}^{N/2-1} |G_S(\tfrac{K}{N})|^2 \right| , \qquad (3)$$

where $G_S(\frac{J}{N})$ are the numerical FFT estimates of the sampling error spectrum, defined by equation (2), for J = 0,....N/2.

With regard to the computation of the amplitude or power spectrum of the aliasing error through the use of equation (1), an approximation to $|F_A(\omega)|$ is presented here for use in real time survey design with small scale computers. This technique is particularly appropriate when only the sampling error variance is desired, rather than the sampling error spectrum. This approximation is called a power fold, and is developed in the following manner.

For a real asymmetric f(x), the Fourier transform is a complex quantity of the form $F(\omega) = E(\omega) + i\, D(\omega)$ with an even, real part ($E(\omega)$), and an odd, imaginary part ($D(\omega)$). A complex quantity possessing this type of symmetry is termed Hermitian. An explicit formulation of the power spectrum of the aliasing error component for a sample spacing (T) is, from equation (1),

$$\left|111(\omega)*F(\omega)-F(\omega)\right|^2 = \left|\frac{2\pi}{T}\int_{-\infty}^{\infty} E(u)\sum_{m=-\infty}^{\infty}\delta[(\omega-u)-\frac{2\pi m}{T}]du\right.$$

$$\left. + i\,\frac{2\pi}{T}\int_{-\infty}^{\infty} D(u)\sum_{m=-\infty}^{\infty}\delta[(\omega-u)-\frac{2\pi m}{T}]du - [E(\omega)+iD(\omega)]\right|^2$$

Changing the order of integration and summation, and utilizing the property of $\delta(\omega)$ given by $\int_{-\infty}^{\infty} E(\omega)\delta(\omega)d\omega = E(o)$, yields

$$\left|111(\omega)*F(\omega)-F(\omega)\right|^2 = \left|\left\{\frac{2\pi}{T}\sum_{m=-\infty}^{\infty} E(\omega-\frac{2\pi m}{T})\right\} - E(\omega)\right|^2$$

$$+ \left|\left\{\frac{2\pi}{T}\sum_{m=-\infty}^{\infty} D(\omega-\frac{2\pi m}{T})\right\} - D(\omega)\right|^2 \qquad (4)$$

In the power fold approximation, the computer storage requirement and computation time is essentially cut in half by approximating the actual power spectrum of the aliasing error component given by equation (4) by replicating $|F(\omega)|^2$ rather than $F(\omega)$.

Thus, $|111(\omega)*F(\omega)-F(\omega)|^2 \simeq |111(\omega)*|F(\omega)|^2 - |F(\omega)|^2|$ for $|\omega|\leq\frac{\pi}{T}$. Explicitly, we have

$$\left|111(\omega)*\left|F(\omega)\right|^2 - \left|F(\omega)\right|^2\right| = \left|\left\{\frac{2\pi}{T}\sum_{m=-\infty}^{\infty} E^2(\omega-\frac{2\pi m}{T})\right\} - E^2(\omega)\right.$$

$$\left. + \left\{\frac{2\pi}{T}\sum_{m=-\infty}^{\infty} D^2(\omega-\frac{2\pi m}{T}) - D^2(\omega)\right\}\right| . \qquad (5)$$

Comparing equations (4) and (5), it is readily apparent that the accuracy of this power fold approximation is a function of the amplitude of the cross terms in the product of the summations in equation (4). Empirical tests on many different types of geophysical data

indicate that the error of this approximation is within a small percentage of the total mean square sampling error except at folding frequencies equivalent to the first two or three harmonics of the sample data record. Two examples of these tests are shown in Figures 6 and 7. Figure 6 indicates the sampling error estimates obtained from applying equations (4) and (5) to a 32 point numerical test function shown in Figure 8. In this test, the power fold is seen to yield relatively accurate estimates of the sampling error except for sample spacings associated with the first three harmonics of the 32 point test function. Figure 7 shows a similar result obtained by applying equations (4) and (5) to a 128 point digital record of temporal variations of oceanic sound speed. As in the previous example, estimates of the sampling error for sample spacings associated with folding frequencies equivalent to the first three harmonics of the 128 point data record are relatively inaccurate.

In order to illustrate these concepts in a numerical example, a digital test function containing predominantly high frequency energy was generated utilizing equations (A-1) and (A-2) from Appendix A to produce a set of high-pass filter weights. The filter control parameters were set to $V_c = 0.08$, $H = 0.2$, $N = 15$. The numerical weight function generated by this process is shown in Figure 8. Note that the central values of this function should be scaled by the factor 100. The power spectrum of this function $|F(\omega)|^2$, computed via the FFT, is shown in Figure 9 as well as the estimate of the aliased spectrum produced for a ΔX sample spacing of two data intervals. This estimate was produced by a numerical solution of $|111(\omega)*F(\omega)|^2$ for the real and imaginary fold and $111(\omega)*|F(\omega)|^2$ for the power fold approximation. In this example, with ΔX = two data intervals, the folding

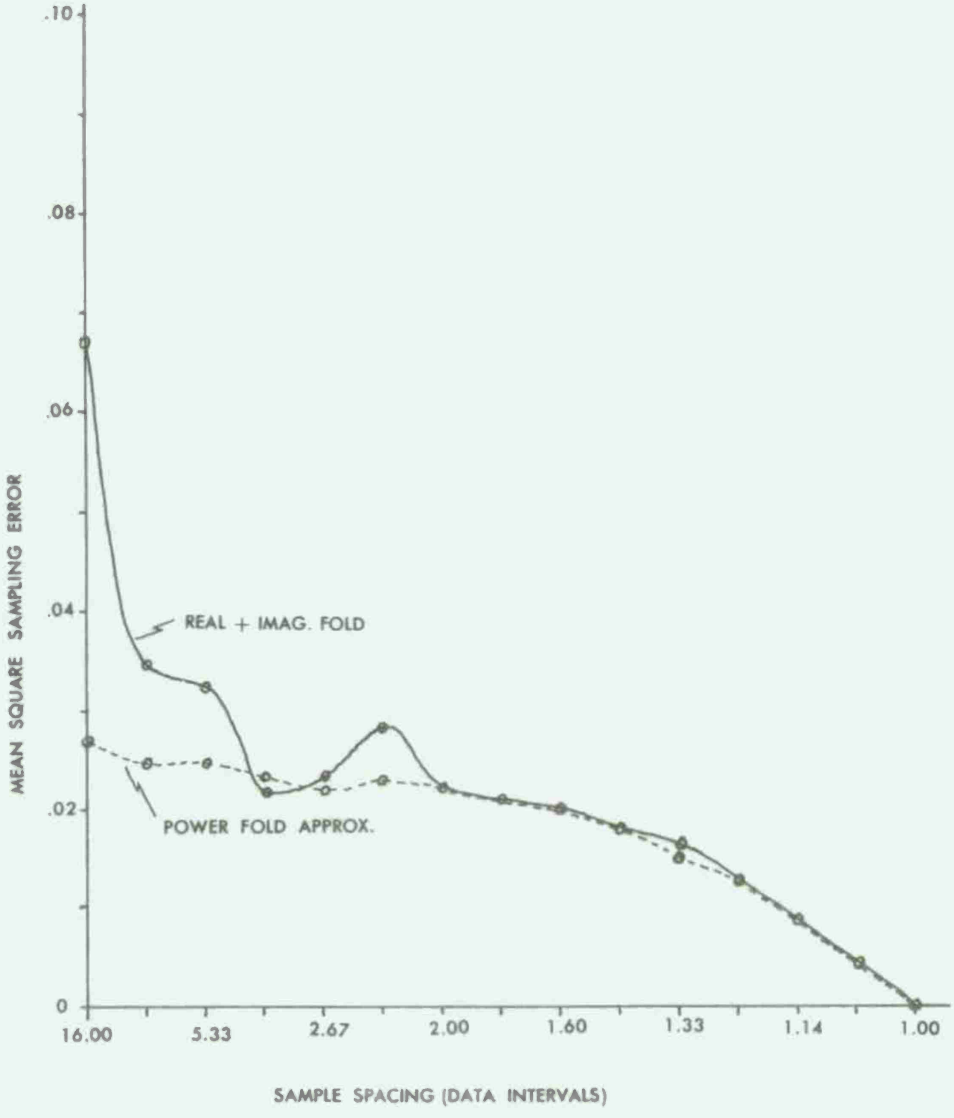

Figure 6. Numerical one-dimensional test - Sampling error vs. sample spacing.

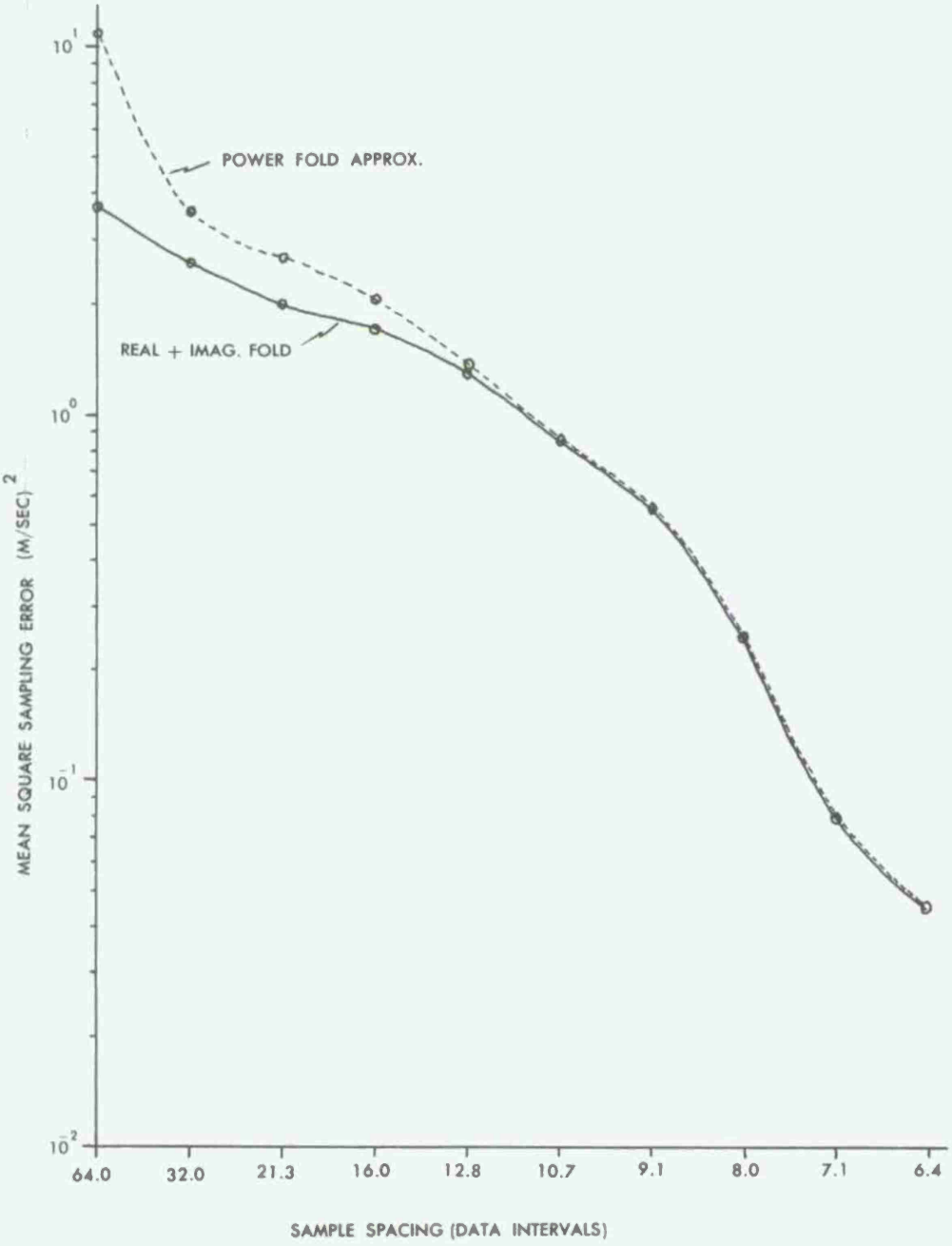

Figure 7. Example of sampling error for temporal variations of oceanic sound speed at a depth of 75 meters—one data interval=25 min.

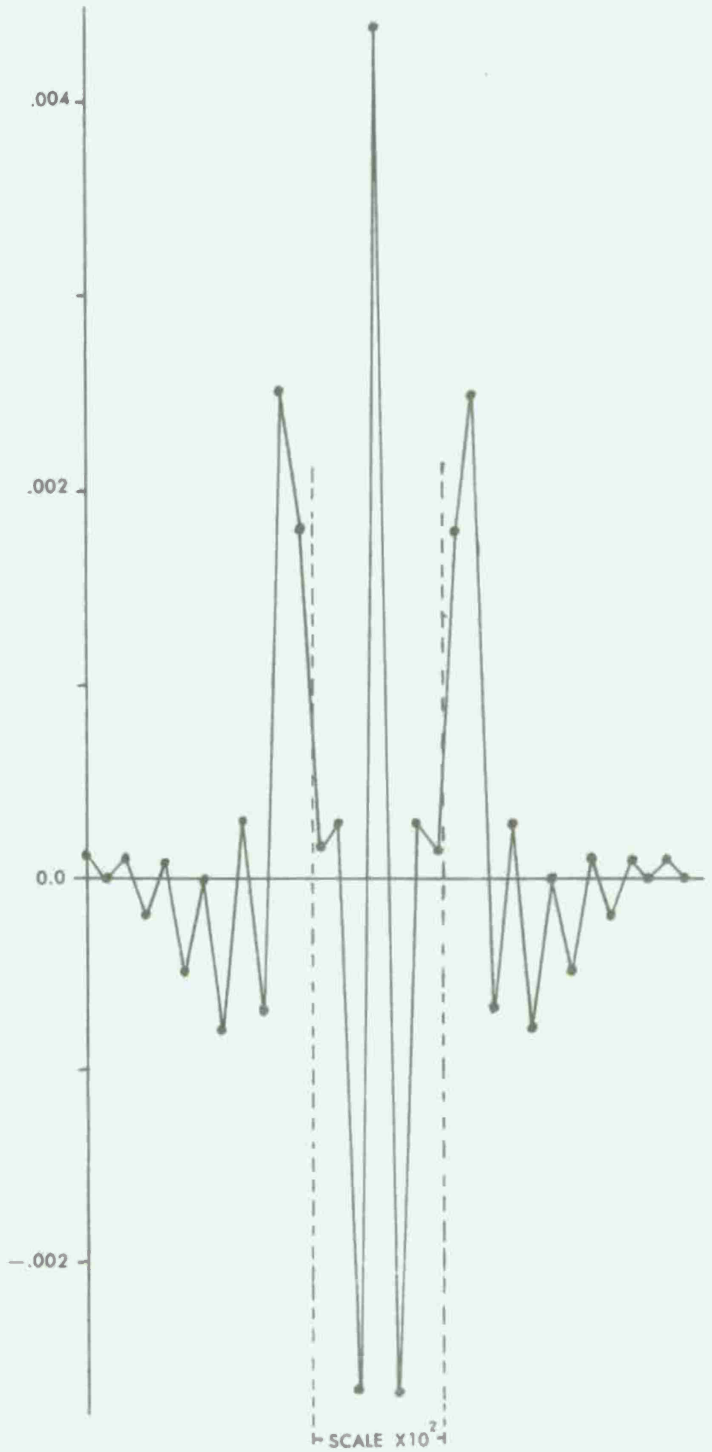

Figure 8. One-dimensional digital test function.

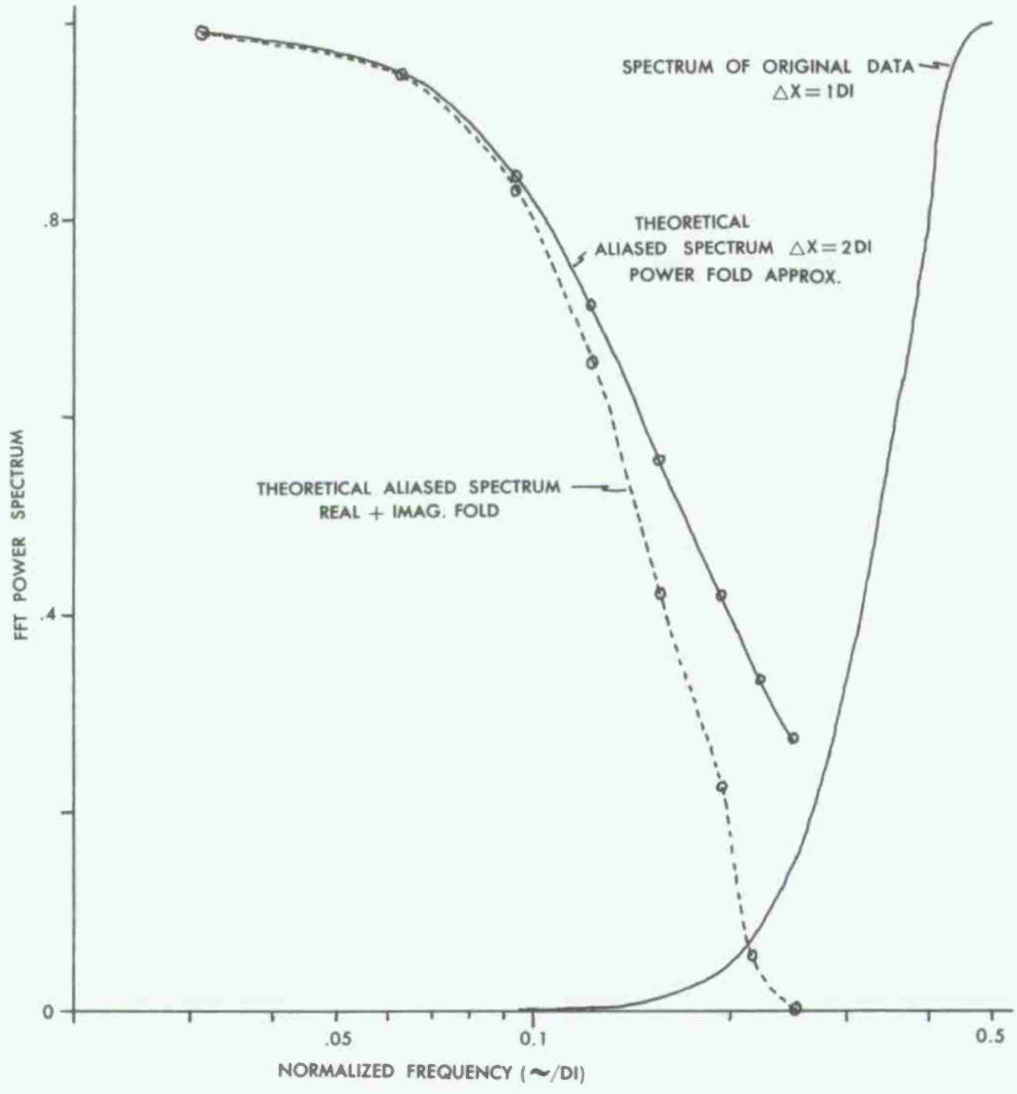

Figure 9. Numerical one-dimensional test—Aliased spectrum for △X=2DI.

frequency is 0.25 cycles per data interval. Figure 10 is a plot of the estimated power spectrum of the sampling error obtained by a numerical solution of equations (4) and (5). At this sample spacing, the sampling error spectrum produced by the power fold approximation was identical to that produced by folding the real and imaginary parts of $F(\omega)$.

As a test of this numerical process, the original test function was sampled at every second data point and a cubic spline interpolation (Davis and Kontis, 1970) was applied to obtain values at the missing points. As shown in Figure 10, the power spectrum of the difference between the interpolated values and the true values of the test function is in excellent agreement with that predicted by the theory. The spectral content of the error for frequencies less than 0.25 cycles per data interval is the error of commission while the error for frequencies greater than 0.25 cycles per data interval is the error of omission.

Utilizing equation (3), the estimated mean square sampling error for both the real and imaginary fold and the power fold approximation is 0.021201. The actual sampling error computed from the interpolated data values was 0.019330. In practice, the sampling error spectrum and mean square error may be estimated for any folding frequency which is a harmonic of the original data record. Figure 6 is a plot of the sampling error estimates for all possible folding frequencies of this test function. It is interesting to note that, with the total sampling error defined as consisting of both the error of commission and the error of omission, it is perfectly feasible to generate a mean square sampling error that is greater than the mean square value of the original function. In this particular example, the mean square value

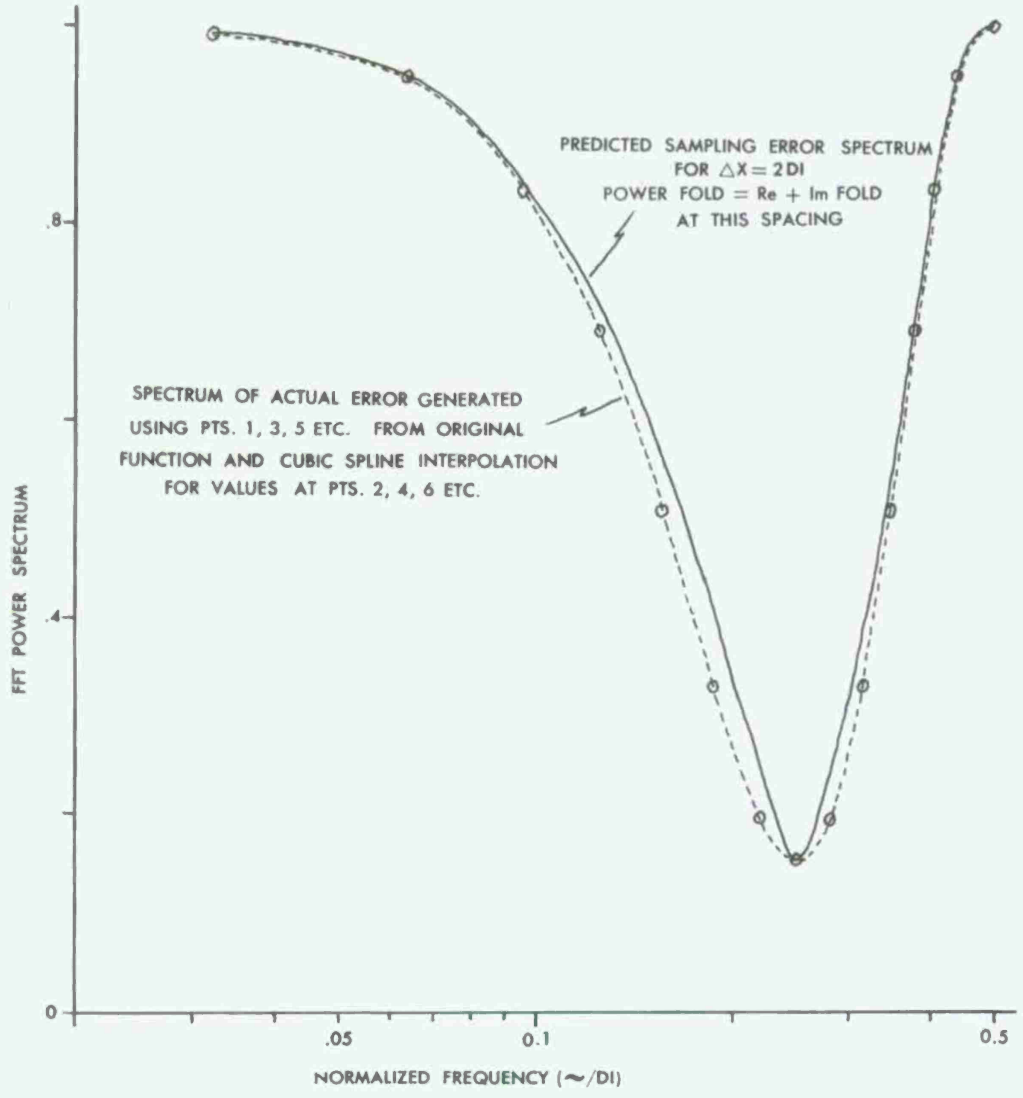

Figure 10. Numerical one-dimensional test—Spectrum of sampling error for △X=2DI.

of the original test function is 0.010625. Referring to Figure 6, it is clear that the sampling error may be expected to exceed this value for any sample spacing greater than 1.14 data intervals.

Two-Dimensional Track Sampling

At the present time, most large scale geophysical survey operations are conducted by collecting data along nominally parallel survey tracks by the use of aircraft, ships, helicopters, and satellites. The basic concept of geophysical survey design involves determining the optimum track spacing, track direction, and down-track sample rate which will produce digital data to describe these continuous fields to a predetermined accuracy.

With the current widespread use of digital recording systems and the utilization of the one-dimensional sampling theory for selecting the appropriate down-track sample rate, we can reasonably assume that the down-track sample rate is sufficient to define exactly a two-dimensional function f(x,y) along each survey track. Under this assumption, the appropriate mathematical model for defining two-dimensional track-type surveys is the raster sampling model utilized by Bracewell (1965) as a model for the formation of television images. This model is essentially a set of parallel delta function ridges generated by considering the one-dimensional shaw symbol as a two-dimensional function, ie:

$$S_T(x,y) = g(x) \sum_{m=-\infty}^{\infty} \delta(y-mT) \text{ where } g(x) \equiv 1 \text{ for}$$

survey tracks parallel to the x axis and spaced a distance T apart in the y direction.

Since the Fourier transform of a two-dimensional function which is

a product of two one-dimensional functions is the product of the one-dimensional transforms, the Fourier transform of $S_T(x,y)$ is given by

$$S_T(u,v) = 2\pi\delta(u)\,\frac{2\pi}{T}\sum_{m=-\infty}^{\infty}\delta\left(v-\frac{2\pi m}{T}\right)$$

where $2\pi\delta(u)$ is the Fourier transform of the constant $g(x)=1$. This model is shown in Figure 11. The survey data $D(x,y)$ collected along a set of equally spaced survey tracks oriented parallel to the x axis is then given by $D(x,y) = f(x,y)\ S_T(x,y)$. Since multiplication in the two-dimensional space domain results in a convolution in the two-dimensional spatial frequency domain, the result of the survey operation is to replicate the true two-dimensional Fourier transform of $f(x,y)$ in the cross-track direction by convolving $F(u,v)$ with $S_T(u,v)$). As in the one-dimensional case, the two-dimensional sampling error is defined as consisting of an aliasing error or error of commission for frequencies less than the folding frequency and an error of omission for frequencies greater than the folding frequency. The real part of the spectrum of this sampling error ($F_S(u,v)$) is shown in Figure 11.

An explicit formulation for the two-dimensional power spectrum is given by

$$\begin{aligned}
\left|F_A(u,v)\right|^2 &= \left|F(u,v)*S_T(u,v)-F(u,v)\right|^2 \\
&= \left|\left\{\frac{4\pi^2}{T}\sum_{m=-\infty}^{\infty}R\left(u,v-\frac{2\pi m}{T}\right)\right\} - R(u,v)\right|^2 \\
&+ \left|\left\{\frac{4\pi^2}{T}\sum_{m=-\infty}^{\infty}I\left(u,v-\frac{2\pi m}{T}\right)\right\} - I(u,v)\right|^2 \qquad (6)
\end{aligned}$$

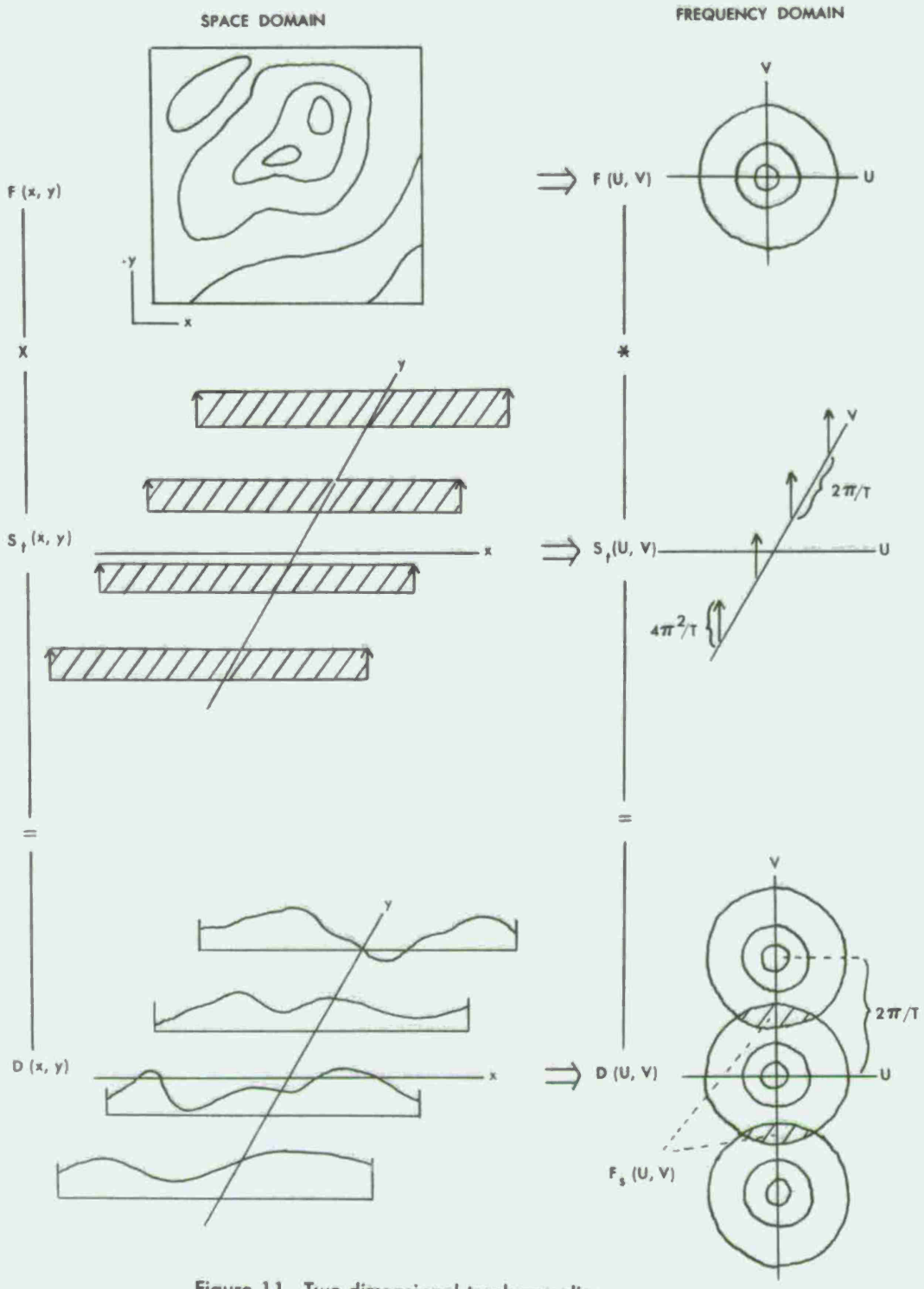

Figure 11. Two-dimensional track sampling.

where R(u,v) and I(u,v) are the real and imaginary parts of F(u,v). As in the one-dimensional case, the error of omission for tracks parallel to the x axis is simply $|F_o(u,v)|^2 = |F(u,v)|^2$ for v greater than the folding frequency. It should be noted that, in contrast to the one-dimensional transform, the real and imaginary parts of the two-dimensional transform of an arbitrary f(x,y), which does not exhibit circular symmetry, are composed of both even and odd components. In practice, the numerical evaluation of equation (6) is faciliated by separating both R(u,v) and I(u,v) into their respective even and odd components by use of the identity $f(t) = \frac{1}{2}[f(t)+f(-t)]$ for the even component and $f(t) = \frac{1}{2}[f(t)-f(-t)]$ for the odd component (Wylie, 1960).

With the preceding definitions, the power spectrum of the sampling error for two-dimensional track type sampling is defined as

$$|F_S(u,v)|^2 = |F_A(u,v)|^2 + |F_o(u,v)|^2 \qquad (7)$$

As in the one-dimensional case, the estimated mean square sampling error is obtained by numerically solving the two-dimensional form of Parseval's formula. That is, for an NxN grid of equally spaced values ($\Delta x=\Delta y$ = one data interval) of a two-dimensional function $f_{n,m}$, the mean square sampling error is

$$\frac{1}{N^2}\sum_{n=o}^{N=1}\sum_{m=o}^{N=1} f_{n,m}^2 = \frac{1}{N^4}\sum_{K=-\frac{N}{2}}^{N/2-1}\sum_{J=-\frac{N}{2}}^{N/2-1} |F_S(\tfrac{J}{N},\tfrac{K}{N})|^2 \qquad (8)$$

Figure 11 illustrates the relationship which exists between the two-dimensional spatial and frequency domains for track-type surveys. Practical application of this track-sampling theory involves the application of a two-dimensional FFT, with appropriate prewhitening,

and the numerical solution of equations (6) - (8) to obtain an estimate of the mean square sampling error and the two-dimensional sampling error spectrum at any desired folding frequency which is a harmonic of the test sample field.

As a numerical test of this theory, consider the contour chart shown in Figure 12 to be the result of a small detailed survey within a much larger homogeneous province. These test data, with units of arc seconds ($\widehat{sec}$), actually consist of 16x16 digital values derived from a model of the north component of vertical deflection at a grid spacing as shown in Figure 12. In this example, the y axis is assumed to be oriented in the north direction. Figure 13 is a contour chart of all four quadrants of the two-dimensional amplitude spectrum of this base data after appropriate prewhitening and correction. This figure, as well as subsequent contour charts of computed two-dimensional spectra, indicates a region centered at $F_x = F_y = 0.0$ in which the spectral content is undefined. This is a consequence of the prewhitening operation which essentially removes wavelength components longer than the data record, and the result of applying a two-dimensional low-pass smoothing filter to the spectral estimates in order to show the general character of the spectrum.

The numerical solution of equations (6) - (8) for north-south tracks spaced at varying multiples of the original data spacing produced estimates of the sampling error as shown in Figure 14. For comparison, the error estimates resulting from the utilization of a spectrum computed without prewhitening are also shown. In this particular example, the effect of spectral leakage on the estimated sampling error spectrum is not particularly pronounced.

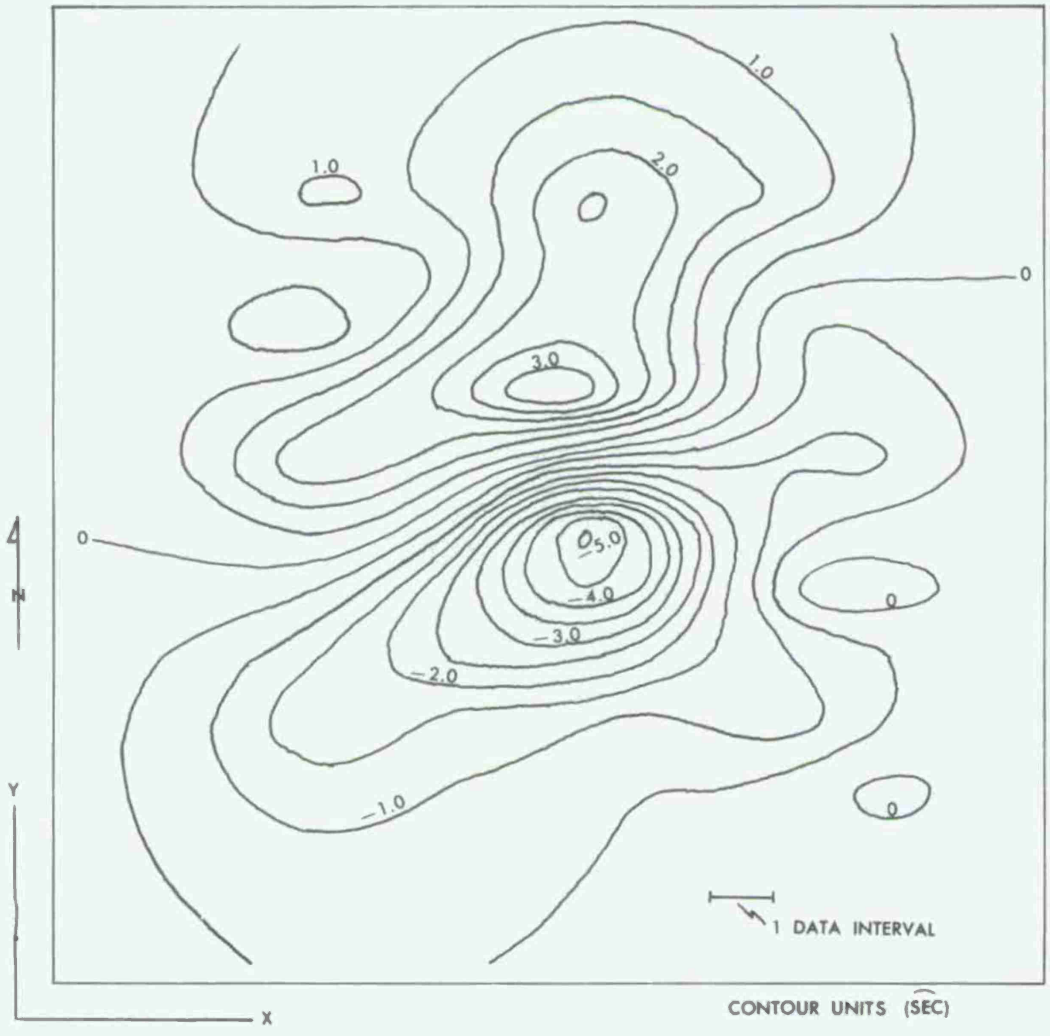

Figure 12. Base data for two-dimensional sampling test—16 × 16 point grid.

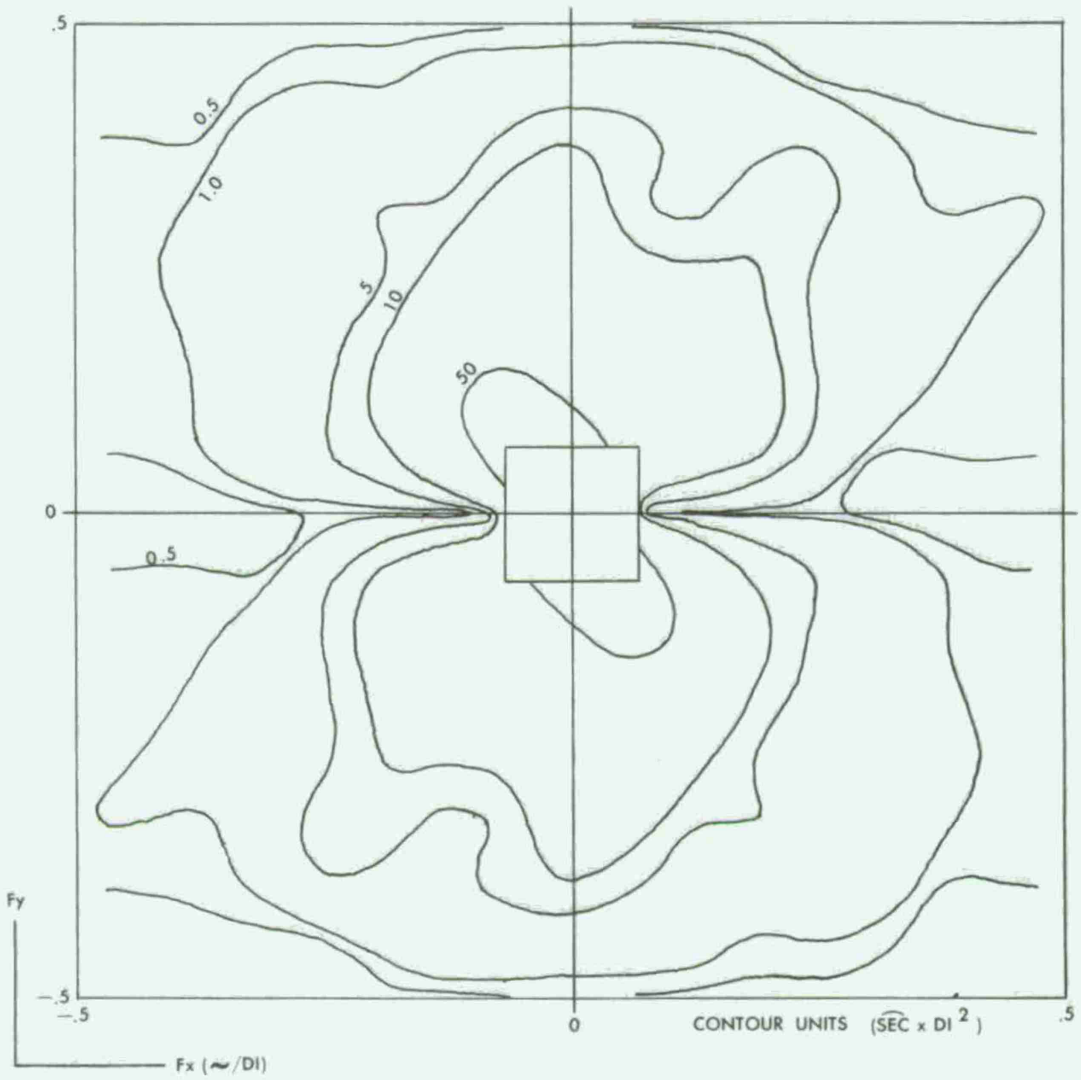

Figure 13. Two-dimensional amplitude spectrum of base data.

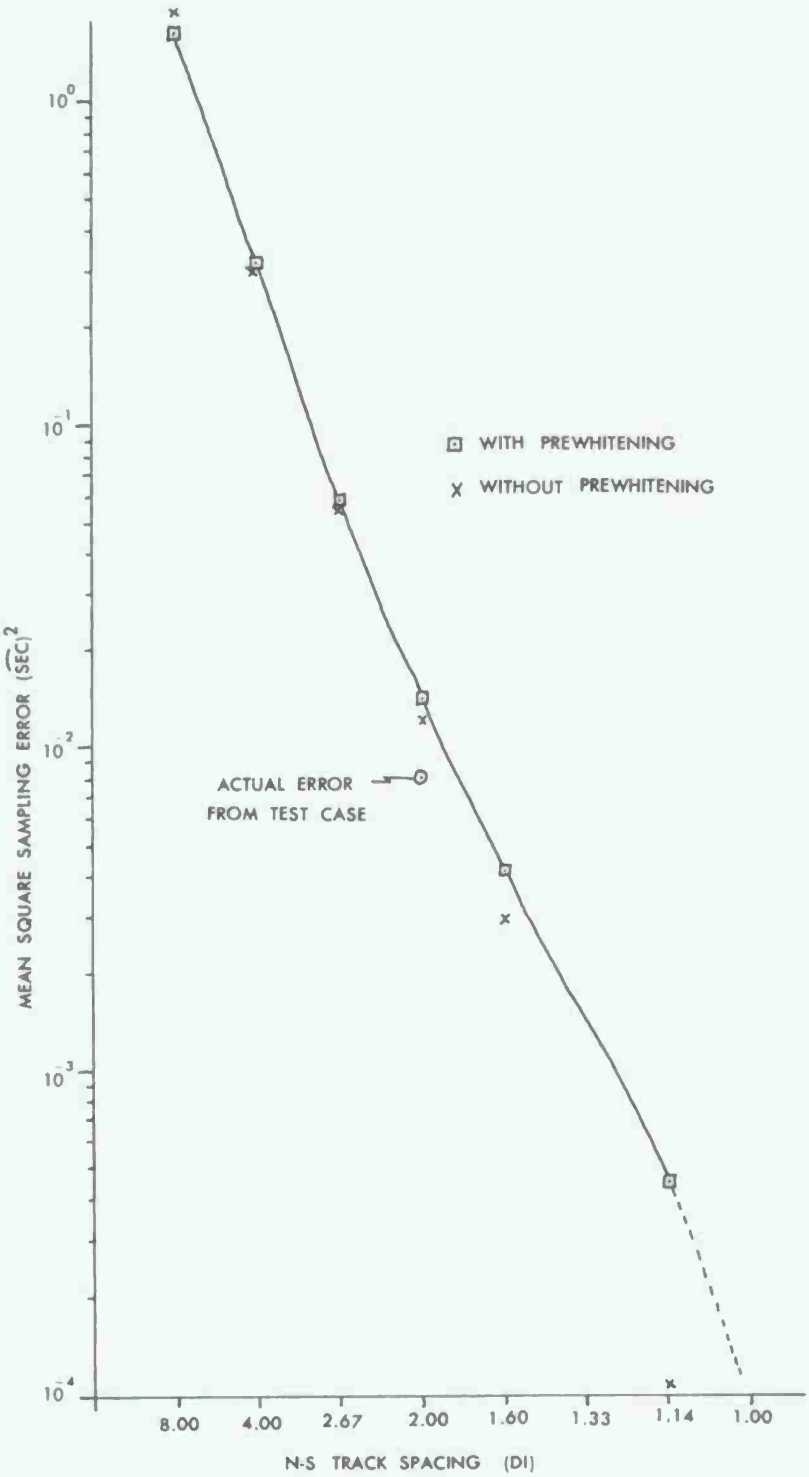

Figure 14. Numerical two-dimensional test—Sampling error vs. N-S track spacing.

At each track spacing, the solution of equations (6) and (7) produce an estimate of the two-dimensional spectrum of the sampling error. Figures 15-17 are contour charts of the two-dimensional amplitude spectrum of the sampling error at selected track spacings. As expected from the preceding discussion concerning the operations of $S_T(u,v)$, and the general "red noise" type character of the spectrum of the base data (Figure 13), Figures 15-17 indicate that the maximum amplitude of the sampling error spectrum decreases as the spacing between tracks decreases, and that the maximum amplitude is located quite close to the folding frequency.

As a numerical test of the accuracy of these sampling error estimates, every second column of data was extracted from the base data grid to simulate the survey data which would be collected along north-south tracks spaced two data intervals apart. Values of the field at the missing grid points were generated by the application of a cubic spline interpolation procedure (Davis and Kontis, 1970) designed specifically for gridding data from track - type surveys. The actual mean square error computed for this test case is shown in Figure 14. The two-dimensional amplitude spectrum of this error is contoured in Figure 18. A comparison of Figures 16 and 18 indicates the generally excellent agreement between the theoretical estimate of the error spectrum and the actual spectrum from this numerical test. Figure 19 is a profile through these two error spectra along the line $F_x=F_y$. The slight disagreement between the two curves at the lower frequencies is undoubtedly generated by two-dimensional spectral leakage since no prewhitening filter was applied to the sampling error produced by the numerical test.

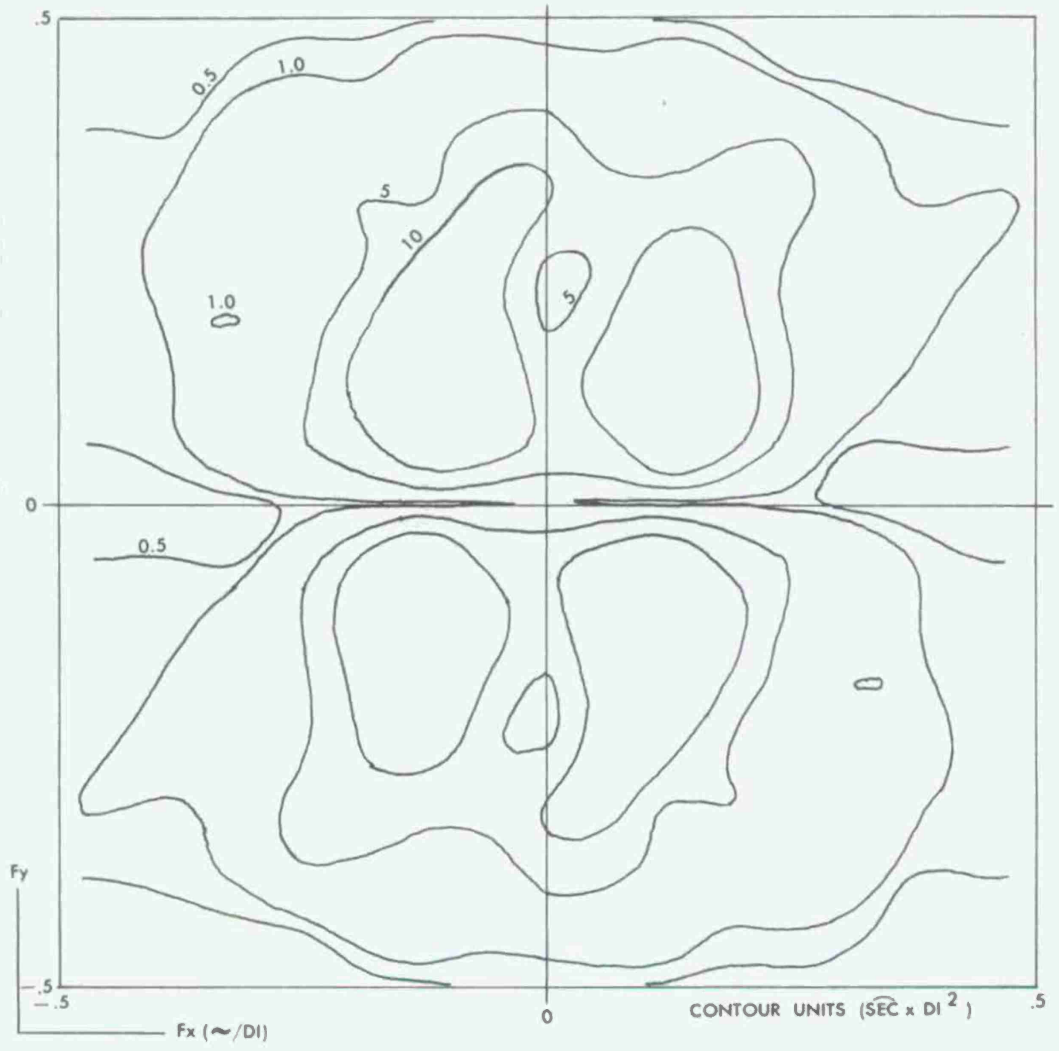

Figure 15. Two-dimensional error spectrum, N-S track spacing=4.0 DI.

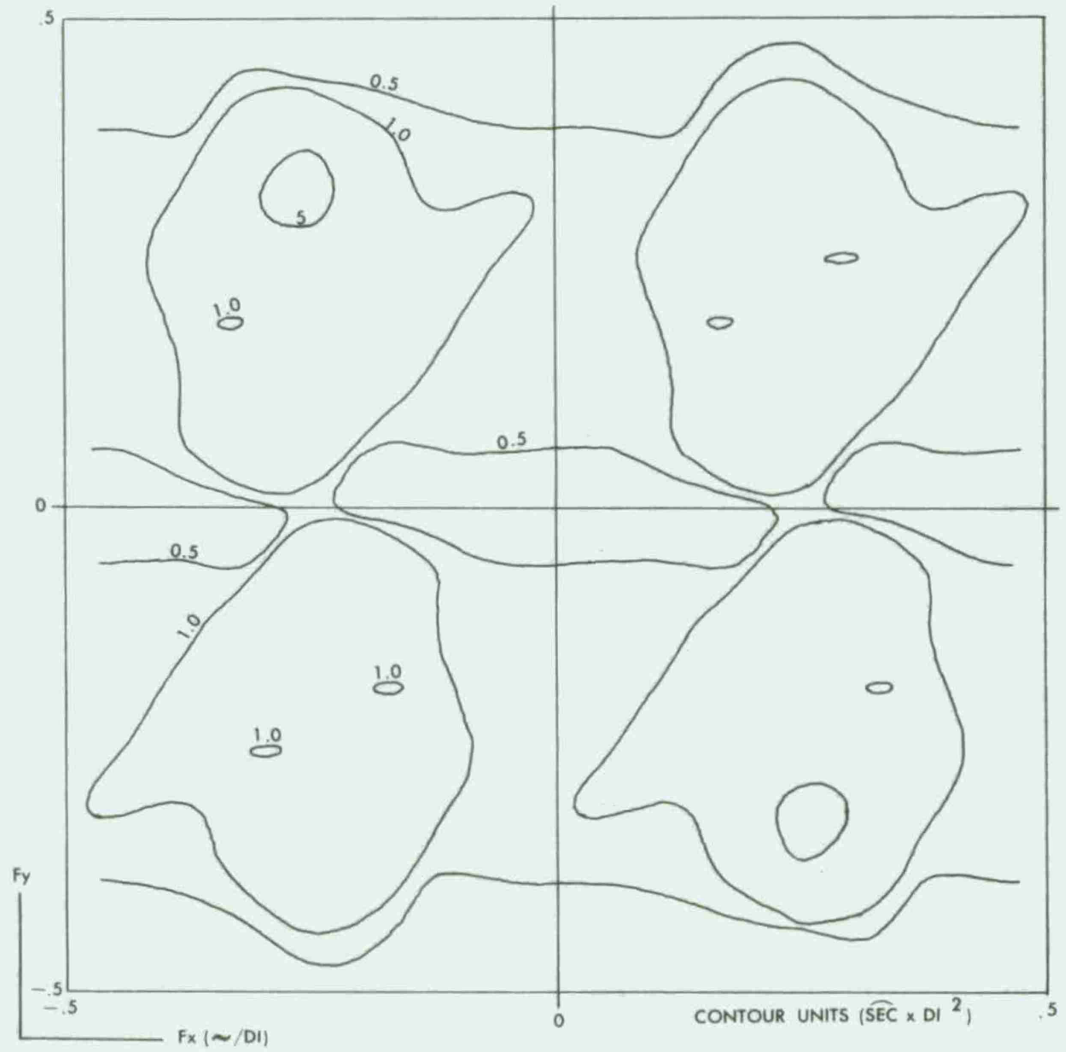

Figure 16. Two-dimensional error spectrum, N-S track spacing=2.0 DI.

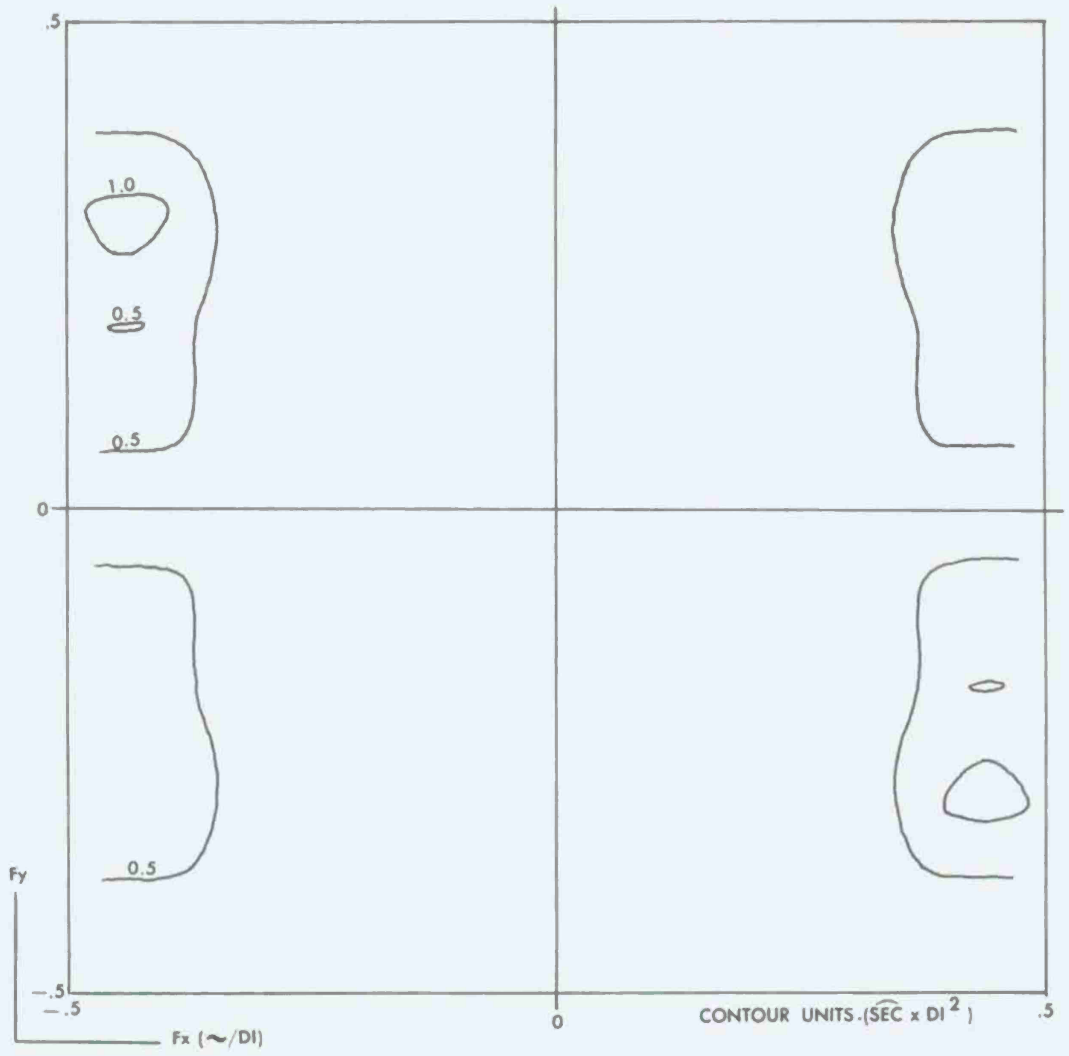

Figure 17. Two-dimensional error spectrum, N-S track spacing=1.14 DI.

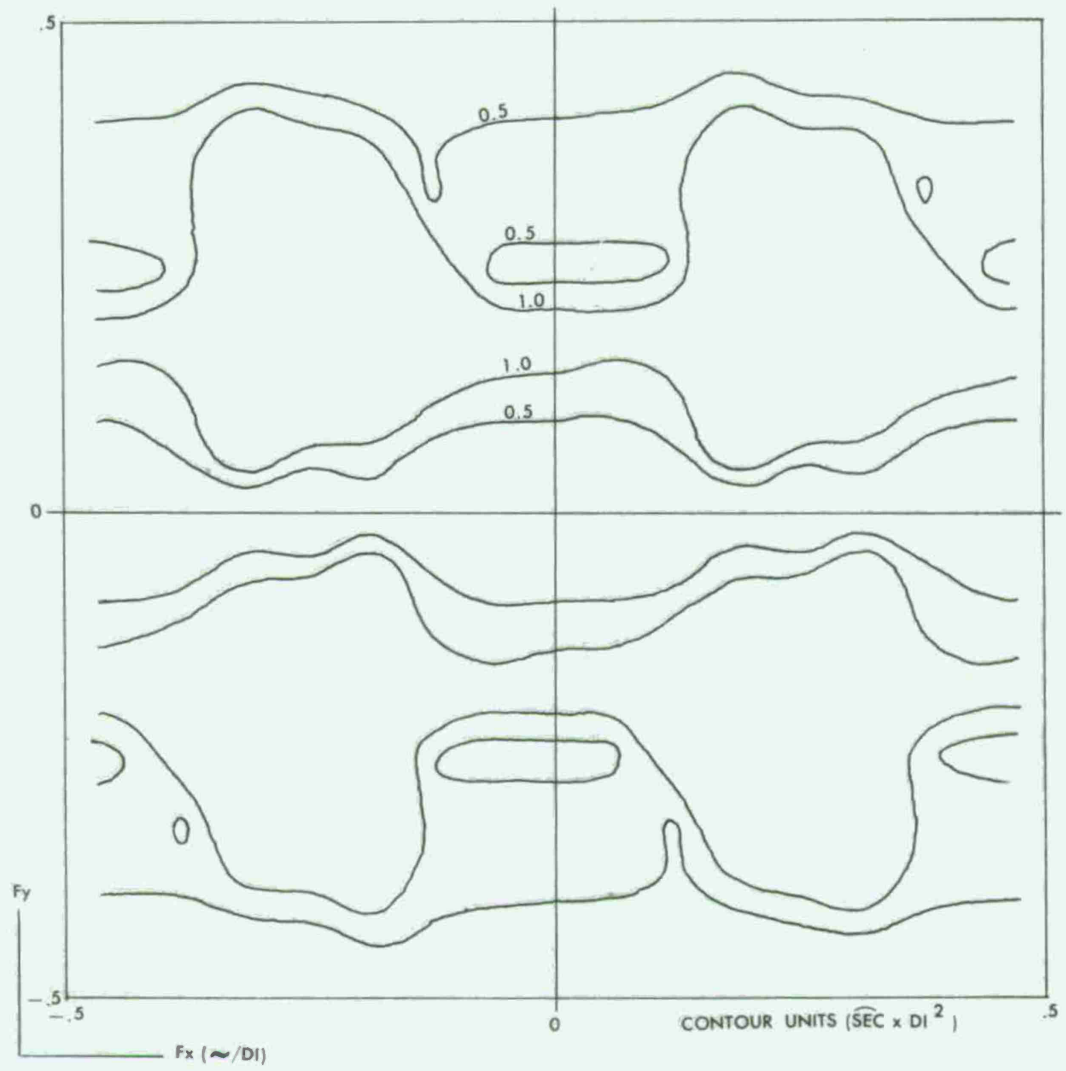

Figure 18. Actual error spectrum for a N-S track spacing of 2.0 DI.

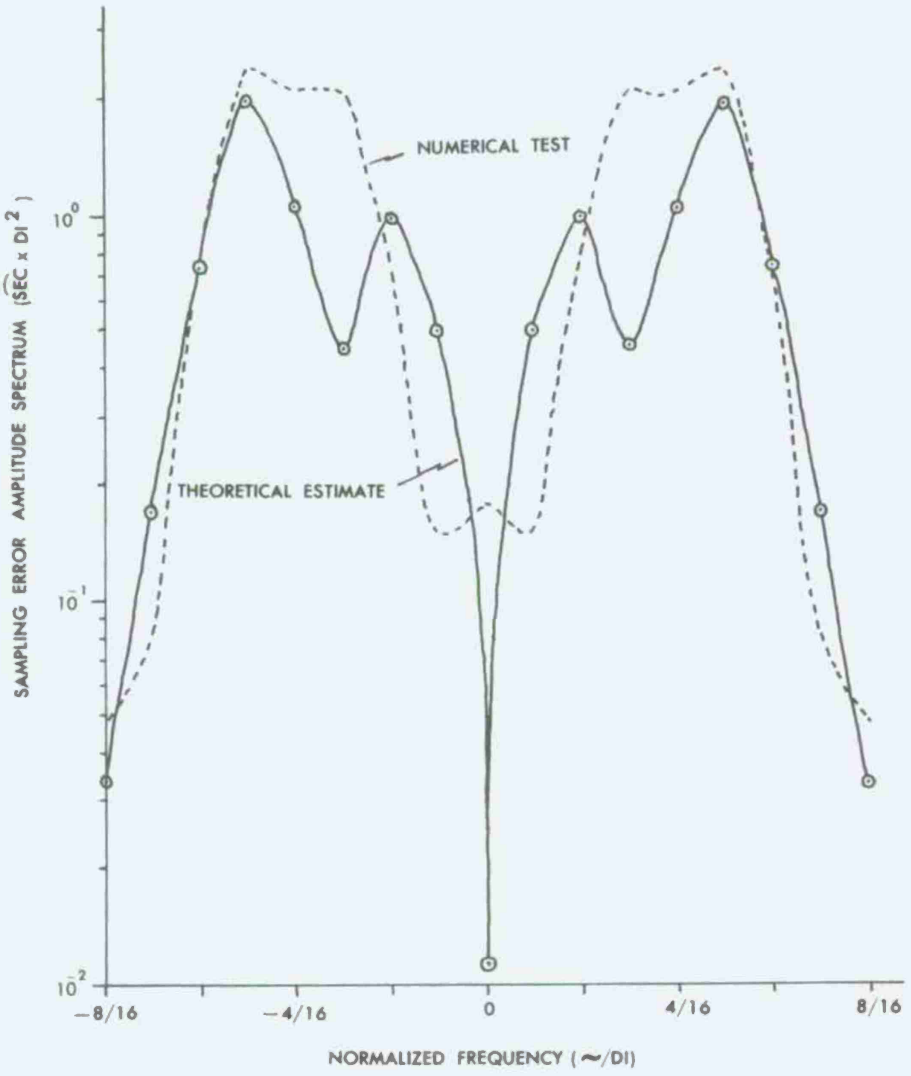

Figure 19. Profile of sampling error spectrum along Fx=Fy from numerical test.

In the practical application of this theory, these base data are obtained by a detailed survey of a small test area located within a large homogeneous province. Since this detailed survey should be designed to adequately sample the base data in all directions, a simple rotation of the geographic direction of the x-y grid will allow the survey design process to be utilized to produce contours of the estimated sampling error as a function of both track spacing and track direction.

Effect of Pre-Filtering on Sampling Error

At first glance, it would appear reasonable that low-pass filtering the digital data collected along survey tracks would be an efficient means of reducing the mean square sampling error. The fact that this is generally not the case may be shown in the following manner.

The two-dimensional filter weight function $W(x,y)$, which represents the application of a one-dimensional digital filter $G(y)$ to the track data assumed parallel to the y axis, is given by $W(x,y) = \delta(x)g(y)$. The two-dimensional Fourier transform of $W(x,y)$ is

$$W(u,v) = \int_{-\infty}^{\infty} \int_{-\infty}^{\infty} \delta(x)g(y)e^{-i(ux+vy)}dxdy = G(v).$$

Figure 20 is a plot of this model. Notice that, although in practice the sampling function $S_T(x,y)$ is applied first and then a one-dimensional filter is applied to this sampled data, this is identical to applying $W(x,y)$ first and then sampling the result. Thus, in this case,

$$D_F(x,y) = [f(x,y)*W(x,y)]\ S_T(x,y) = [f(x,y)S_T(x,y)]*W(x,y), \qquad (9)$$

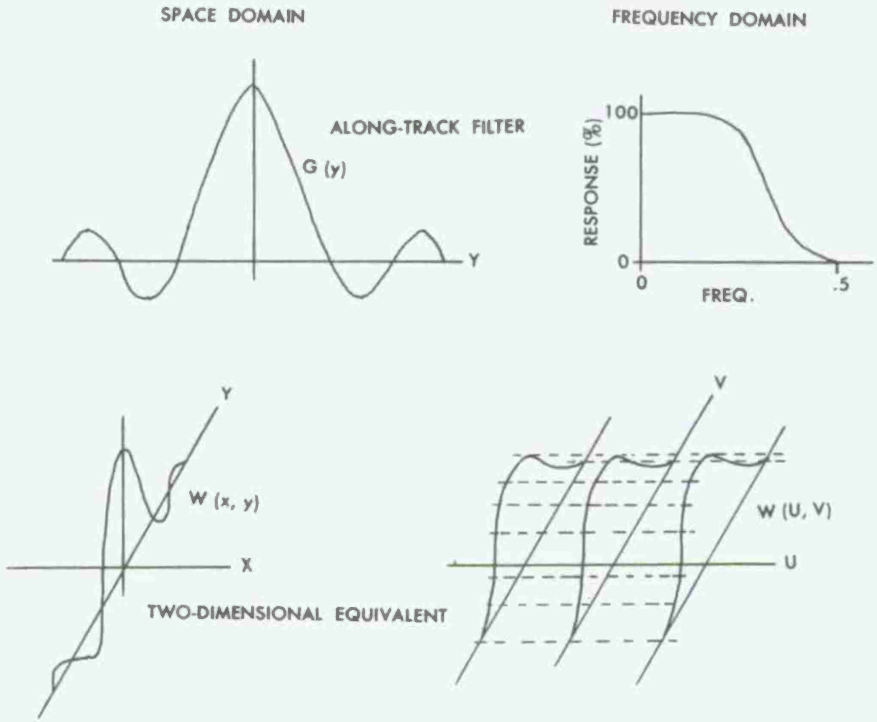

Figure 20. The two-dimensional equivalent of along-track filtering.

where $D_F(x,y)$ is the filtered data. In the frequency domain, the right hand side of equation (9) is equivalent to $[F(u,v)*S_T(u,v)]W(u,v)$. Figure 21 illustrates this operation. It is clear that the net result of pre-filtering the track data is to introduce an error of omission for frequencies in the along-track direction while having no effect on either the error of commission or the error of omission in the cross track direction. For frequencies in other directions, the application of W(u,v) may reduce the sampling error to some extent, but this effect must be evaluated on a case by case basis in order to determine if the net reduction in the error of commission is significant in light of the increase in the error of omission.

The inherent limitation in prefiltering track data by the application of a low-pass filter to the digital data should not be construed to mean that nothing may be done to reduce sampling error. On the contrary, in many practical situations it is possible to exert a considerable amount of control over this error. This control may be accomplished either through the use of the inherent physical properties of the data which are being sampled or through the control of the two-dimensional frequency response of the measuring device. For example, in airborne surveying of magnetic or gravity fields, the natural exponential decay of the two-dimensional spectrum as a function of height above the source (Grant and West, 1965) results in the natural application of a two-dimensional low-pass filter. As the flight elevation is increased, the amplitude of the short wavelength components of the field are reduced. Thus, while the error of omission is increased, the error of commission will be appreciably reduced. This results in a relatively undistorted measurement of the longer wavelength components of the field.

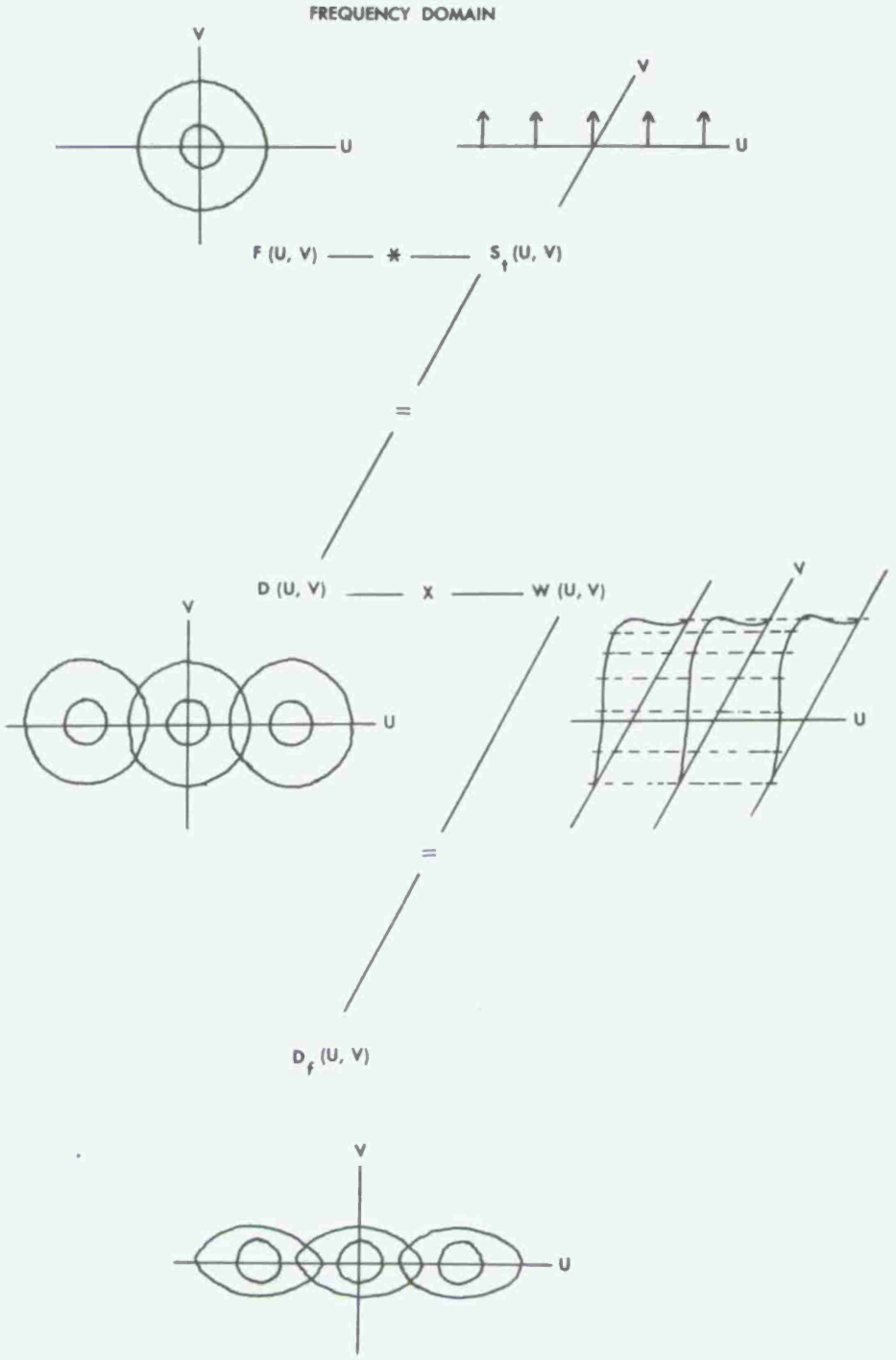

Figure 21. The effect of along-track filtering on sampling error.

An example of the control of sampling error through the design of instrumentation may be found in the measurement of geoid height by the use of a satellite mounted radar altimeter. Adjusting the beam width of the receiver controls the size of the illuminated spot on the sea surface resulting in a two-dimensional filtering operation which reduces the error of commission at the expense of increasing the error of omission.

ALGORITHMS FOR DETERMINING HOMOGENEOUS PROVINCES

The successful practical application of the theory of survey design depends to a great extent upon the accuracy with which the determination of the boundaries of relatively homogeneous provinces may be made. In a statistical sense, a stochastic process is defined as being stationary, in the wide sense, if its mean and autocorrelation function are independent of position (Papoulis, 1962). This is equivalent to requiring that the two-dimensional amplitude or power spectrum be independent of position. It is clear from the preceeding description of the way in which the track sampling model ($S_T(u,v)$) operates on the Fourier transform of the data, that the requirement for stationarity may be somewhat relaxed for survey design. Within this context, a province is defined as homogeneous if the sample data are nearly stationary only for those frequency components that will contribute to sampling error at a particular track spacing.

Even with this relaxation of the requirement for stationarity, a rigid adherence to this definition is not practically feasible since this would require that different province boundaries be defined for each track spacing and each track direction. The particular process which is utilized to define these province boundaries depends upon several factors such as the availability and extent of reconnaissance data and whether the data is basically a function of two-dimensions such as gravity and bathymetry, or three dimensions such as oceanic temperature and salinity. In addition, the appropriate orientation of the survey lines may, in some instances, be controlled by factors other than the local spectral content which is normally used to delineate provinces. One example of this is the effect of errors in the

determination of heading and velocity for computing the Eotvos correction to be applied to shipboard gravity survey data. In this case, the Eotvos correction contains less error if the survey tracks are oriented east-west (Glicken, 1962). The following discussion consists of a detailed description of the numerical algorithms which have been developed for determining the location of the boundaries of homogeneous provinces through the use of reconnaissance data. Fortran IV computer programs are available from the author for implementing each of these algorithms.

Two-Dimensional Fields

In general, the reconnaissance data which are available for delineating provinces for gravity, magnetic, or bathymetric surveys consist of widely spaced tracks of generally random orientation. Since the application of $S_T(u,v)$ results in a replication of the transform of the data in the cross-track direction, it is desirable that a sufficient amount of reconnaissance data, or related geophysical information, be available for determining the general direction of any major lineation of the field. In order to minimize the mean square sampling error, the most efficient orientation of the final survey tracks is in a direction normal to these lineations. This assumes, of course, that there is no overriding constraint on track direction such as that imposed by the Eotvos correction. The object of this province selection process is to outline regions in which short wavelength energy in the cross-track direction is expected to be uniform based on the reconnaissance information.

At the present time, the algorithm which has been developed for

this type of province selection consists of the following steps:

1. Those reconnaissance tracks which are most nearly parallel to the major lineations are selected for analysis. Each of these tracks is separated into relatively straight line segments and, following the procedure of Davis and Kontis (1970), a least-squares straight line is fitted to the positions of the data points in each segment. The actual position of each data value is then mapped onto this straight line and the data value is adjusted by utilizing the local gradient of the field. A cubic spline is then applied to interpolate new data values which are equally spaced in terms of distance down-track. The numerical details, as well as tests indicating the accuracy of this procedure, are given in Davis and Kontis (1970).
2. At this point, a practical decision must be made concerning the maximum track spacing which one would be willing to allow in the final survey design. This decision is based on an estimate of sampling error as a function of sample spacing obtained by applying equations (2) and (3) to a segment of reconnaissance data selected in step (1). This segment of data should be selected to contain a relatively small amount of short wavelength energy. This maximum track spacing defines a folding frequency which is used in conjunction with equations (A-1) and (A-2), shown in Appendix A, to design a high-pass, one-dimensional, digital filter which will pass only those frequencies that will contribute to sampling error.

3. The equally spaced reconnaissance data produced in step (1) are high-pass filtered with the filter designed in step (2), and an approximation to the envelope is computed. The variability of the amplitude of this envelope is used as a practical means for locating the boundaries of stationary data segments.

Although the means for computing a mathematically correct envelope via the frequency domain application of a Hilbert transform (Papoulis, 1962) are available on a large scale computer, an approximation is used here for application to small shipboard computers. This approximation consists simply of computing the absolute value of the high-passed data and applying a low-pass filter with a very low frequency cutoff and a small number of weights to conserve data.

4. In order to generate the locations of the province boundaries from the envelope estimates, two additional decisions must be made at this point. These are:

   A. What is the minimum size, ie. horizontal extent, of a province which one would be willing to accept in terms of modifying the track spacing?

   B. In terms of the envelope of the high-passed data, how much variability will be allowed within a province?

While these are obviously rather arbitrary decisions, in general, the appropriate values of these control parameters usually become apparent after several test runs on the reconnaissance data. As a point of reference, the present

minimum province size selected for shipboard gravity survey design is 32 nautical miles (NM) with an allowable envelope variability of 1.5 mgals.

5. Utilizing the above control parameters, provinces are selected which are of at least minimum size and within which, the envelope variability is within the acceptable range. If reconnaissance tracks are available at various orientations, these steps may be repeated to delineate provinces for any desired orientation of the final survey.

Given these province boundaries estimated from the selected reconnaissance data segments, the final steps in the survey design procedure consist of conducting a detailed, closely-spaced, track-type survey of a small test area within each province and applying the previously defined procedure to obtain the design parameters for each type province. These design parameters, or decision products, consist of the mean square sampling error as a function of track spacing, as well as track direction if appropriate, and the two-dimensional spectral content of the sampling error at selected track spacings. Combining these error estimates with a predetermined accuracy specification results in the final survey design. As a consequence of having available the spectral content of the sampling error, it is possible to accommodate a wide range of accuracy specifications. For example, if an accuracy specification is stated in terms of the allowable mean square sampling error within a particular frequency band, the application of equation (8) to the sampling error spectrum over this restricted frequency band will produce the required estimates of sampling error. Figure 22 is a

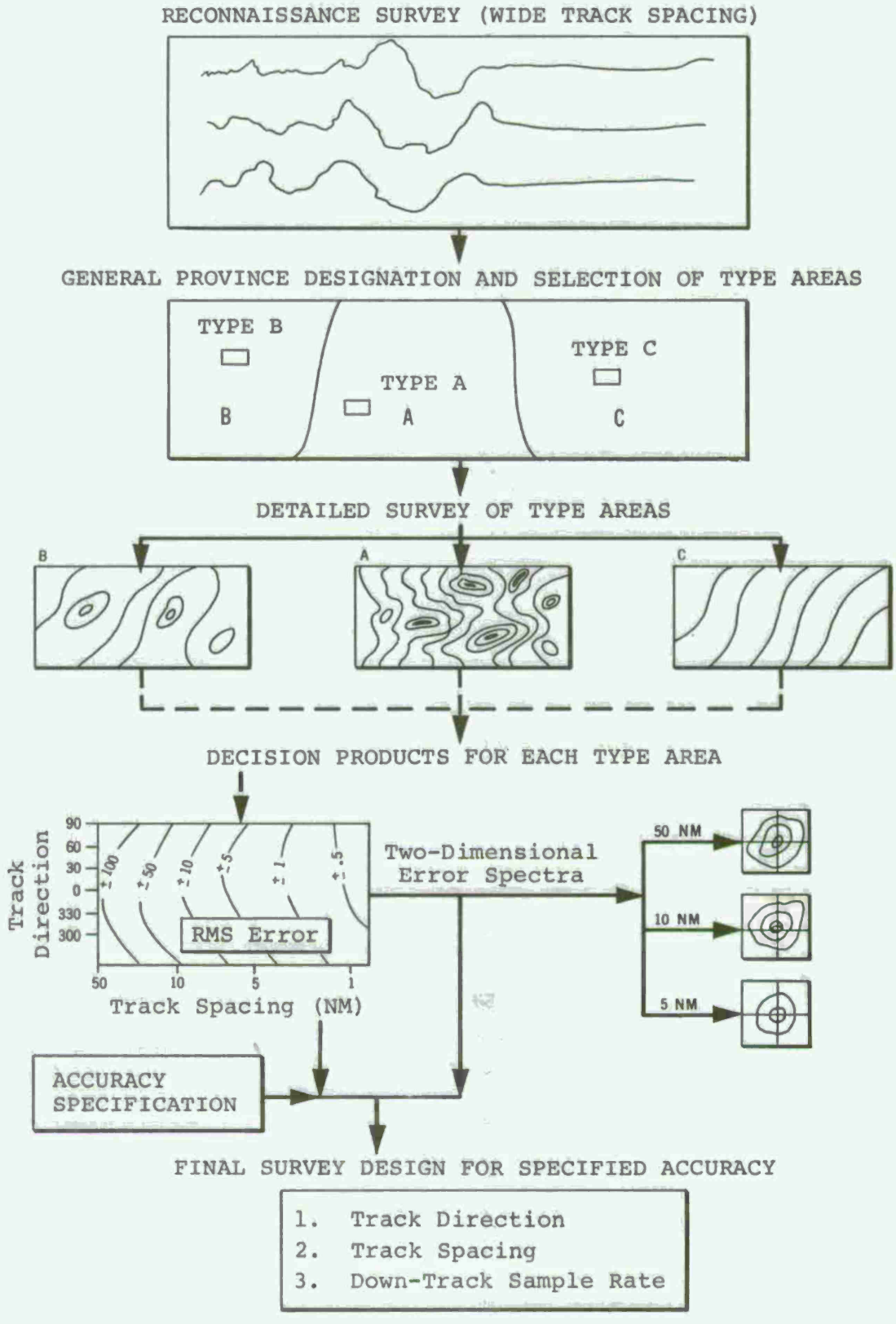

Figure 22. Survey design procedures for two-dimensional fields.

general flow diagram outlining the procedure which is utilized for designing oceanographic surveys of gravity, magnetics, or bathymetry.

One additional point should be made with regard to selecting the proper track spacing for the detailed type area surveys. At the present time, the most appropriate procedure appears to consist of selecting a section of reconnaissance track data which exhibits the greatest magnitude of short wavelength energy within each selected province. A two-dimensional Fourier transform or equivalently, a Hankel transform, is applied to this selected data set which is assumed to possess circular symmetry. This transform is then used with equations (7) and (8) to select a track spacing for the type area survey such that a minimum amount of sampling error will be generated in the type area data.

Three-Dimensional Fields

The process which has been developed for determining the boundaries of homogeneous provinces for three-dimensional fields such as oceanic temperature, salinity, or sound speed is considerably more complex than the two-dimensional case. It should be pointed out that these fields are, in reality, four-dimensional, since, as will be shown in a later example, temporal variability is quite pronounced in some ocean areas. Despite this fact, the present lack of appropriate data restricts the survey design procedure to consider only three dimensions.

As the basis for this process, a generalized procedure has been developed for modeling three-dimensional fields through the utilization of reconnaissance data consisting of randomly spaced vertical profiles. The historical data which are available for models of oceanic

temperature, salinity, and sound speed are processed in the form of a digital data bank by the National Oceanographic Data Center (NODC, 1964). The pertinent information in this data bank consists of the latitude, longitude, and time of each ocean station along with the recorded values of temperature and salinity, and the computed values of sound speed at what are defined as standard oceanographic depths. As a consequence of the large vertical gradients of these fields at the shallower depths, the vertical spacing between samples normally varies as a function of depth. These standard oceanographic depths were determined by the International Association of Physical Oceanography in 1936 (Sverdrup et al, 1942) and are presented in Table (1).

Table 1. Standard Oceanographic Depths

Depth (m)				
10	75	300	800	2000
20	100	400	1000	2500
30	150	500	1200	3000
50	200	600	1500	and every 1000 thereafter

At each standard depth, sound speed is computed via the empirically derived relationship equating sound speed to the measured values of temperature, salinity, and pressure (Wilson, 1960).

Taking sound speed as an example, a primary three-dimensional model is constructed in the following manner. To reduce the effect of

seasonal variations, the station data are separated into appropriately defined winter and summer stations. Working with one vertical profile at a time, a cubic spline interpolation procedure is applied to the sound speed values at the standard depths to generate data values at an equal depth spacing of 50 meters. A seven degree least squares orthogonal polynomial (Van Voorhis and Davis, 1964) is then fitted to these equally spaced profile values over the depth range 200 to 2450 meters. The starting depth of 200 meters was selected because of the high frequency temporal variations which normally occur at the shallower depths. Extensive tests indicate that a seven degree polynomial will generally yield an RMS residual of less than 1 m/sec. This level of residual was selected on the basis of a study by Pickett (1972) which indicates that the error in computed sound speed is within 0.8 to 2.8 m/sec depending on salinity and depth.

Taking the first coefficient of the polynomial thus determined for each profile within a selected area, a two-dimensional gridding algorithm is applied to interpolate the value of this coefficient at equally spaced grid points. As a consequence of the paucity of existing data, the grid spacing for sound speed is presently selected to be 30 minutes of latitude x 30 minutes of longitude. This two-dimensional gridding algorithm, which was developed by Rankin (1974), is essentially a three phase algorithm consisting of local averaging, distance weighting (Shepard, 1968), and cubic spline interpolation. Applying this interpolation procedure to each of the eight polynomial coefficients derived at each station produces a set of eight coefficient surfaces which comprise the primary three-dimensional sound speed model.

In order to develop province boundaries from this numerical model,

a two-dimensional low-pass filter is applied to the gridded coefficient surfaces for degree one through four. The weight function for this filter is derived from equation (A-3) of Appendix A with a K_c of 100 data intervals and a K_T of 5 data intervals. For a 30x30 minute grid spacing, this produces a filter which effectively removes wavelengths shorter than 2.5 degrees of latitude or longitude, thus reducing the effect of steep local horizontal gradients in the coefficient surfaces. These local gradients are normally generated by short term temporal variations occurring at closely spaced stations, or by erroneous data. By restricting the two-dimensional frequency content of the polynomial surfaces in this way, the province boundaries are defined on more of a regional basis than on a local basis. Only the degree one through four coefficient surfaces are used to define the sound speed province boundaries since these have been found to account for most of the variability in acoustic propagation over this depth range.

The next step in the process consists of applying a two-dimensional bicubic spline (Davis and Kontis, 1970) to each of the filtered coefficient surfaces in order to determine the partial derivatives $(\frac{\partial \phi}{\partial x}, \frac{\partial \phi}{\partial y})$, and the magnitude of the gradient at each grid point. As was the case for provinces defined for two-dimensional fields, a decision must be made as to the minimum acceptable size of a province. Utilizing this minimum province size, an appropriate magnitude of the gradient is selected from the contoured gradient values to define the province boundaries for each coefficient surface. A composite of these four boundary charts produces the final estimates of what are defined as secondary province boundaries for survey design. Figure 23 is a general flow diagram for this province selection algorithm.

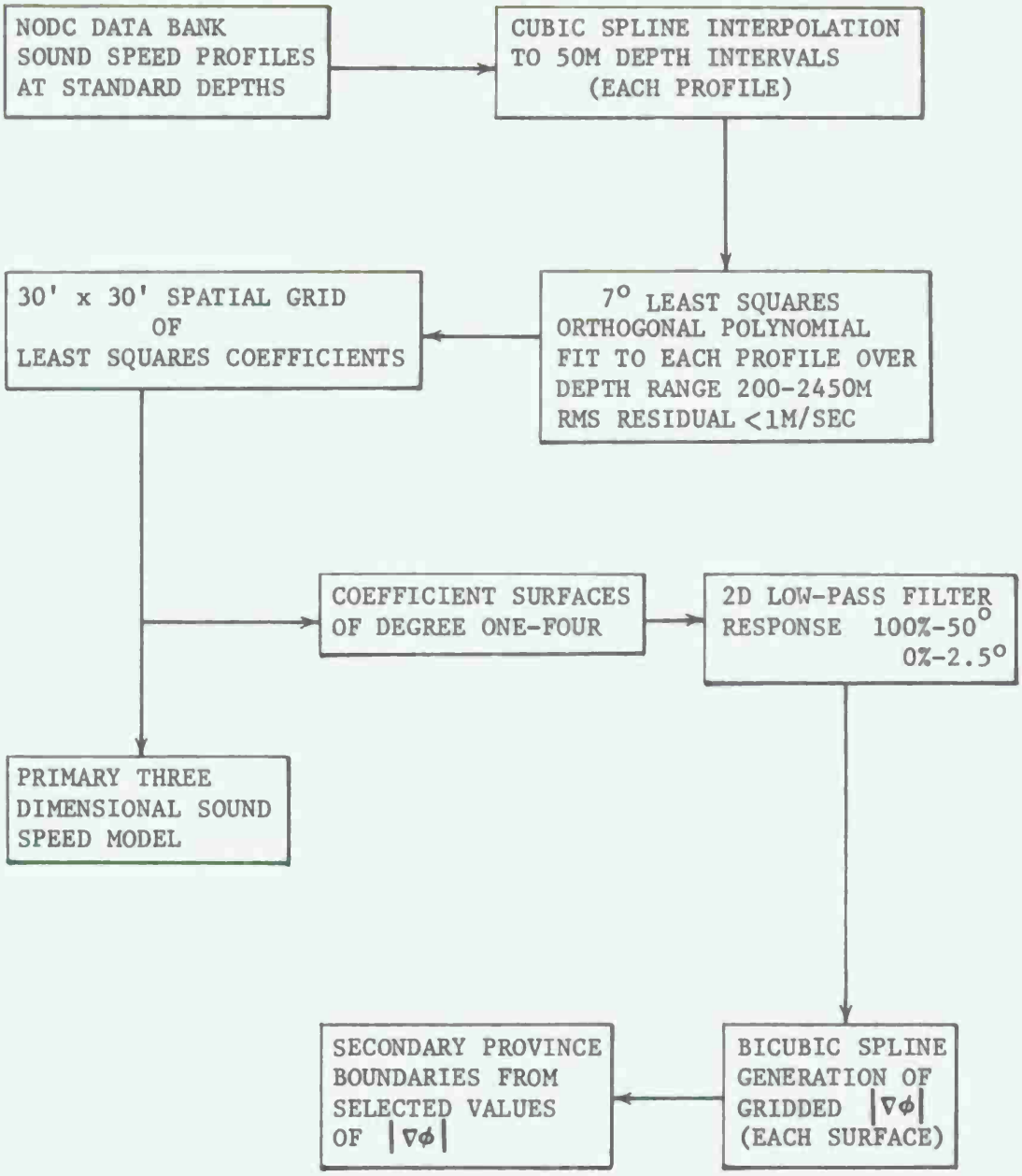

Figure 23. Algorithm for defining sound speed province boundaries.

In summary, the present technique for selecting province boundaries for the three-dimensional oceanic fields is based on locating those areas in which the overall character of a vertical profile changes abruptly in the horizontal direction. This is in contrast to the two-dimensional case in which the province boundaries are defined by a prescribed change in the magnitude of the high frequency spectral content.

PRACTICAL APPLICATIONS

Several practical applications are presented in order to demonstrate the adaptability of the preceeding theory of survey design, and the efficiency with which the two-dimensional frequency domain representation of sampling error may be propagated through various linear operations.

The application of survey design to hydrographic surveying illustrates the utilization of a one-dimensional modification of the two-dimensional theory for use with small scale computers in near real-time. This modification is possible if the appropriate orientation of the survey tracks is known a priori, and the desired accuracy specification is in terms of a broad-band mean square or RMS error rather than the spectral content of the error.

The application of the two-dimensional theory to the design of gravity surveys for computing vertical deflection and geoid undulation was selected to illustrate one of the more intriguing and useful aspects of the theory. In this application, the desired accuracy specification is stated in terms of both a broad band mean square error, and the two-dimensional spectral content of the error in geoid undulation as well as the error in the north and east components of vertical deflection. The procedure for satisfying this type of specification consists of propagating the two-dimensional spectrum of the sampling error generated by the basic gravity survey through the linear operations required for computing undulation and deflection components. This application of the survey design theory illustrates the accuracy and inherent efficiency of this frequency domain procedure as well as the effect of regional lineations on sampling error.

The application of the two-dimensional survey design theory to three-dimensional fields is illustrated by an example of a survey design for oceanic sound speed. This application also illustrates the facility with which this sampling theory may be adapted to provide a very useful estimate of the sampling error as a function of depth.

One final practical application of the two-dimensional theory illustrates the effect of sampling error on a classical problem of geophysical interpretation. This example was specifically designed to show that an apparently insignificant amount of sampling error can severely influence an interpretation if the interpretation technique is sensitive to the high-frequency components of the anomalous field.

Near Real-Time Hydrographic Survey Design

At the present time, the U. S. Naval Oceanographic Office is in the process of developing a high-speed hydrographic survey and charting system (HYSURCH) for defining the topography of the ocean bottom in shallow coastal areas. This automated system is designed to enable the Navy to rapidly and economically conduct hydrographic surveys to a predetermined accuracy as well as on-site data evaluation and automated field production of contour charts. The basis for the economy of this approach is the near real-time application of survey design procedures in the following manner.

Figure 24 shows the general concept which is essentially a one-dimensional modification of the two-dimensional sampling theory developed for the design of gravity, magnetic, and deep ocean bathymetric surveys. The major regional trends of the field normally are parallel to the coastline. On this basis, the appropriate direction of

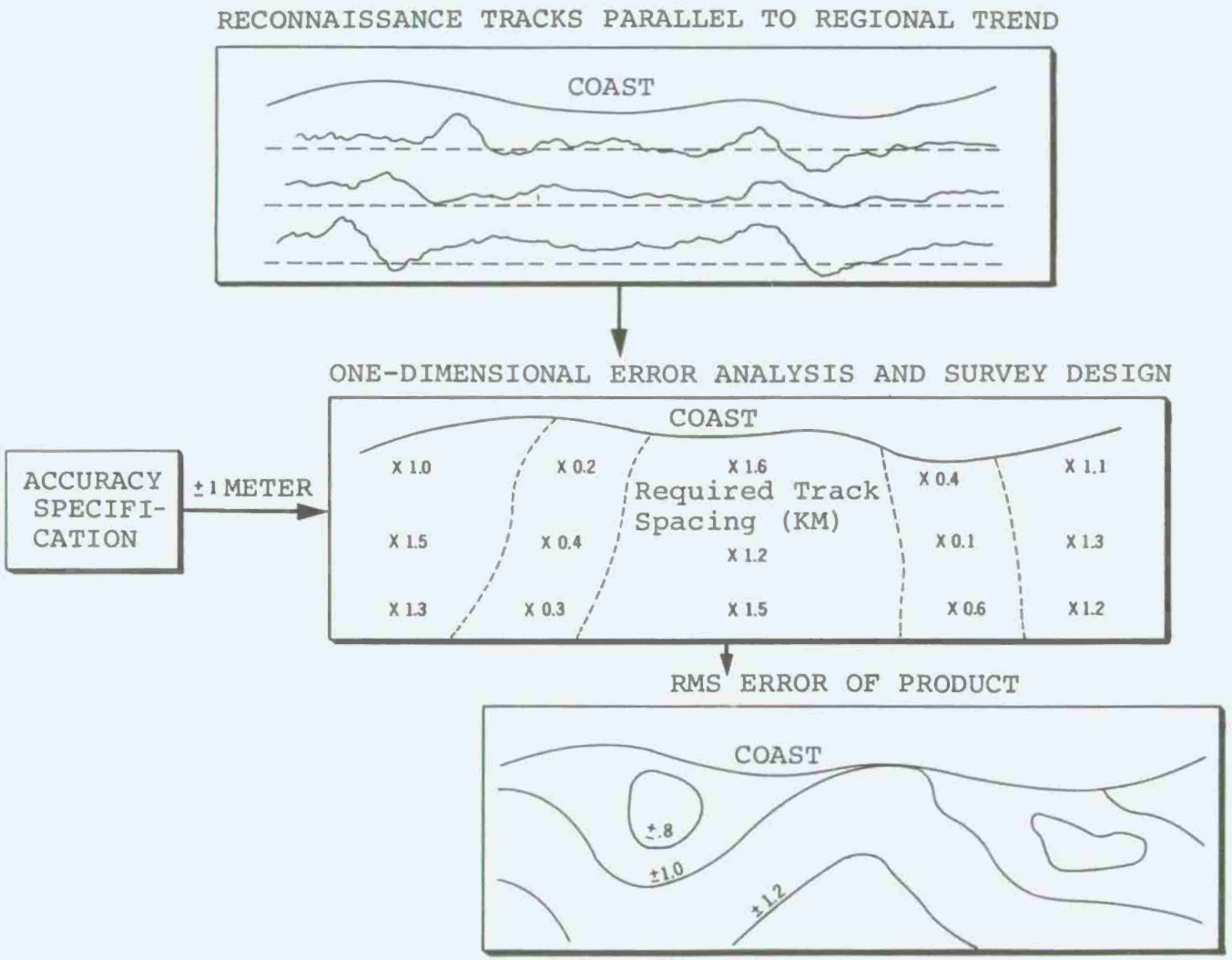

Figure 24. Near real-time hydrographic survey design (HYSURCH).

the survey tracks is normal to the coastline. With this constraint on the survey orientation, data are collected along reconnaissance lines run generally parallel to the coastline. The digital data collected along these lines is then used to define the locations of homogeneous province boundaries utilizing the algorithm developed for application to two-dimensional fields.

A one-dimensional Fourier transform is applied to the data within each of these selected provinces for each of the available reconnaissance tracks. With these spectral estimates, equations (3) and (4) are numerically evaluated to obtain an estimate of the sampling error as a function of sample spacing. Since the actual survey tracks will be oriented normal to these reconnaissance lines, this sampling error is, in reality, a function of the survey track spacing. Given a required survey accuracy specification, the appropriate sample/track spacing is selected for each defined province and the final survey is completed using the average specified track spacing for each area.

At the conclusion of the survey operation, the track data are examined to determine if any significant provinces were missed by the preliminary reconnaissance tracks. In this case, additional short survey lines will be run as necessary and the sampling error will be estimated at the actual track spacing achieved within each of these additional provinces.

Figure 25 is an example of a test of the province selection process applied to survey data collected along one reconnaissance track. The lower curve is a plot of the original sounding data collected at five-meter intervals along the track. The upper curve is a plot of the original data after high-pass filtering with a frequency response set to

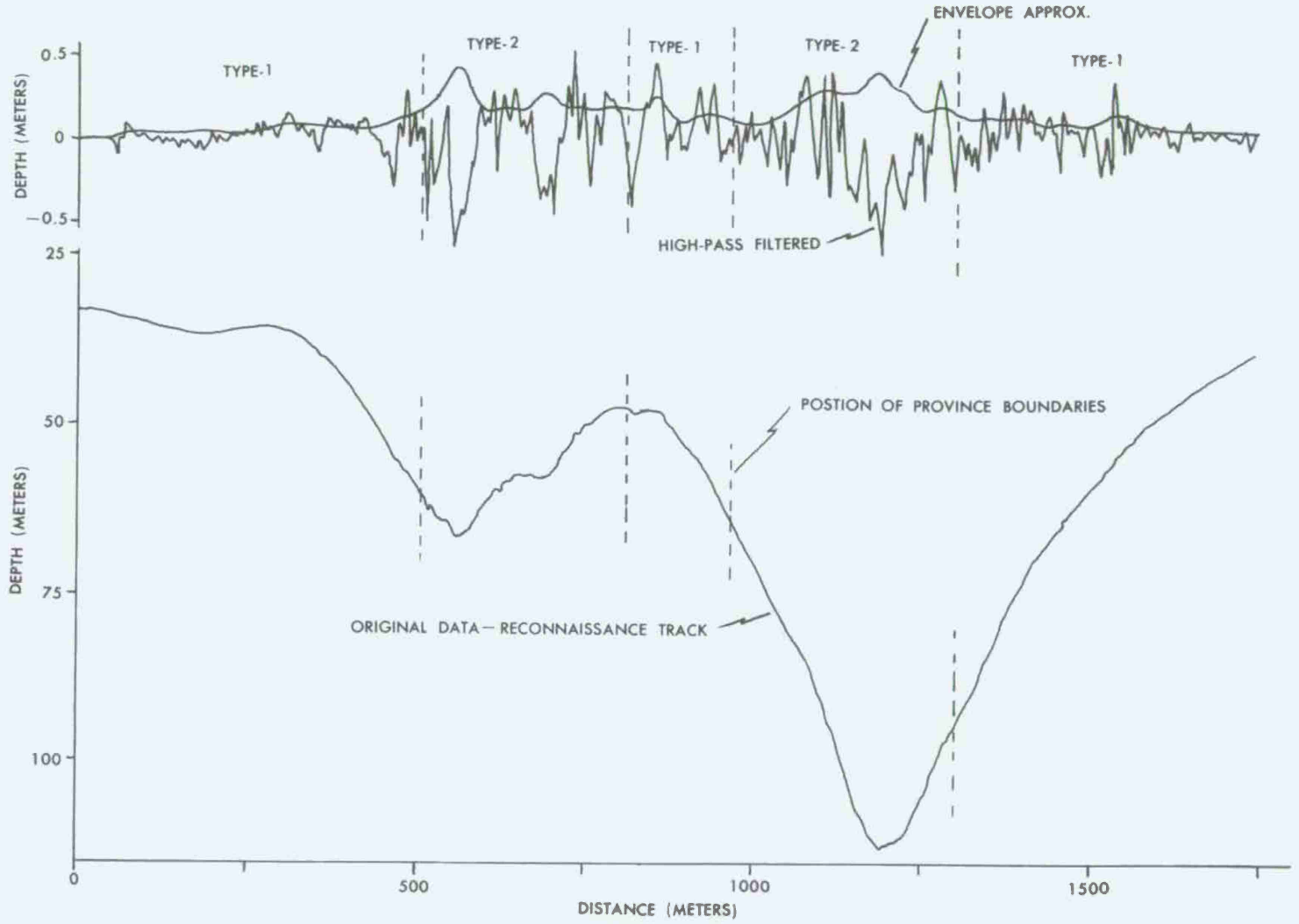

Figure 25. Example of HYSURCH province selection process.

pass spectral components which would contribute to the sampling error at a maximum allowable track spacing of 2000 meters. A plot of the approximation to the envelope of this high frequency energy is also shown. Selecting a minimum province size of 160 meters in the horizontal dimension, and a maximum variability of the envelope within a province of 0.2 meters, the province selection algorithm produced positions for the province boundaries as shown by the dashed lines. On this particular test, there were three type-one provinces selected with envelope amplitudes within the range 0-0.2 meters, and two type-two provinces with amplitudes in the range 0.2-0.4 meters. Figure 26 is a plot of the estimated RMS of the sampling error as a function of sample/track spacing for the first province type one segment. The geographic coordinates, in x-y units, of this province are also noted. Figure 27 shows the relationship which exists, for this data set, between the FFT amplitude spectrum computed on the raw data without window modification or prewhitening, the spectrum of the prewhitened data, the rough spectrum corrected for the prewhitening operation, and the final smoothed corrected spectrum. As was the case for the gravity example shown in Figure 3, the requirement for prewhitening is readily apparent.

Survey Design for Vertical Deflection and Geoid Undulation

In this example, the requirement is to design a track-type survey operation to produce products of a specified accuracy in which the accuracy requirement is placed not on the data actually being collected, but upon two quantities (vertical deflection and geoid undulation)

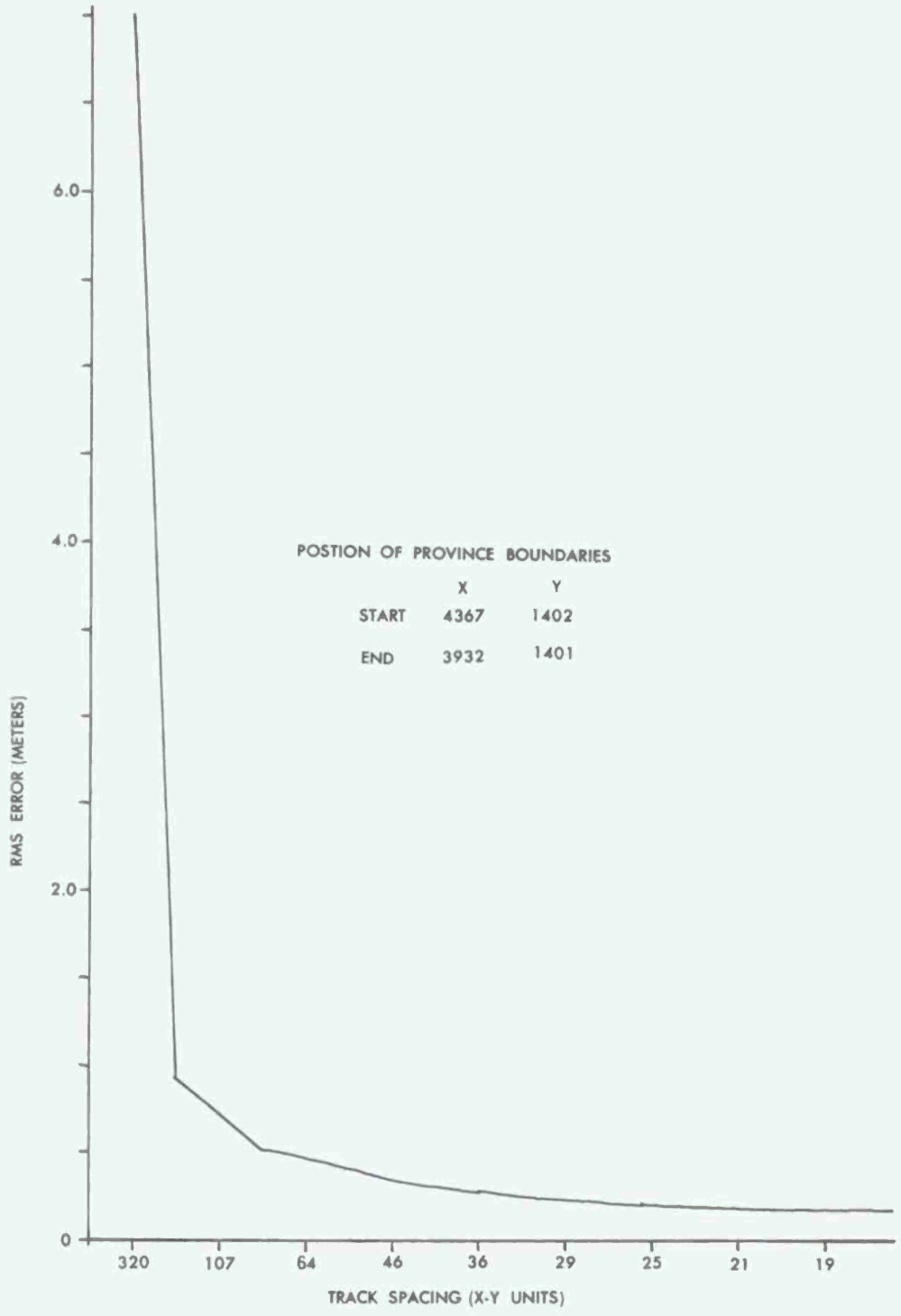

Figure 26. Sampling error vs. sample/track spacing for first province segment.

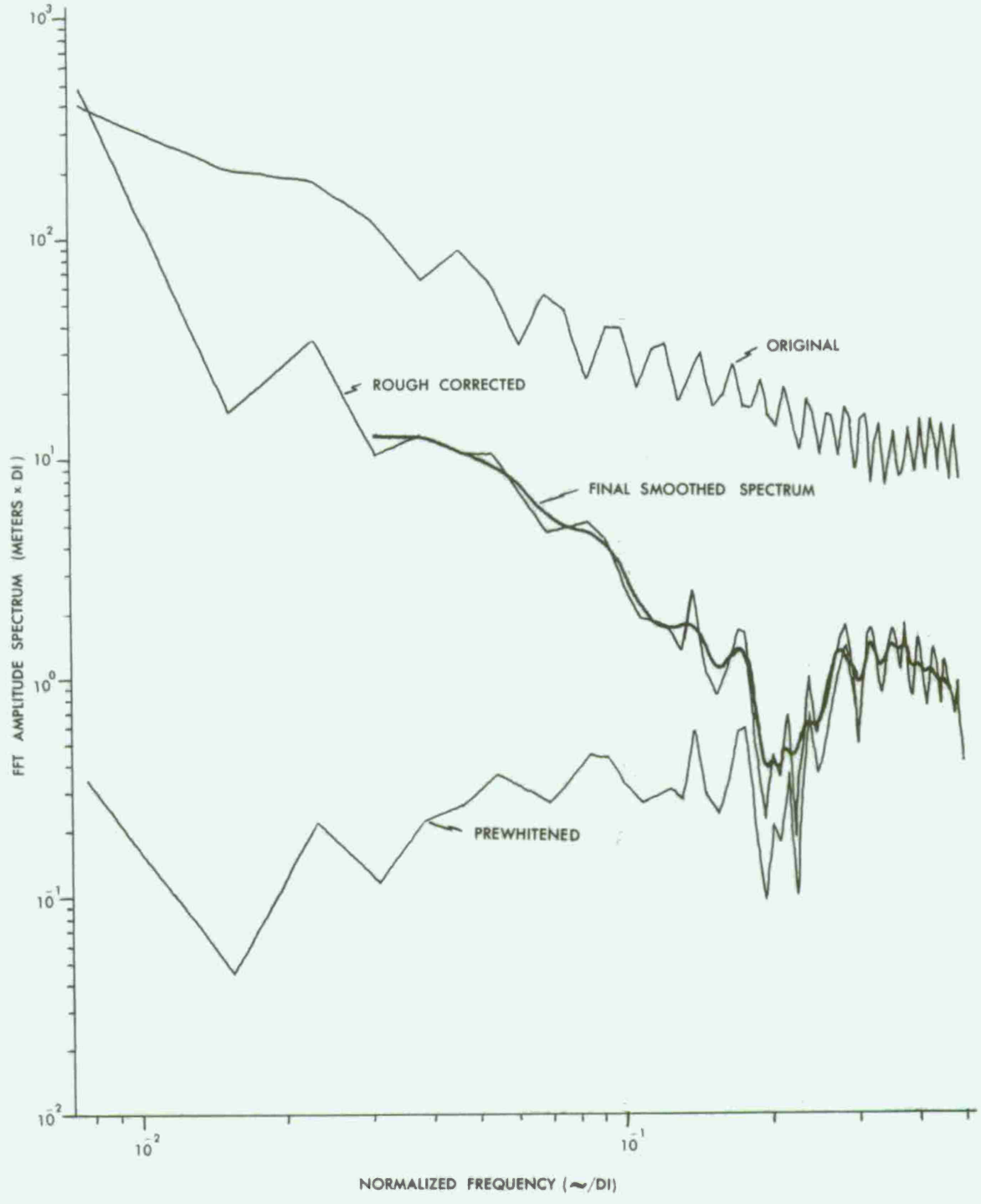

Figure 27. Amplitude spectrum of data from first province segment.

computed from these data. In addition, although the overall broad-band mean square sampling error is of general interest, particular emphasis is placed on estimating the two-dimensional spectral content of the sampling error in order to provide a means for determining the mean square error of the computed quantities within a specified frequency band.

At the present time, the vast majority of existing values of vertical deflection and geoid undulation are computed utilizing worldwide measurements of the earth's gravity field and the mathematical techniques of physical geodesy. Deflection of the vertical is defined, at a point, as the angular difference between the normal to an equipotential surface of the earth's gravity field, and the normal to a smooth mathematically defined reference ellipsoid having the same potential (Heiskanen and Moritz, 1967). This vertical deflection is normally computed in terms of a north-south component (ξ) and an east-west component (η). The geoid undulation is defined as the distance between these two equipotential surfaces measured along a line normal to the reference ellipsoid.

In order to compute geoid undulation and the components of vertical deflection from measurements of the gravity field, Stokes integral (Heiskanen and Moritz, 1967) is numerically solved to produce the undulation estimate, and the Vening Meinesz integral (Vening Meinesz, 1928) is utilized to produce the values of the vertical deflection components. In each of these integrals, the integrand is infinite at the origin of the computation system which is centered over the point at which the deflection or undulation estimate is desired. This presents some numerical difficulties which require special techniques in order to evaluate

this so-called inner-zone contribution (Kontis, et al, 1974). Excluding this inner-zone of some radius ψ_o, the Vening Meinesz integral in spherical polar coordinates (R,ψ,α) (Figure 28) is

$$\begin{bmatrix}\xi_p \\ \eta_p\end{bmatrix} = \frac{\csc 1''}{2\pi\gamma R^2} \int_{\psi=\psi_o}^{\pi} \int_{\alpha=o}^{2\pi} \Delta g(\psi,\alpha)\ V(\psi) \begin{bmatrix}\cos\alpha \\ \sin\alpha\end{bmatrix} R^2 \sin\psi d\psi d\alpha, \qquad (10)$$

where ξ_p and η_p are the north and east deflection components, in $\widehat{sec}$, at the computation point, p, γ is the mean value of the earth's gravity field, ψ is the angular distance between the radius vector to p and a surface element of area $R^2 \sin\psi d\psi d\alpha$, R is the mean radius of the earth, and α is the azimuth, measured from north, of the surface element relative to p. $\Delta g(\psi,\alpha)$ is the mean value of free-air gravity in each surface element, and $V(\psi)$ is the Vening Meinesz function given by

$$V(\psi) = \frac{1}{2}\left[\frac{-\cos\psi/2}{2\sin^2\psi/2} - 6\cos\psi/2 + 8\sin\psi + 3\sin\psi \ln(\sin^2\psi/2+\sin\psi/2) - \frac{3(1-\sin(\psi/2))}{\sin\psi}\right]$$

Utilizing the same system of spherical polar coordinates, and exluding the inner-zone, the Stokes integral for computing undulation (N_p) is

$$N_p = \frac{1}{2\pi\gamma R} \int_{\psi=\psi_o}^{\pi} \int_{\alpha=o}^{\pi} \Delta g(\psi,\alpha) S(\psi) R^2 \sin\psi d\psi d\alpha, \qquad (11)$$

where $S(\psi)$ is the Stokes function given by

$$S(\psi) = \frac{1}{2}\left[\frac{1}{\sin\psi/2} - 6\sin\frac{\psi}{2} + 1 - 5\cos\psi - 3\cos\psi\ln(\sin^2\psi/2+\sin\psi/2)\right].$$

Since the magnitude of both $V(\psi)$ and $S(\psi)$ decreases rapidly as ψ

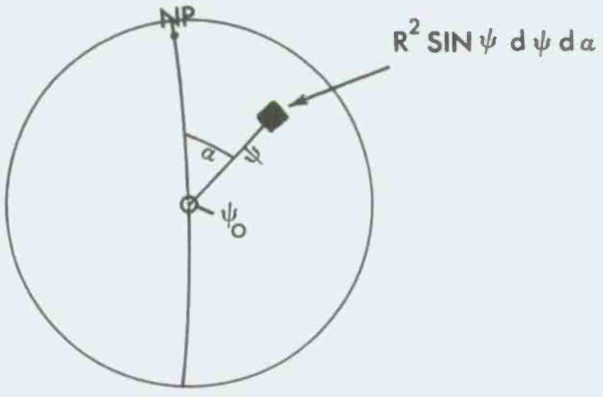

Figure 28. Spherical polar coordinate system.

increases, the gravity field close to the computation point has a much larger effect on the computed undulation and deflection than does the gravity field at greater distances. As a result, as the computation point (p) is moved about to obtain a closely spaced grid of computed values, the high frequency spectral components of deflection and undulation are generated primarily by the local short wavelength components of the gravity field. As a consequence, both $V(\psi)$ and $S(\psi)$ may be approximated locally by the so-called flat-earth approximation (Heiskanen and Moritz, 1967). This approximation for $V(\psi)$ may be derived as follows. On a sphere of radius R, the arc distance between any two points is $R\,\psi$. For large R and small ψ, the arc distance may be approximated by the linear distance r and the spherical surface may be approximated by a plane. For small ψ, the first term in $V(\psi)$ is dominant so that

$$V(\psi) \approx -\frac{\cos \psi/2}{4 \sin^2 \psi/2} \approx \frac{-1}{\psi^2} \approx -\left(\frac{R}{r}\right)^2 .$$

With the element of surface area on the plane given by $rdrd\alpha$, the flat-earth approximation to equation (10) is given by

$$\begin{bmatrix} \xi_p \\ \eta_p \end{bmatrix} \approx \frac{-\csc 1''}{2\pi\gamma} \int_r \int_\alpha \frac{\Delta g(r,\alpha)}{r^2} \begin{bmatrix} \cos\alpha \\ \sin\alpha \end{bmatrix} rdrd\alpha .$$

In cartesian coordinates, with y directed north-south, $rdrd\alpha = dxdy$, $\cos\alpha = \frac{y}{r}$, $\sin\alpha = \frac{x}{r}$, and

$$\begin{bmatrix} \xi_p \\ \eta_p \end{bmatrix} \approx \frac{-\csc 1''}{2\pi\gamma} \int_x \int_y \frac{\Delta g(x,y)}{r^3} \begin{bmatrix} y \\ x \end{bmatrix} dxdy \qquad (12)$$

where $r = \sqrt{x^2+y^2}$.

In a similar manner, (Heiskanen and Moritz, 1967) a flat earth approximation may be derived for geoid undulation. This approximation, in polar coordinates, is given by

$$N_p \approx \frac{1}{2\pi\gamma} \int_r \int_\alpha \frac{\Delta g(r,\alpha)}{r} \, r dr d\alpha \text{ or, in cartesian}$$

coordinates, by $N_p \approx \frac{1}{2\pi\gamma} \int_x \int_y \frac{\Delta g(x,y)}{r} \, dxdy$ (13)

It is apparent that, as the location of the computation point (P) is varied, both equations (12) and (13) describe a two-dimensional cross-correlation process between the free-air gravity observations and the two-dimensional operators $\frac{y}{r^3}$, $\frac{x}{r^3}$, and $\frac{1}{r}$. This observation has been utilized as the basis for a very efficient algorithm for computing deflection and undulation in a large scale production operation (Michlik, 1973).

This process is more readily applicable to the survey design problem when the cross-correlation is converted into a two-dimensional convolution. This is simply accomplished by observing that the ξ operator $(\frac{y}{r^3})$ and the η operator $(\frac{x}{r^3})$ are both even functions with respect to one coordinate axis and odd with respect to the other, and that the undulation operator $(\frac{1}{r})$ possesses circular symmetry. Thus, equation (12) may be changed to a convolution operation by simply changing the sign and equation (13) requires no modification. In this form, the convolution theorem (Bracewell, 1965) may be used with the Fourier transform of these operators to convert the two-dimensional sampling error spectrum of the gravity survey data into the sampling error spectra for undulation and the vertical deflection components. Application of this process, along with the solution of the

two-dimensional form of Parseval's relationship, results in a straightforward design of a gravity survey which will produce a specified error in the geoid undulation and the components of vertical deflection.

The two-dimensional Fourier transform of the deflection operators have been developed by Shaw et al (1969) and are given by

$$\xi_o(f_x,f_y) = \frac{i \csc 1''}{\gamma}\left[\frac{f_y}{(f_x^2+f_y^2)^{1/2}}\right] \tag{14}$$

and

$$\eta_o(f_x,f_y) = \frac{i \csc 1''}{\gamma}\left[\frac{f_x}{(f_x^2+f_y^2)^{1/2}}\right]. \tag{15}$$

A contour of the first quadrant of $\eta_o(f_x,f_y)$ is shown in Figure 29. A 90 degree rotation of the axes in Figure 29 produces a contour of the second quadrant of $\xi_o(f_x,f_y)$. Since the geoid undulation operator possesses circular symmetry, the two-dimensional Fourier transform reduces to a Hankel transform (Bracewell, 1965). Thus, with $N_o(x,y) = \frac{1}{2\pi\gamma r}$, then

$$N_o(u,v) = 2\pi\int_o^\infty \frac{rJ_o}{2\pi\gamma r}\left[r(u^2+v^2)^{1/2}\right]dr$$

$$= \frac{1}{\gamma}\int_o^\infty J_o\left[r(u^2+v^2)^{1/2}\right]dr$$

$$= \frac{1}{\gamma(u^2+v^2)^{1/2}} \quad \text{(Gradshteyn and Ryzhik, 1965)}$$

or, converting to normalized frequency,

$$N_o(f_x,f_y) = \frac{K}{2\pi\gamma(f_x^2+f_y^2)^{1/2}} \tag{16}$$

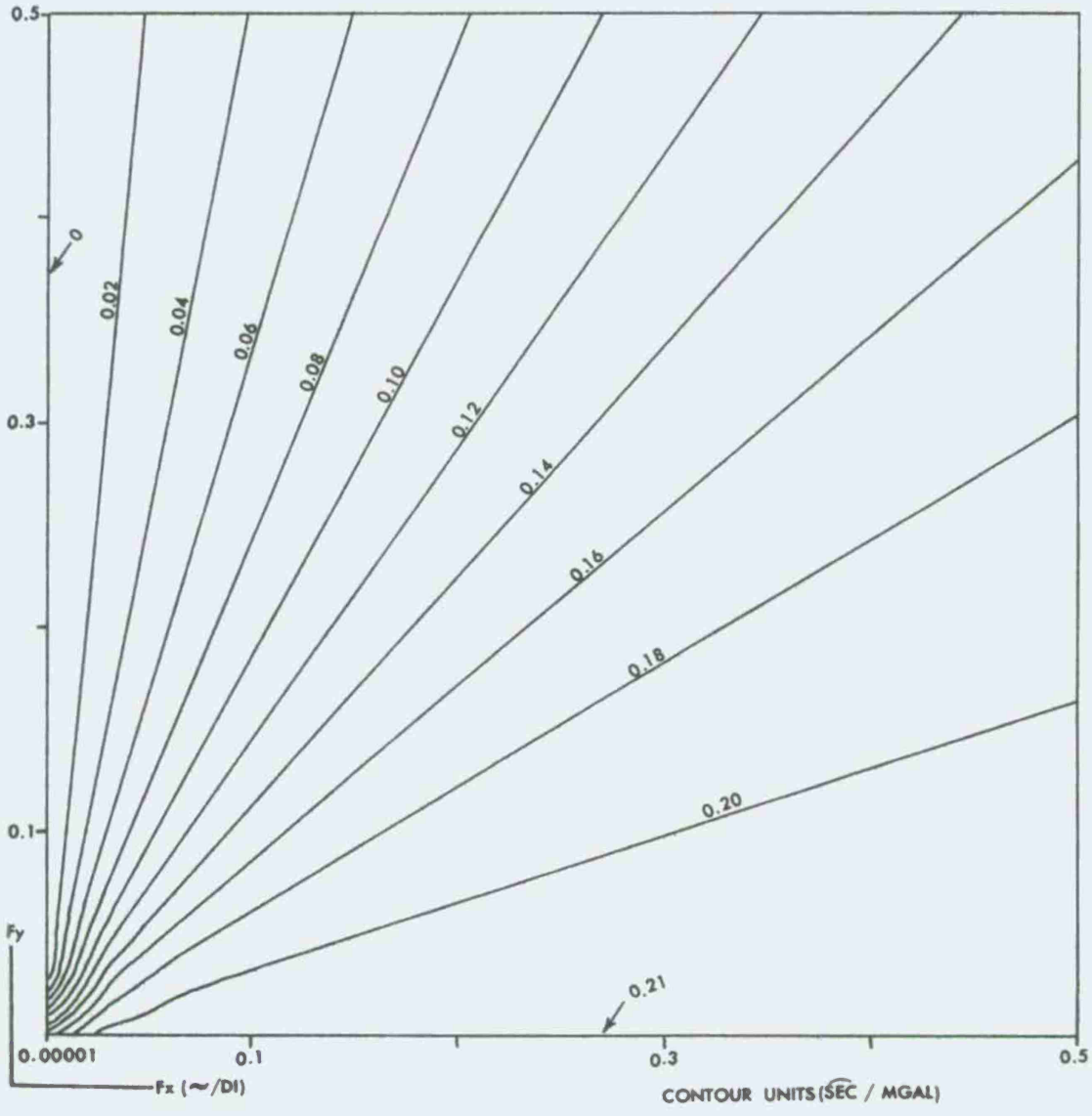

Figure 29. First quadrant of two-dimensional frequency response of the ETA operator.

where K is the length of a data interval in meters.

As an illustration of the accuracy of the flat-earth approximations and, consequently, the accuracy of the spectral domain conversion of the sampling error in the gravity field to error in undulation and deflection components, a theoretical gravity reference surface was developed from a distribution of 16 point masses. The formulation for this process is given in Davis and Kontis, 1970. Figure 30 is a contour chart of this reference gravity field at a contour interval of 5 mgals. The gravity field was computed on a one minute grid covering the entire 80x80 minute area. In addition, the magnitude and direction of the anomalous gravity vector was utilized to compute the ξ and η deflection components at each grid point. Bruns formula (Heiskanen and Moritz, 1967), together with the values for the anomalous potential, was used to determine the undulation reference surface.

Figure 31 is a contour chart of the appropriately prewhitened and corrected two-dimensional amplitude spectrum of this gravity model field. Figures 32-34 are contour charts of the actual two-dimensional amplitude spectra for the gridded ξ, η and N reference model surfaces. Figures 35-37 were generated by applying the frequency responses of the flat-earth operators directly to the two-dimensional spectrum of the reference gravity field. Except for the high frequency roundoff error on the computed undulation reference surface, the accuracy of the flat-earth approximation at these short wavelengths is readily apparent.

In order to illustrate the effect of survey track direction and the utility of these frequency domain operations, these procedures were applied to observed free-air gravity data collected in a small test area from a detailed shipboard survey operation. Figure 38 is a

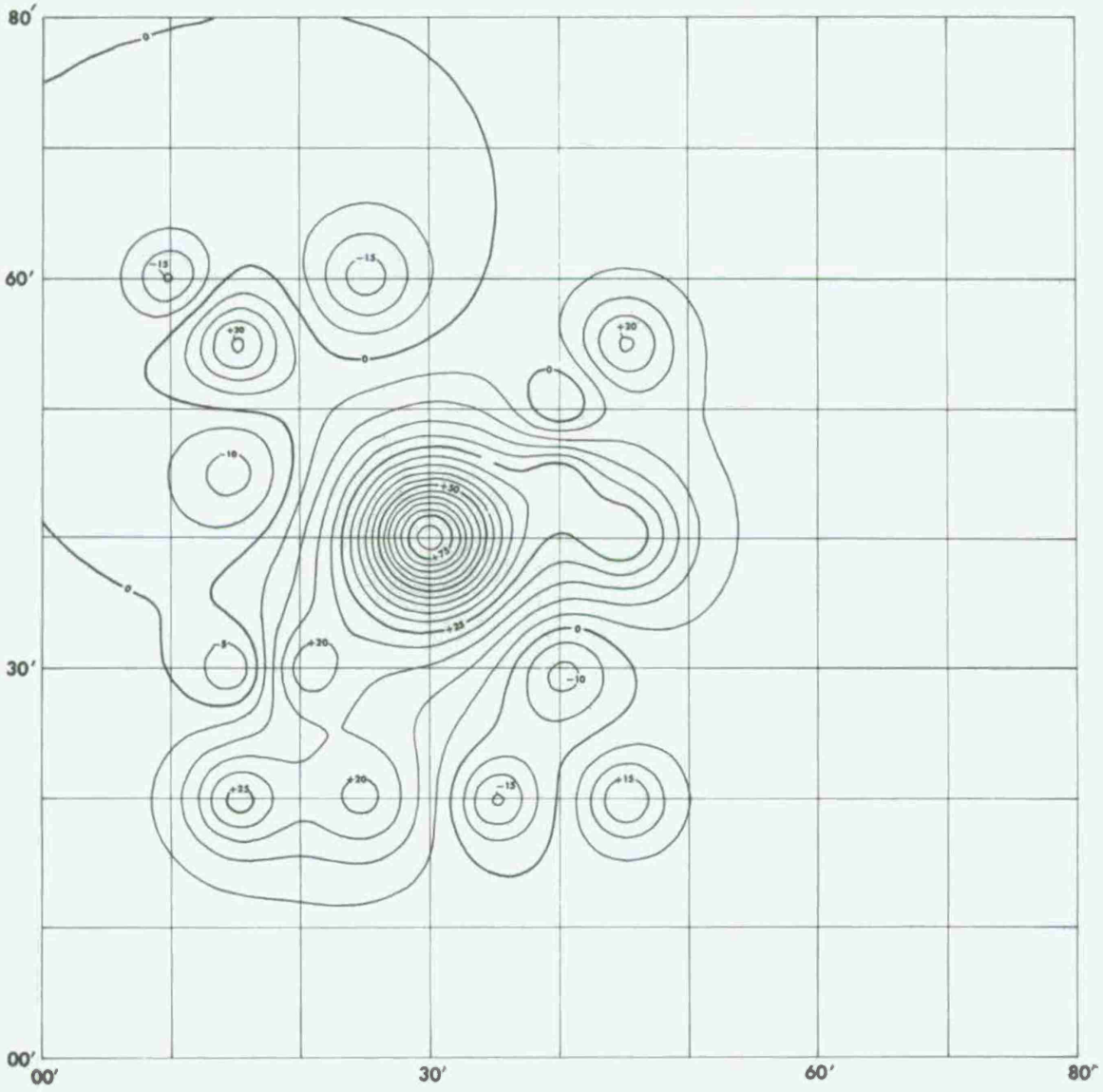

Figure 30. Reference gravity field—81 × 81 minute grid – contour interval (5 mgals).

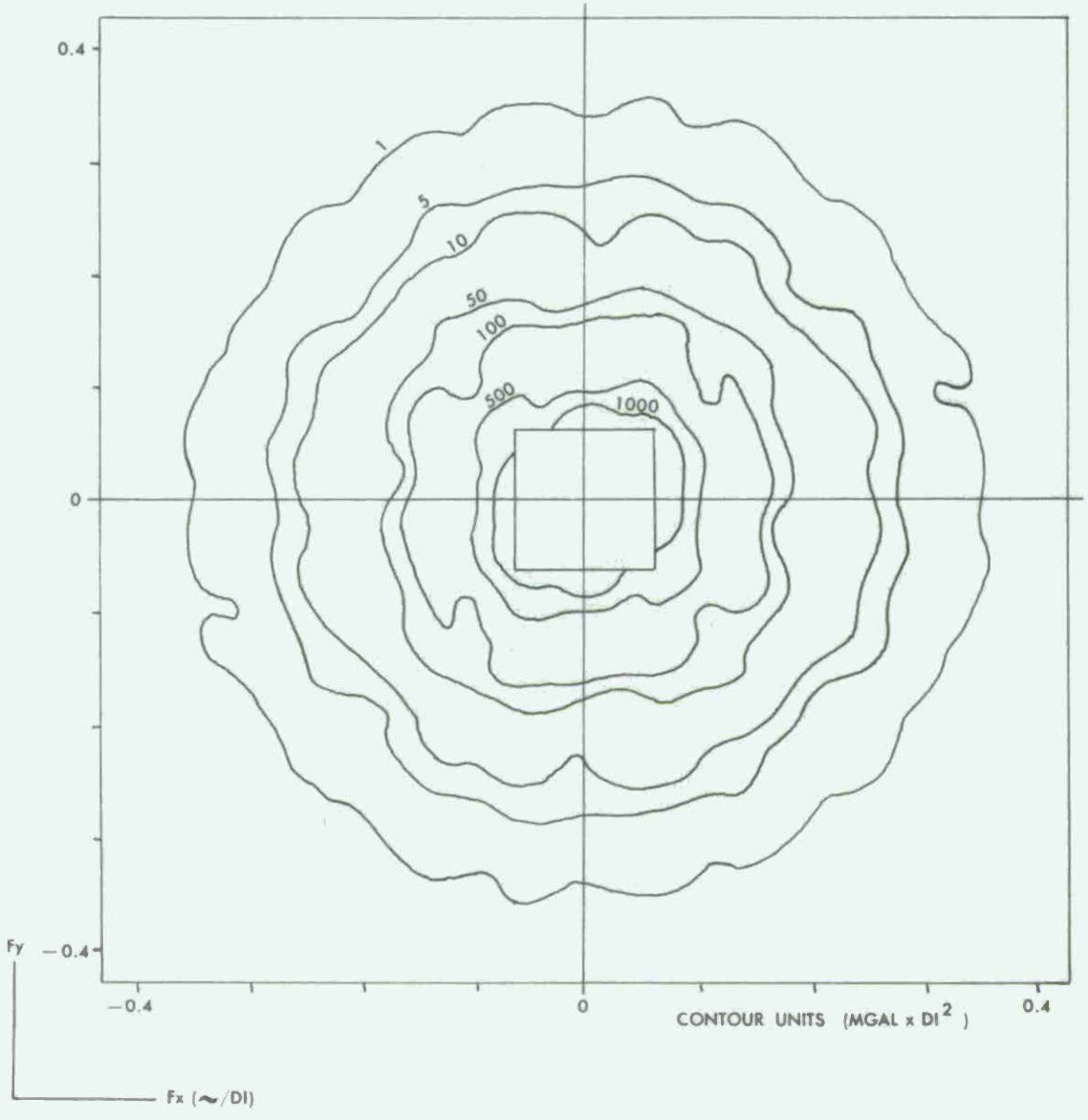

Figure 31. Two-dimensional spectrum of model field (gravity).

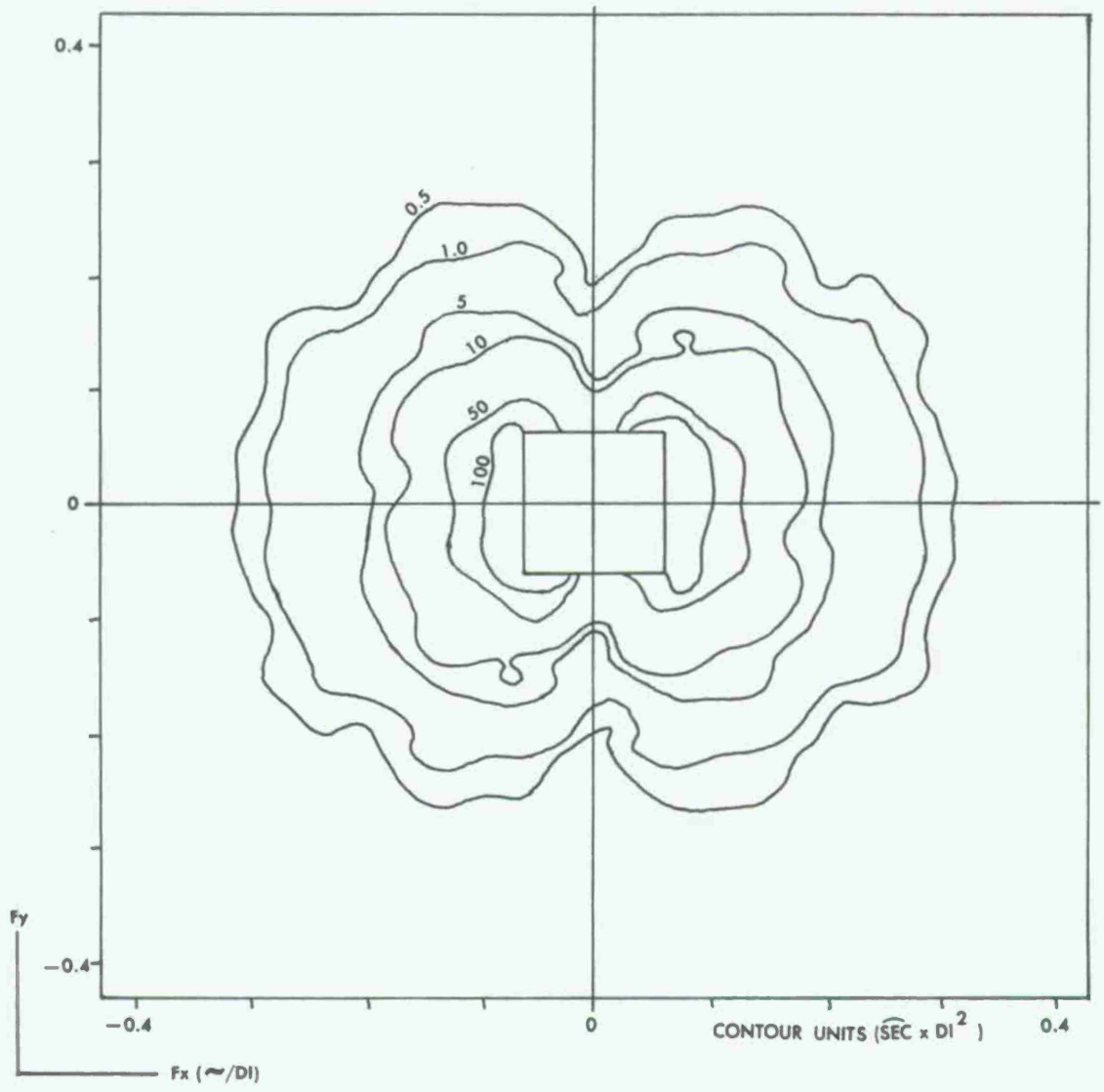

Figure 32. Actual two-dimensional ETA spectrum from model.

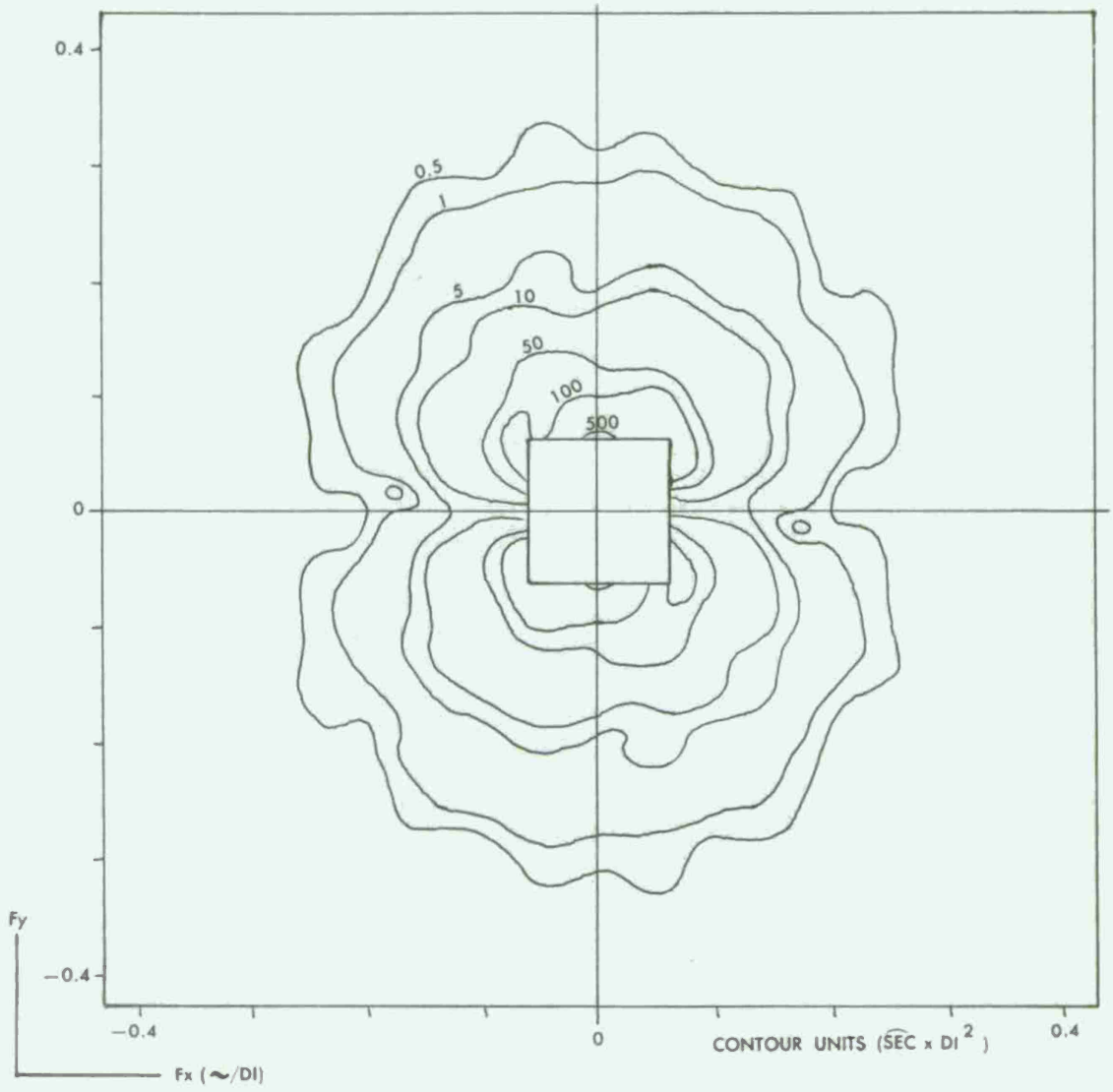

Figure 33. Actual two-dimensional XI spectrum from model.

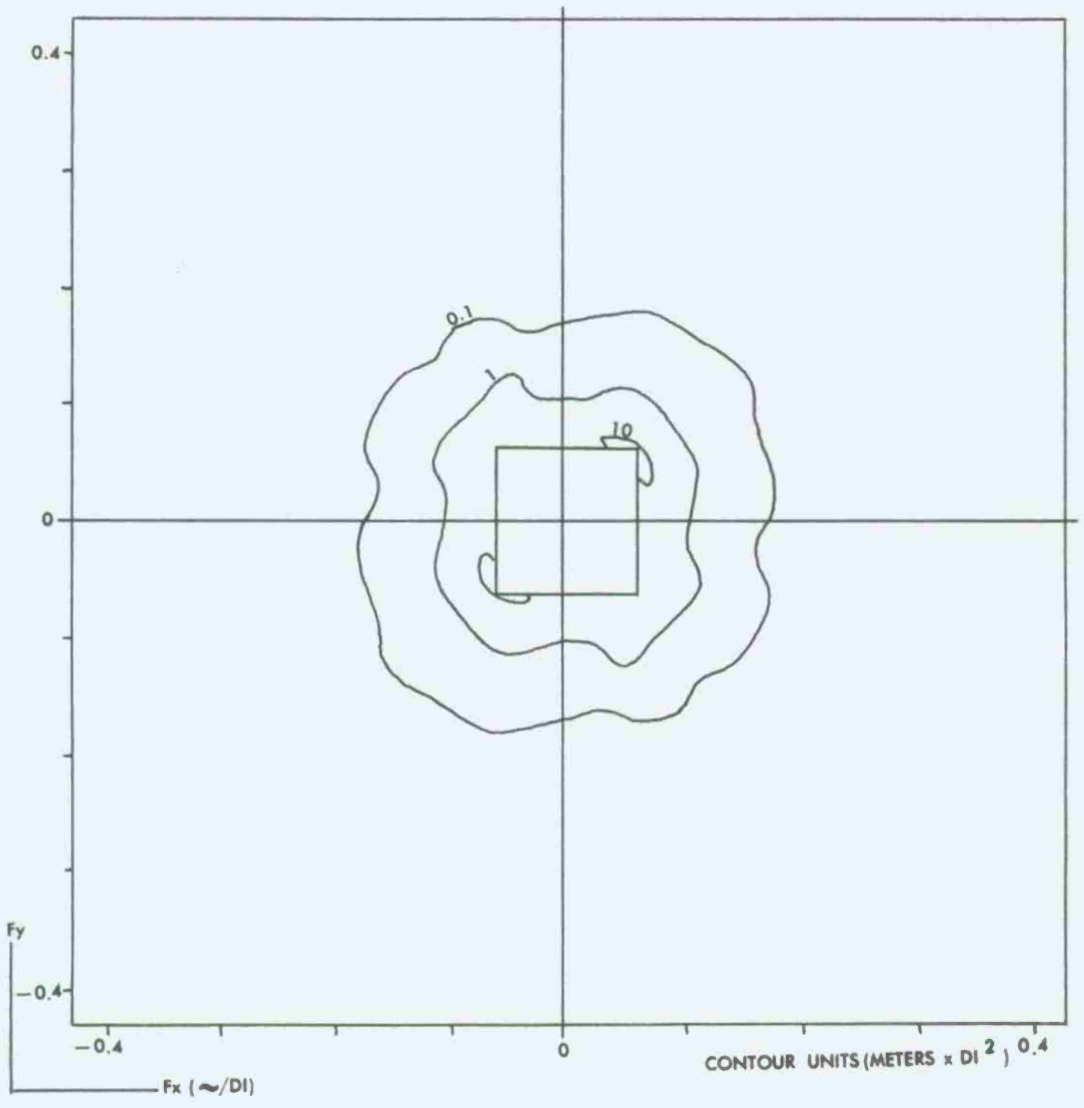

Figure 34. Actual two-dimensional undulation spectrum from model.

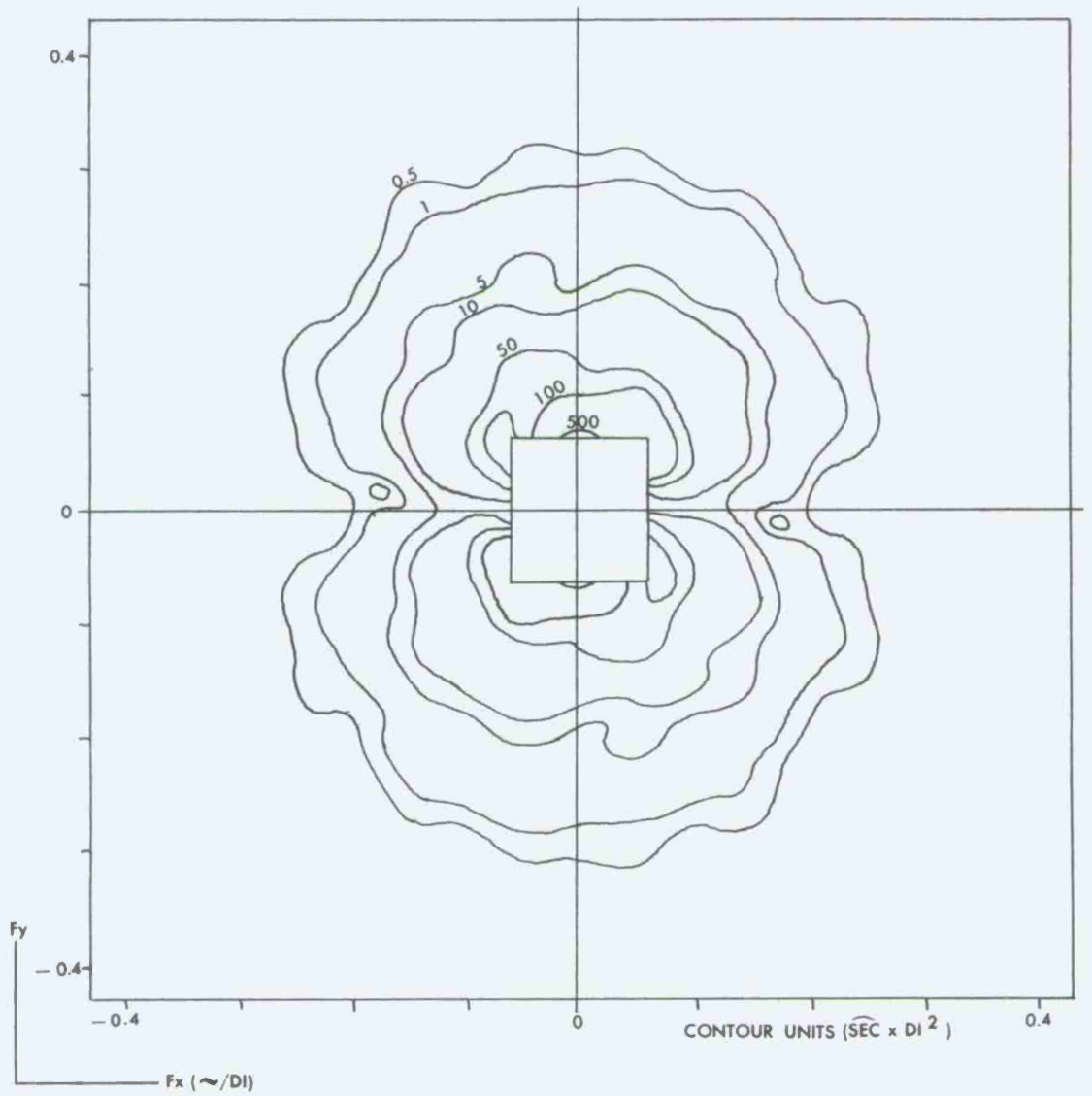

Figure 36. XI spectrum computed with flat-earth frequency domain operator.

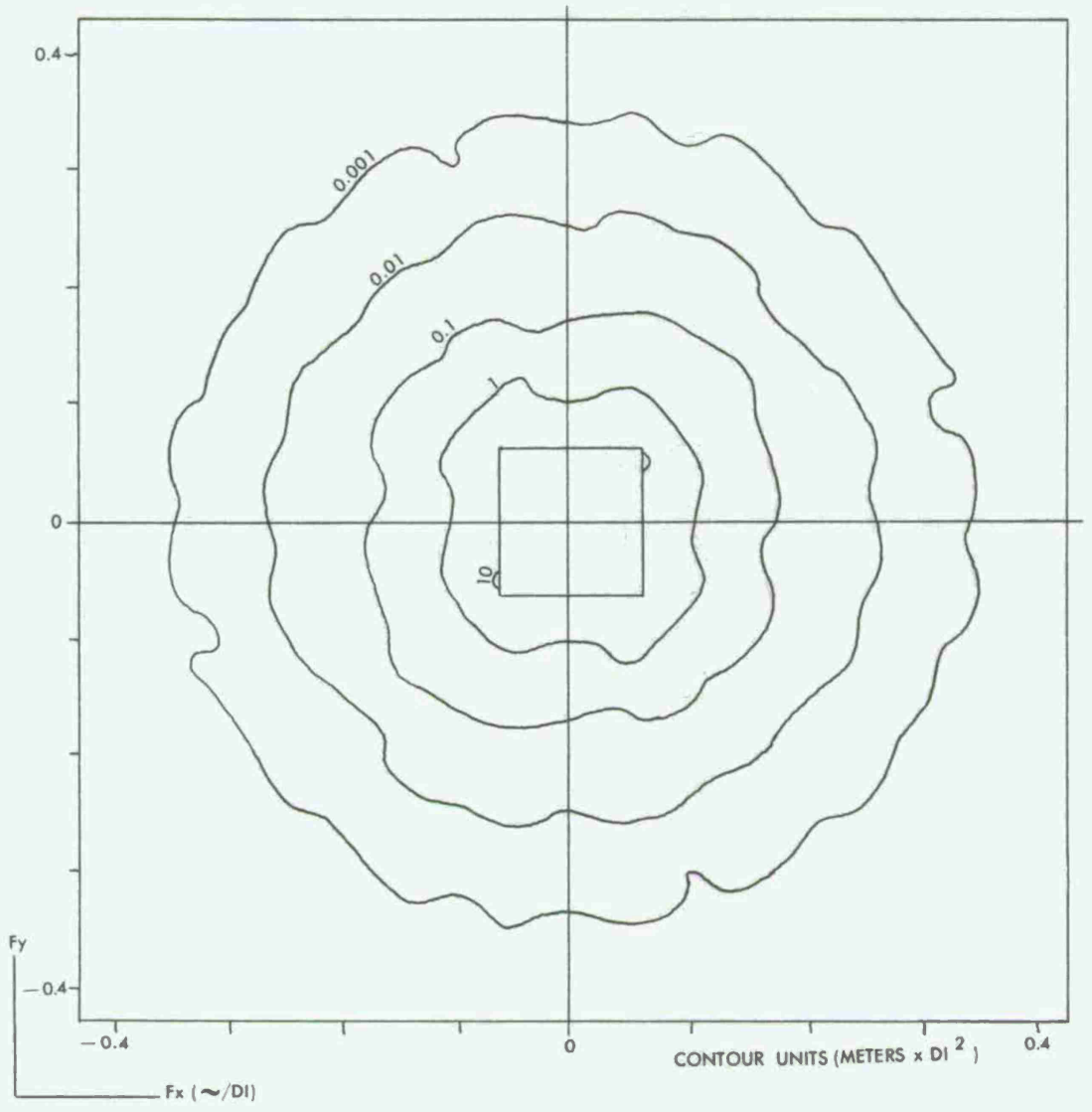

Figure 37. Undulation spectrum computed with flat-earth frequency domain operator.

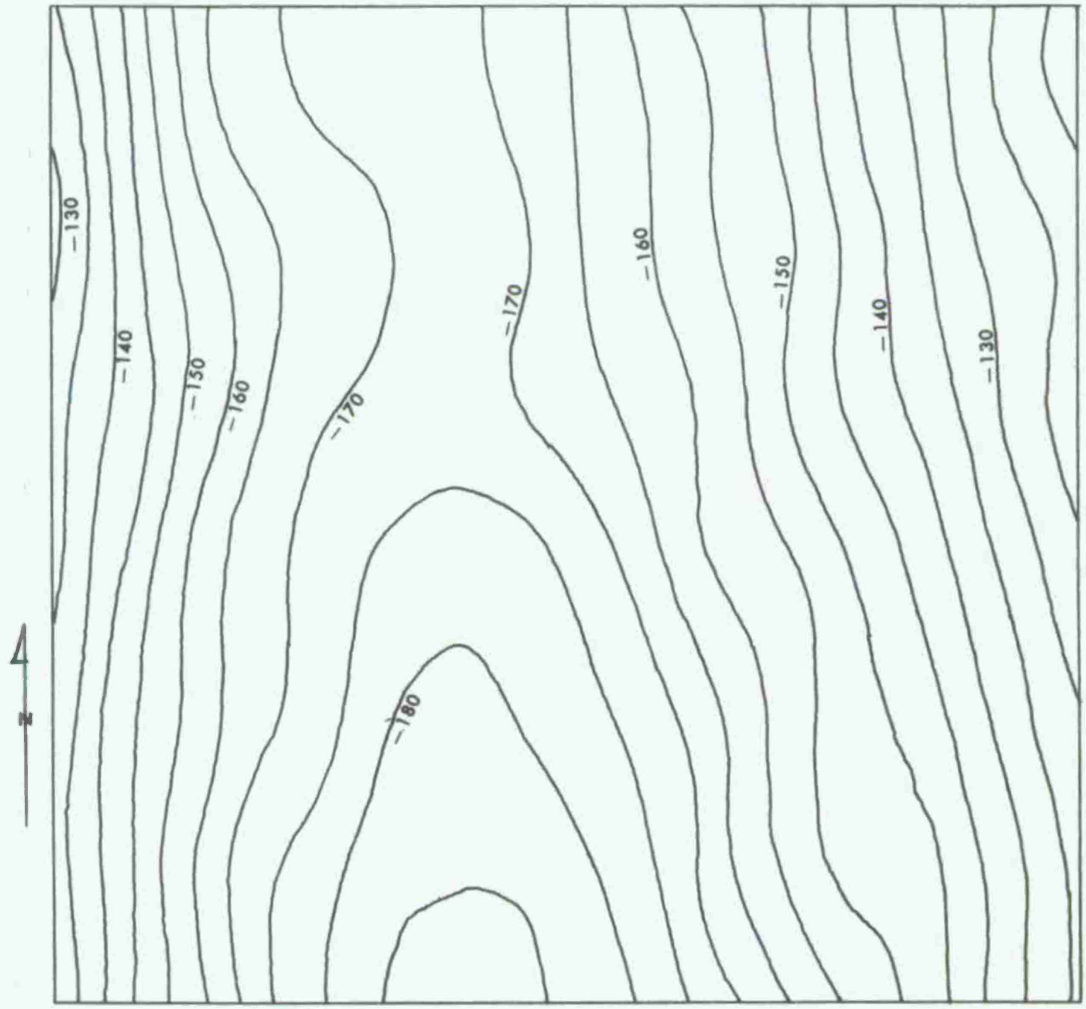

Figure 38. Gravity base data — 21 × 21 point grid, 1 data interval = 1 NM, contour interval (5 mgals).

contour chart of these gridded data at a grid interval of one nautical mile. These data are considered to represent a type area from a large homogeneous province developed in the manner outlined in Figure 22. Figure 39 is a contour chart of the two-dimensional amplitude spectrum of these data after appropriate prewhitening and correction. This figure indicates that, except for a small amount of short wavelength energy, nearly all of the strong lineation shown in Figure 38 is contained in wavelengths much longer than the dimension of the base data. As a consequence, most of the lineation has been removed by the prewhitening process.

Applying equation (6) to the real and imaginary parts of this two-dimensional transform, with $S_T(x,y)$ oriented to model north-south survey tracks at various spacings, results in an estimate of the two-dimensional spectral content of the sampling error for the measured gravity data. Figures 40 and 41 are contour charts of the amplitude spectrum of this sampling error for north-south tracks spaced 16 nautical miles apart and 5.3 nautical miles apart. The lack of long wavelength lineations in the error spectrum at the 16 mile spacing is a consequence of the isotropic character of the low-frequency energy in the base data. As would be expected, the error of omission indicated by the contour levels 1, 5, and 10 is nearly identical to the energy in the base data at these frequencies.

The application of equations (14)-(16) to these estimates of the gravity error spectrum results in straightforward propagation of the gravity error through equations (12) and (13) without the need for performing the two-dimensional convolution operations. Figures 42 and 43 are the resulting estimates of the sampling error spectrum for

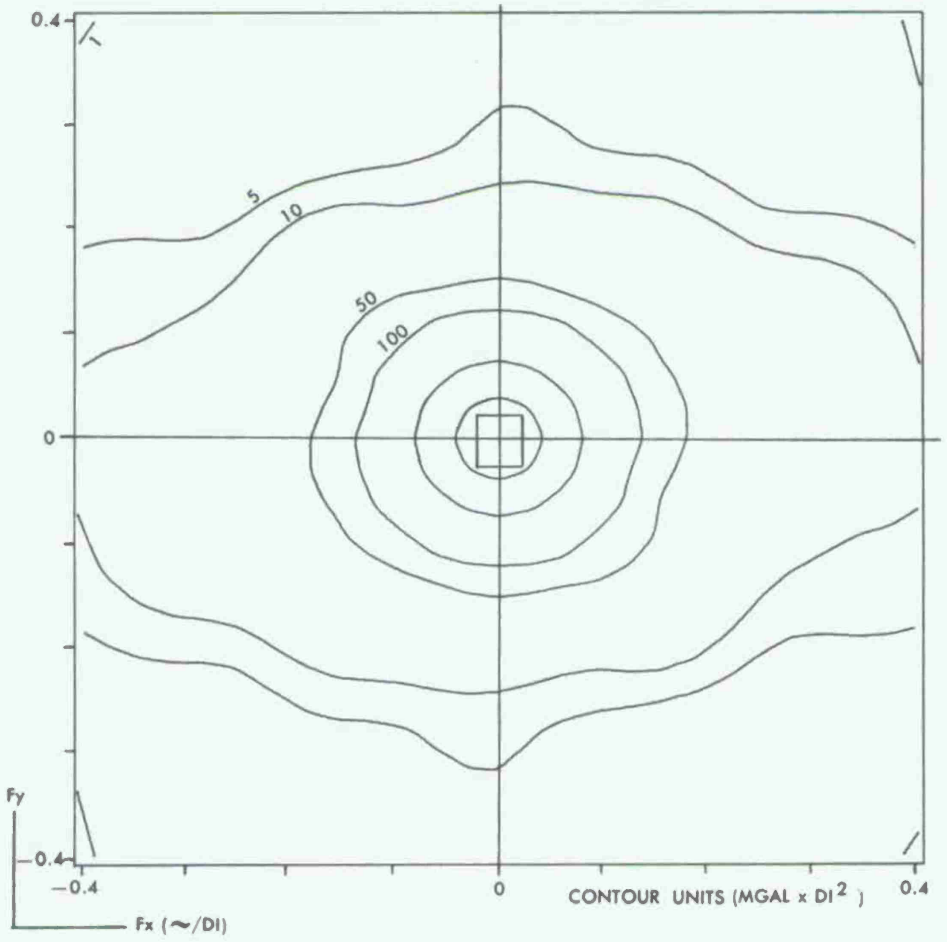

Figure 39. Spectrum of gravity base data.

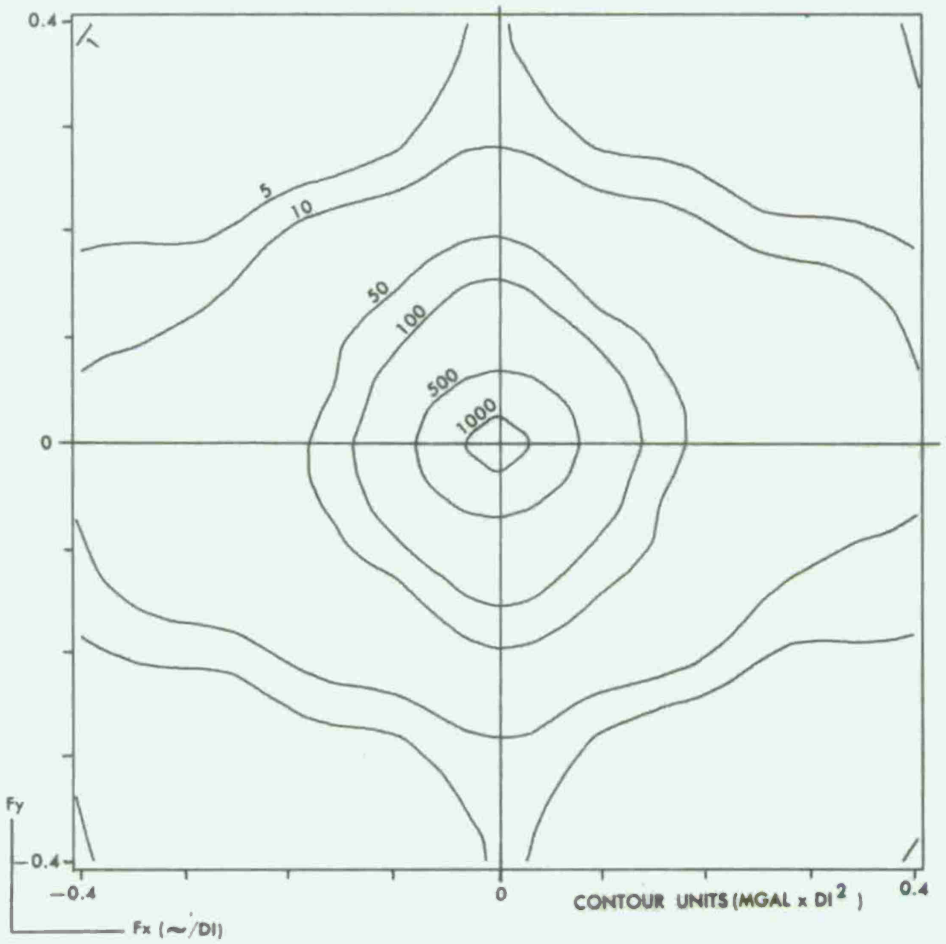

Figure 40. Sampling error spectrum (gravity) N-S tracks—16 NM spacing.

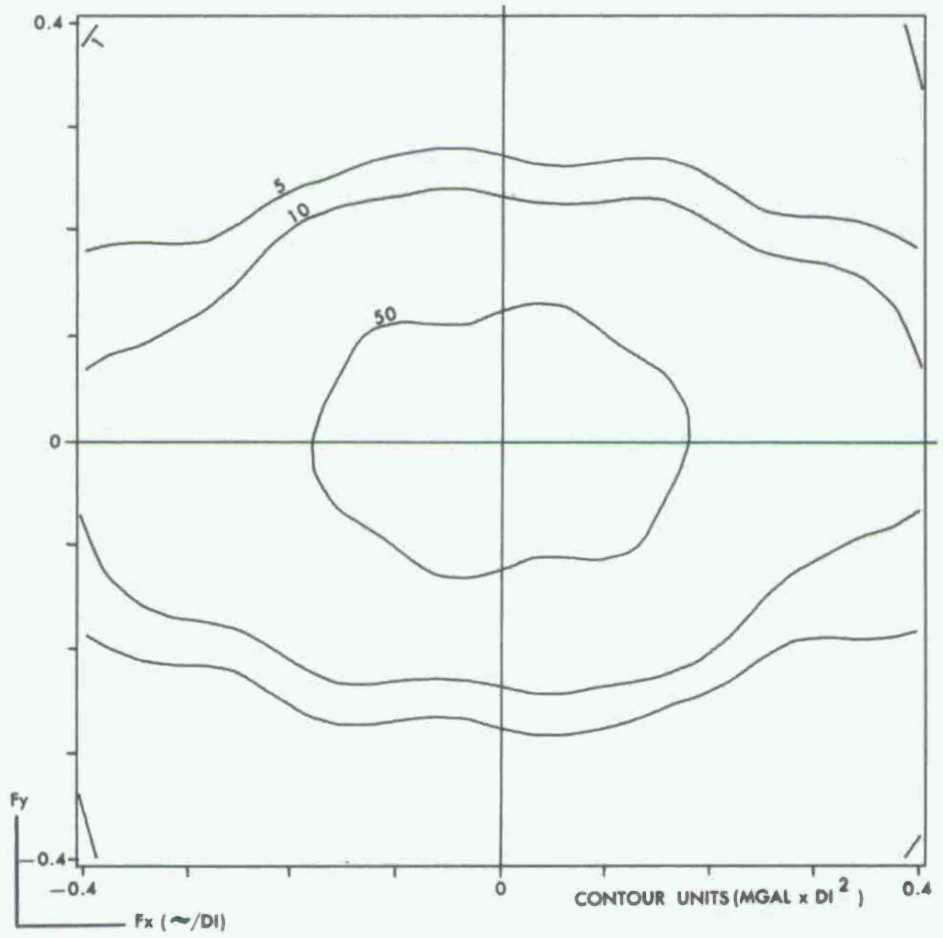

Figure 41. Sampling error spectrum (gravity) N-S tracks—5.3 NM spacing.

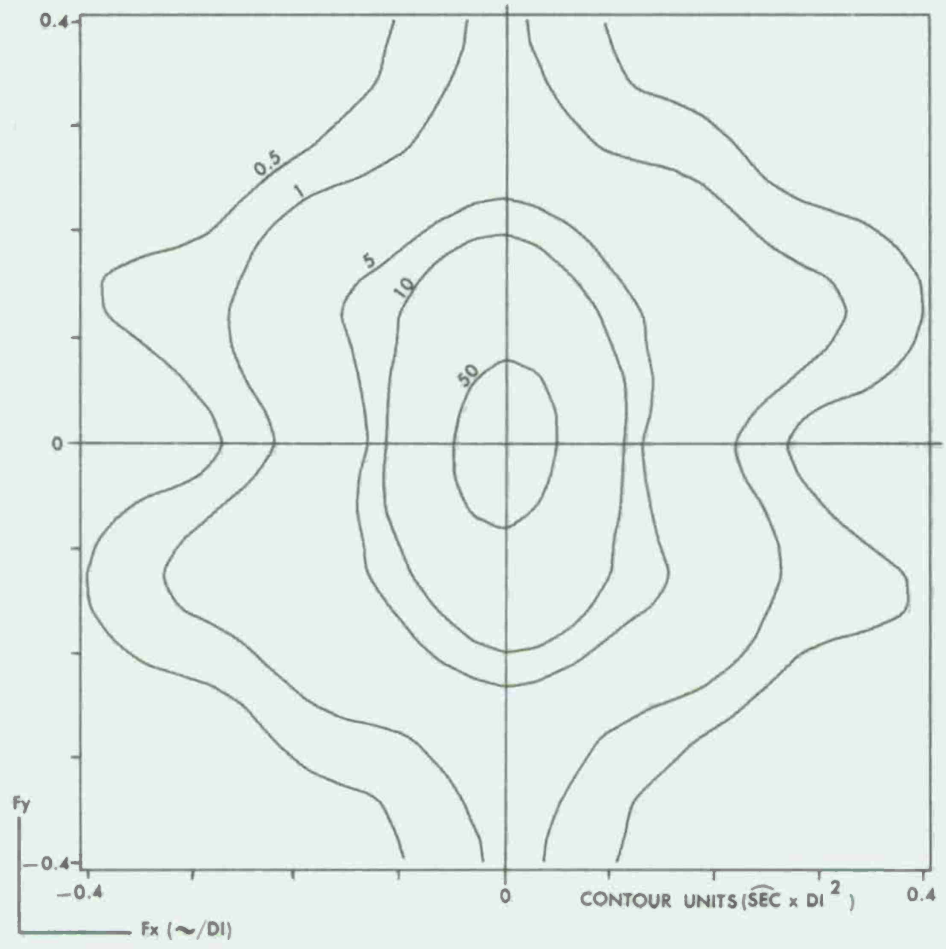

Figure 42. Sampling error spectrum (XI) N-S tracks—16 NM spacing.

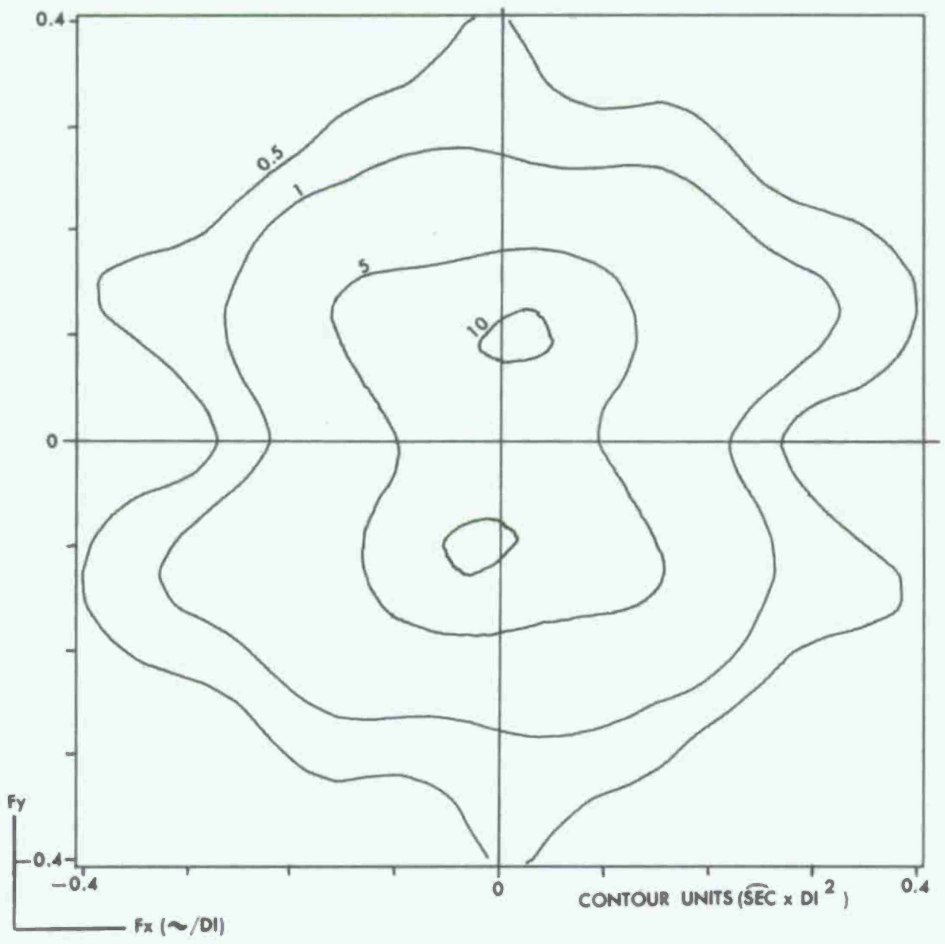

Figure 43. Sampling error spectrum (XI) N-S tracks—5.3 NM spacing.

the along-track deflection component. In this case, for north-south tracks, this is the XI component of deflection. Since the frequency response of the XI operator attenuates all spectral components except those in the north-south direction, these error spectra show a pronounced lineation at all frequencies. As was the case for the gravity error spectra, the error of omission is nearly the same for both track spacings. Figures 44 and 45 are the error spectra for the cross-track (ETA) component. As was the case with the XI operator, the frequency response of the ETA operator generates a strongly lineated error spectrum at both track spacings. Figures 46 and 47 show the error spectra produced by applying the frequency response of the geoid undulation operator. Since this operator exhibits circular symmetry, the undulation error spectrum is simply an attenuated version of the gravity error spectrum at each of the sample track spacings.

Figures 48-55 are similar contours of the estimated error spectra for the case when $S_T(x,y)$ is oriented to model east-west survey tracks at various spacings. For this track orientation, the along-track deflection component is the ETA component, and the cross-track component is the XI component. In this area of high-frequency north-south lineations of the gravity field, the reduction of the sampling error occurring when the survey tracks are oriented normal to the trend is readily apparent. As in the case for north-south tracks, the effect of the frequency responses of the various operators is readily apparent.

The result of applying equation (8) to each of these error spectra is shown in Figures 56 and 57. As in the case of the error spectra, the influence of track direction on the amplitude of the sampling error is quite

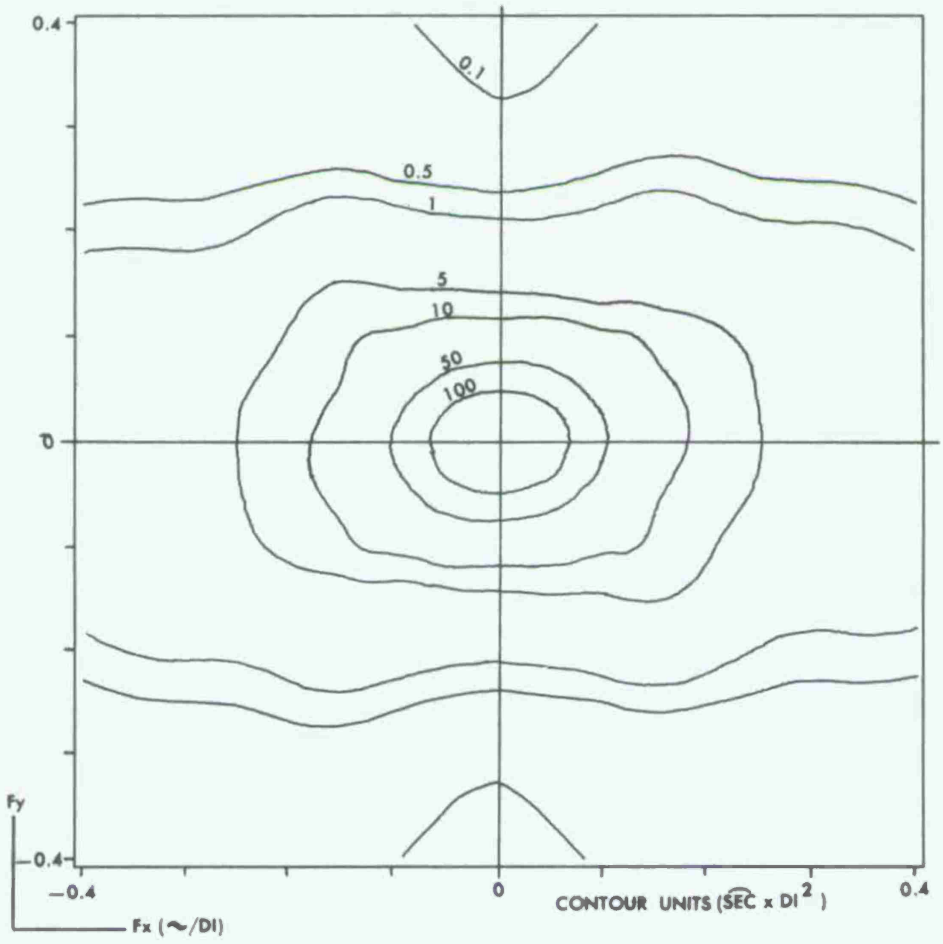

Figure 44. Sampling error spectrum (ETA) N-S tracks—16 NM spacing.

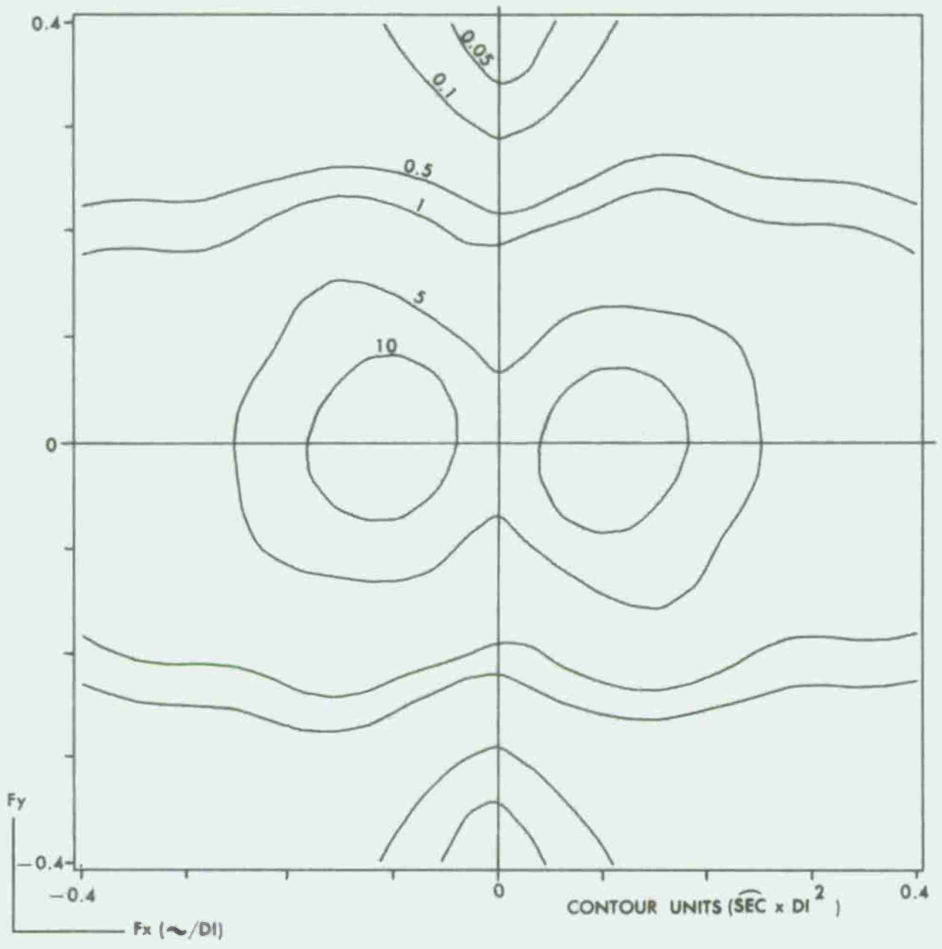

Figure 45. Sampling error spectrum (ETA) N-S tracks—5.3 NM spacing.

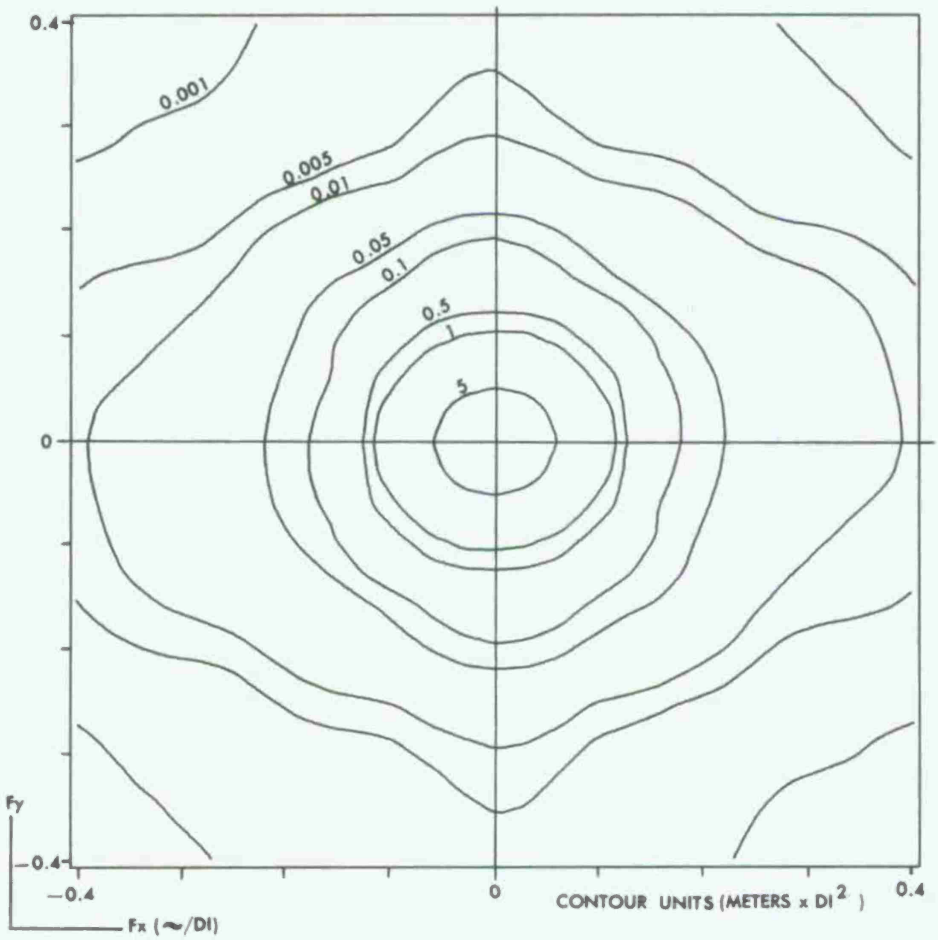

Figure 46. Sampling error spectrum (undulation) N-S tracks—16 NM spacing.

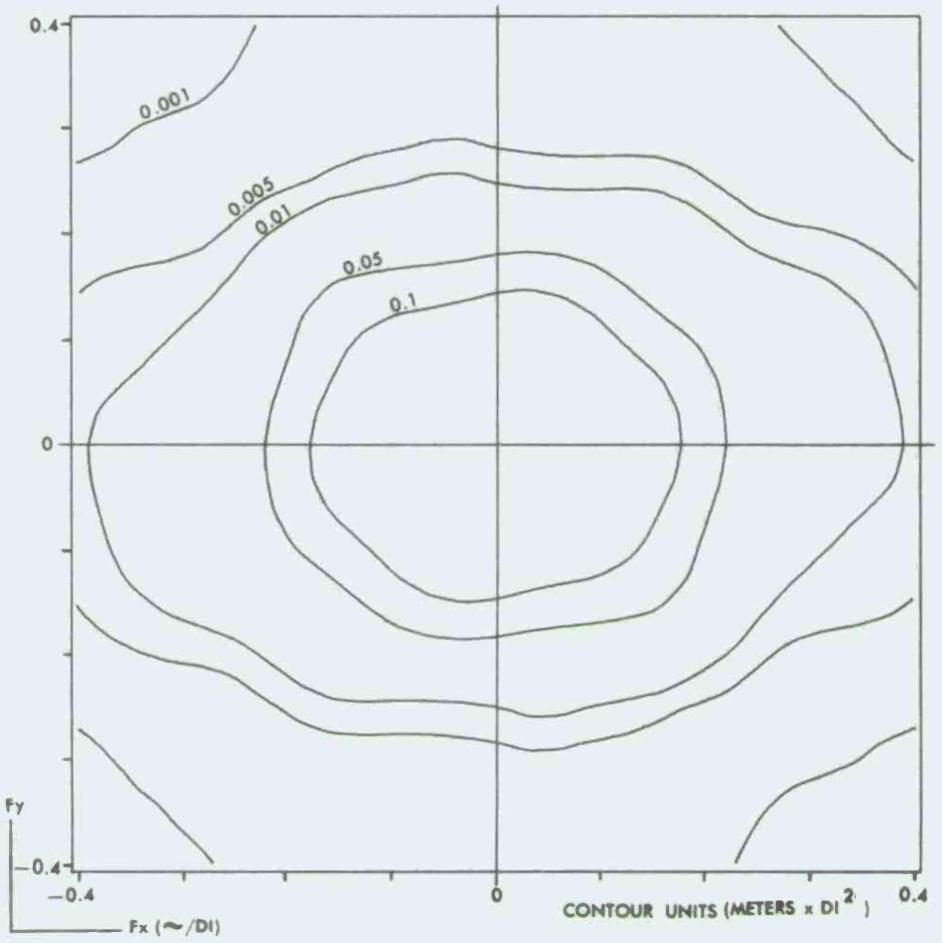

Figure 47. Sampling error spectrum (undulation) N-S tracks—5.3 NM spacing.

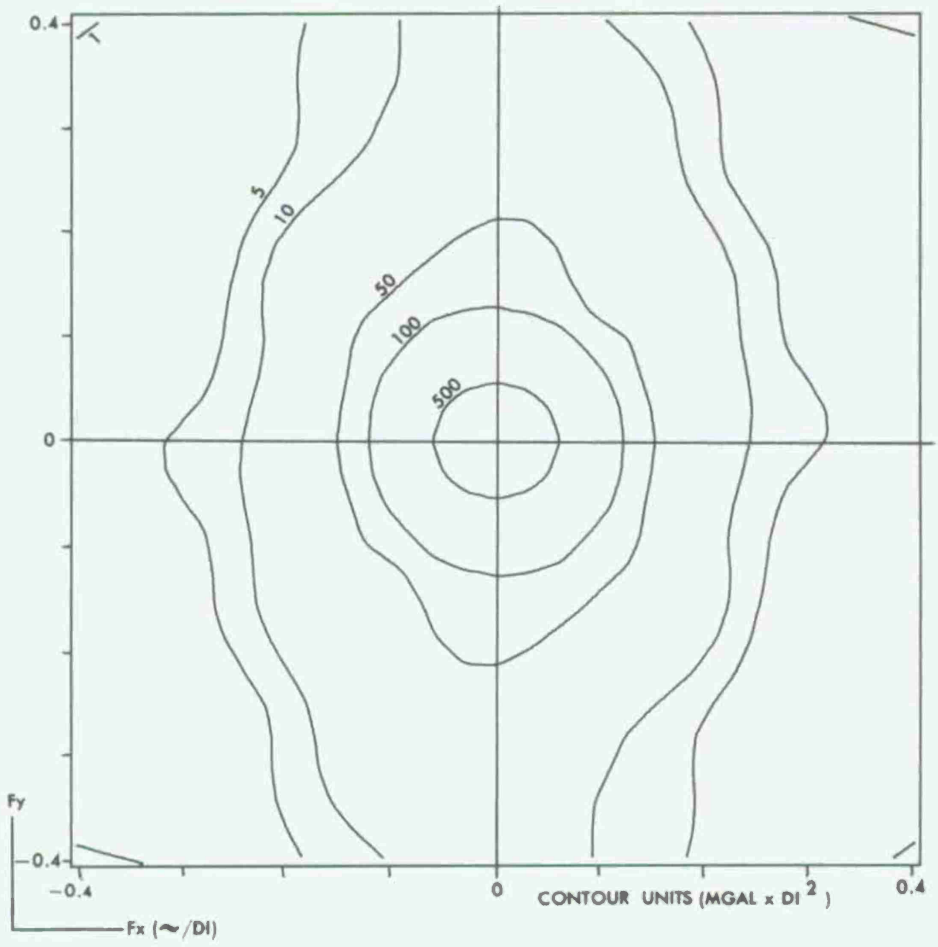

Figure 48. Sampling error spectrum (gravity) E-W tracks—16 NM spacing.

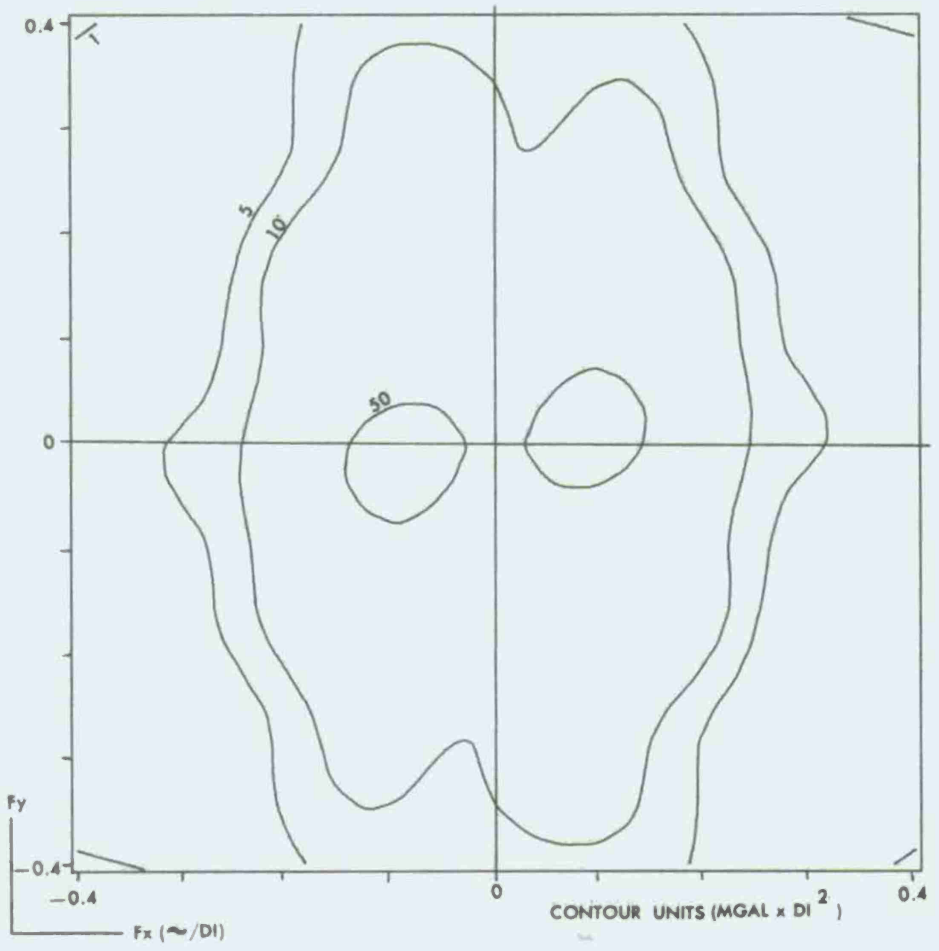

Figure 49. Sampling error spectrum (gravity) E-W tracks—5.3 NM spacing.

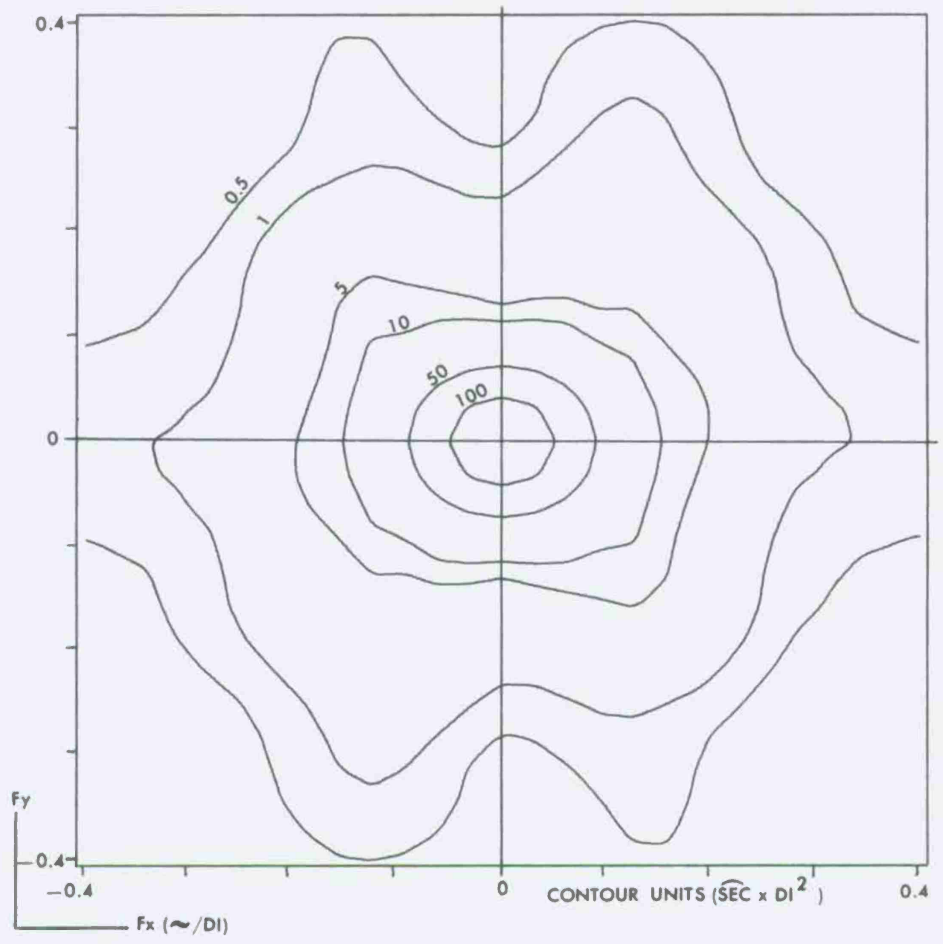

Figure 50. Sampling error spectrum (XI) E-W tracks—16 NM spacing.

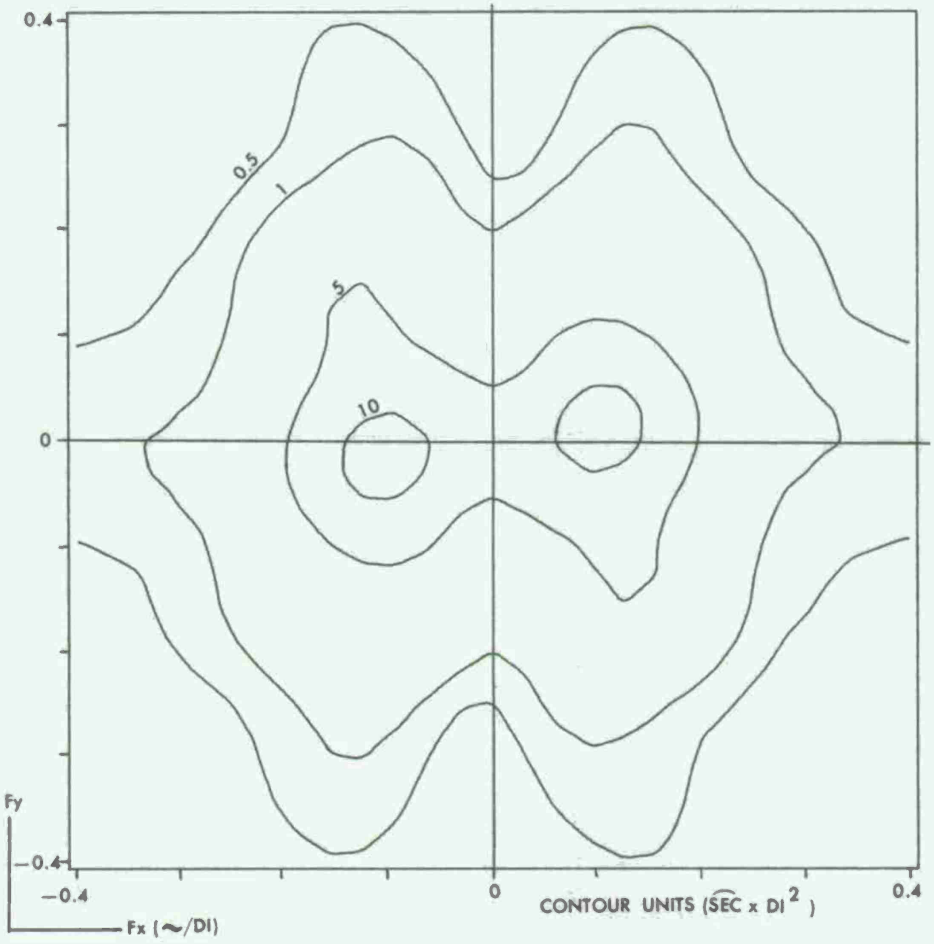

Figure 51. Sampling error spectrum (XI) E-W tracks—5.3 NM spacing.

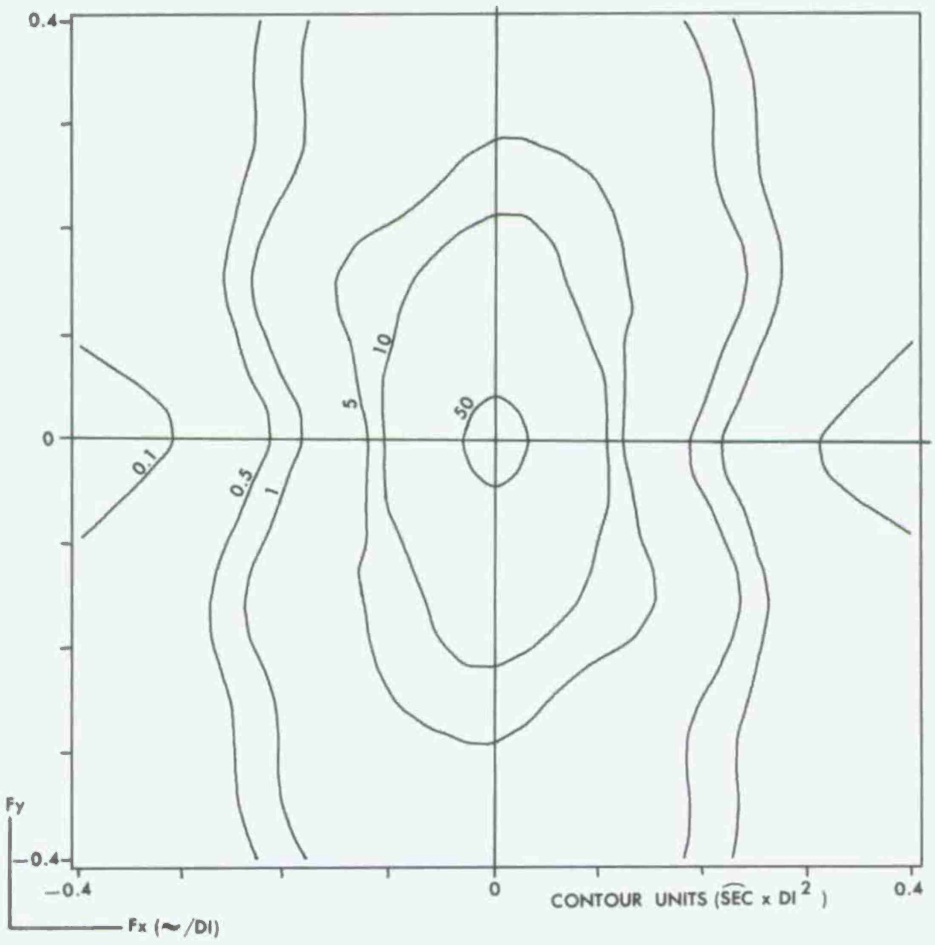

Figure 52. Sampling error spectrum (ETA) E-W tracks—16 NM spacing.

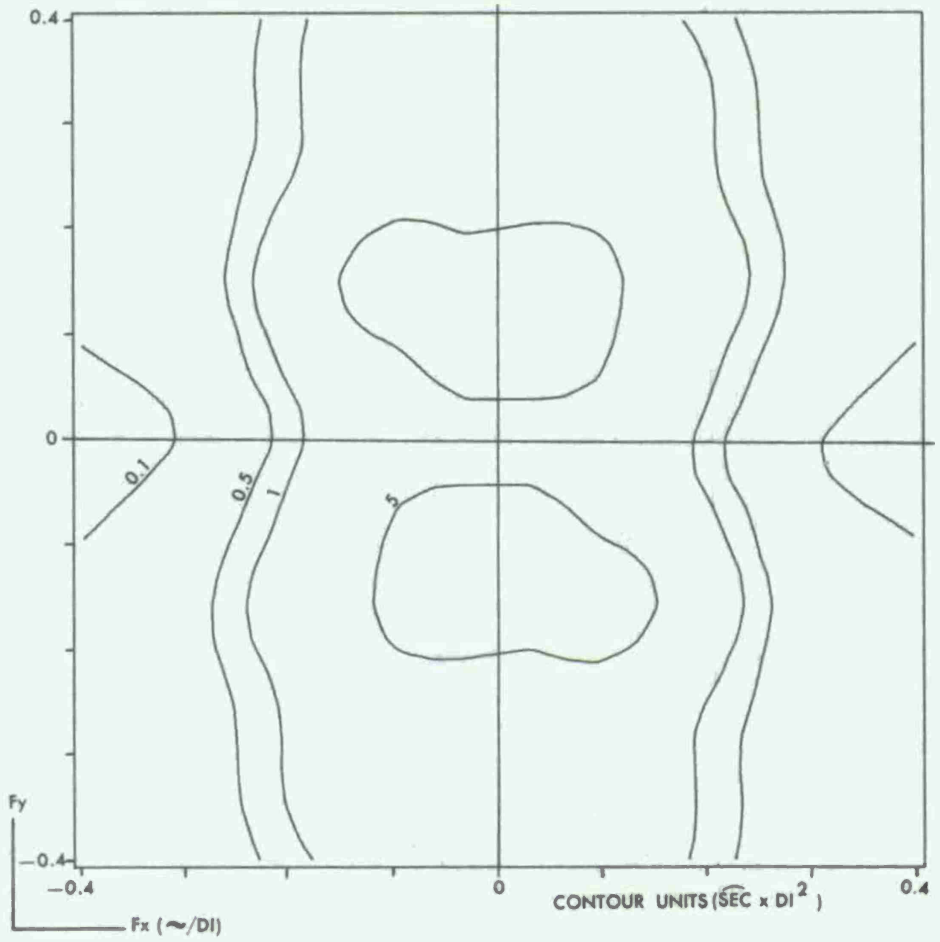

Figure 53. Sampling error spectrum (ETA) E-W tracks—5.3 NM spacing.

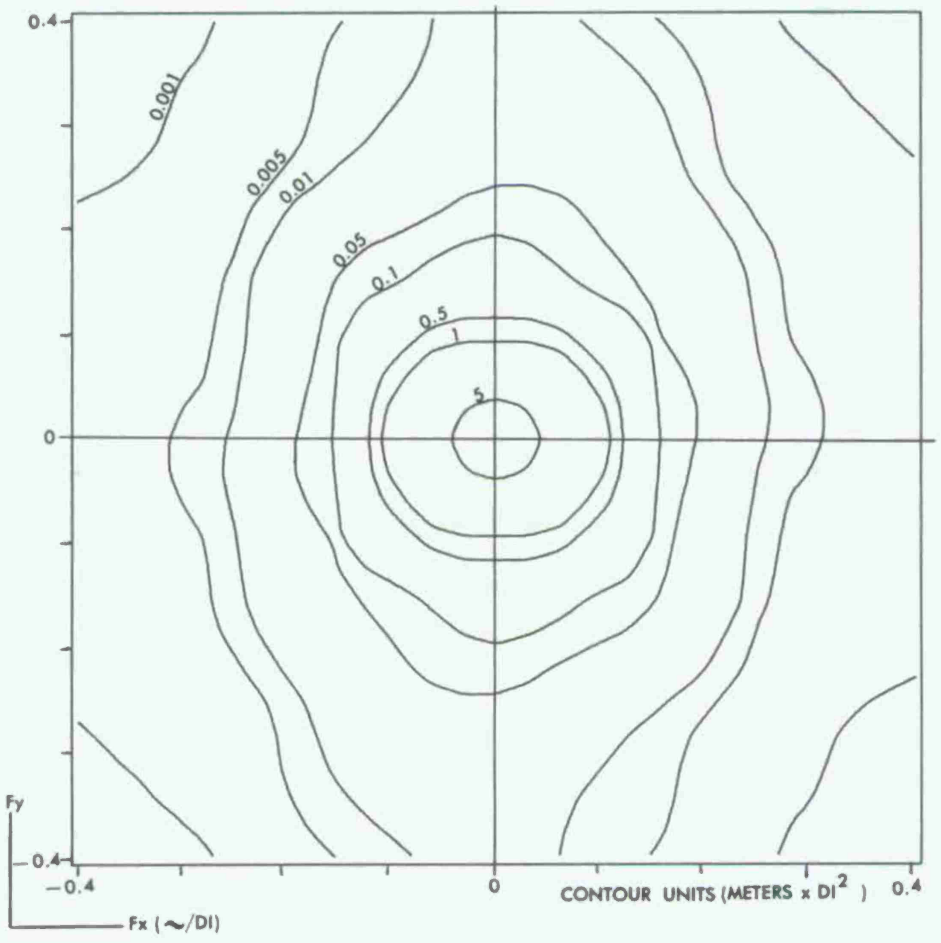

Figure 54. Sampling error spectrum (undulation) E-W tracks—16 NM spacing.

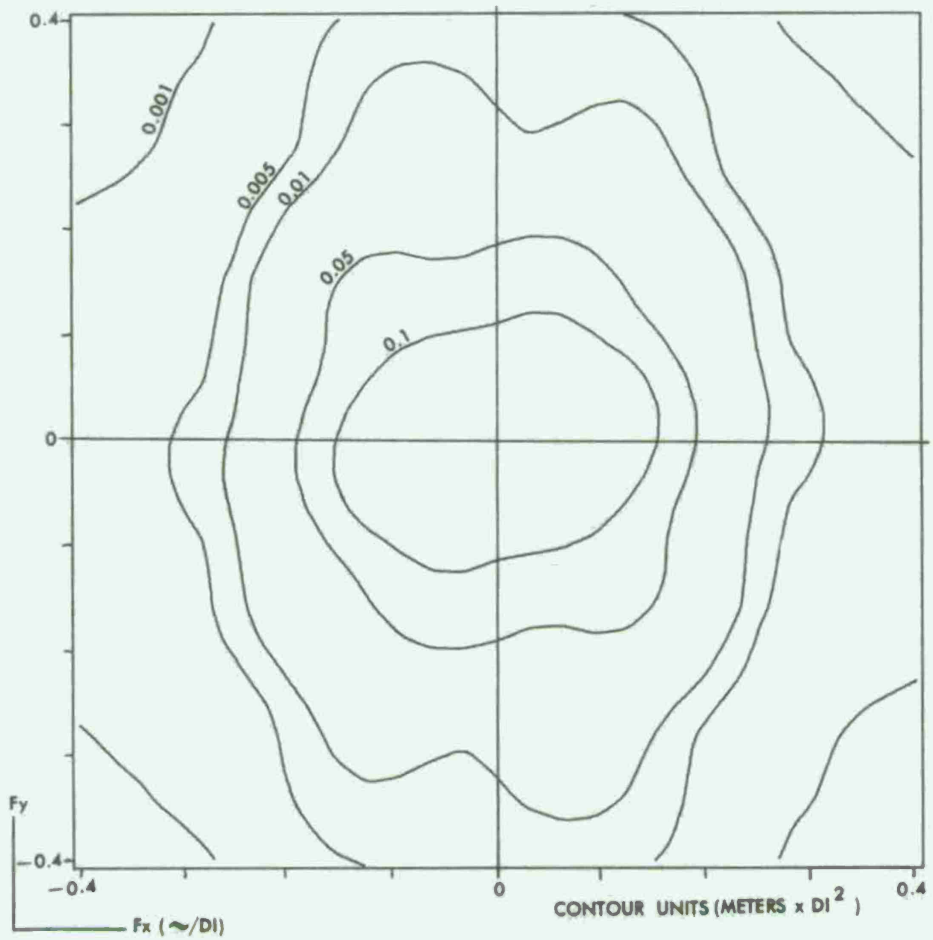

Figure 55. Sampling error spectrum (undulation) E-W tracks—5.3 NM spacing.

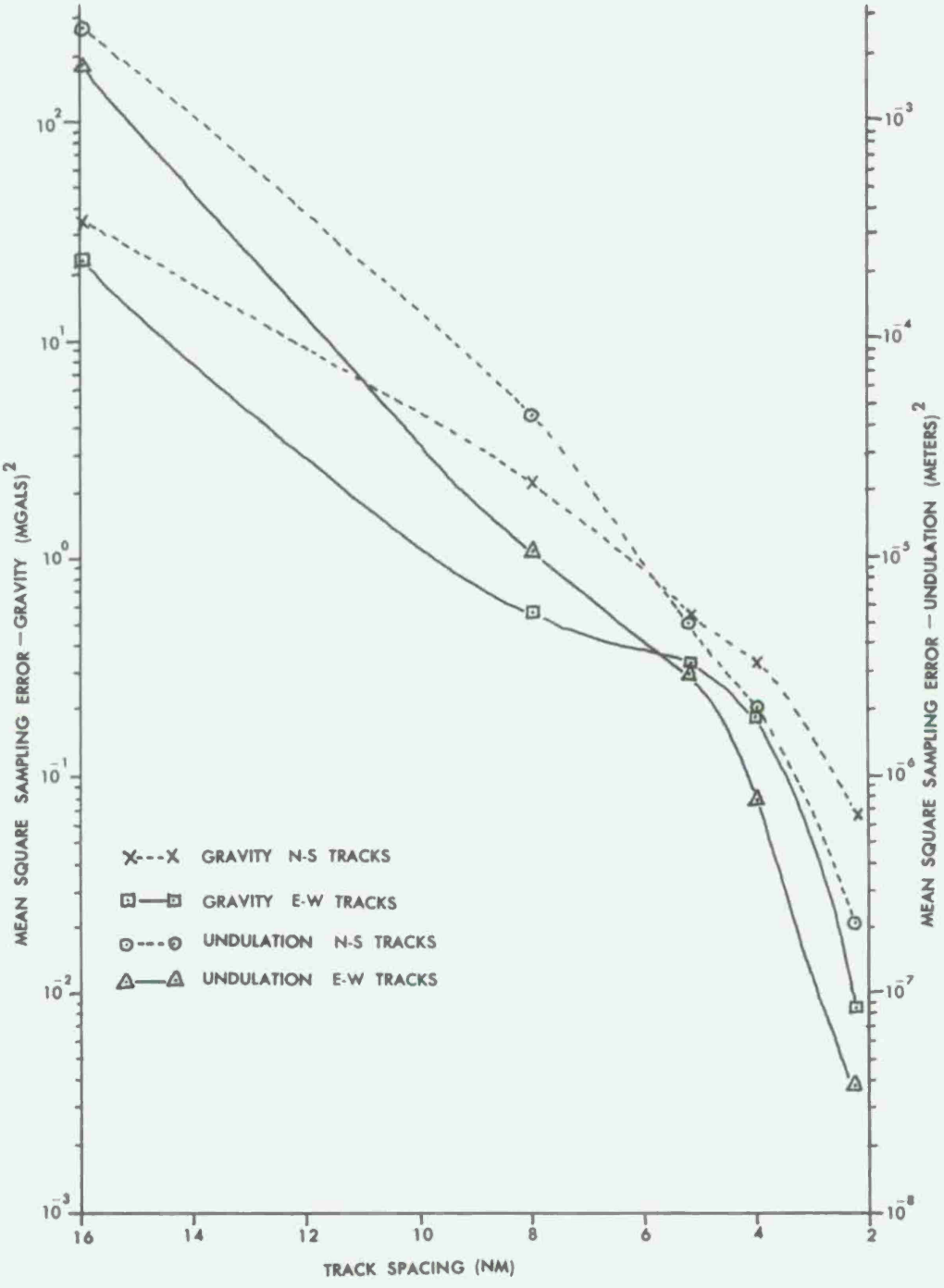

Figure 56. Sampling error vs. track spacing for gravity and undulation.

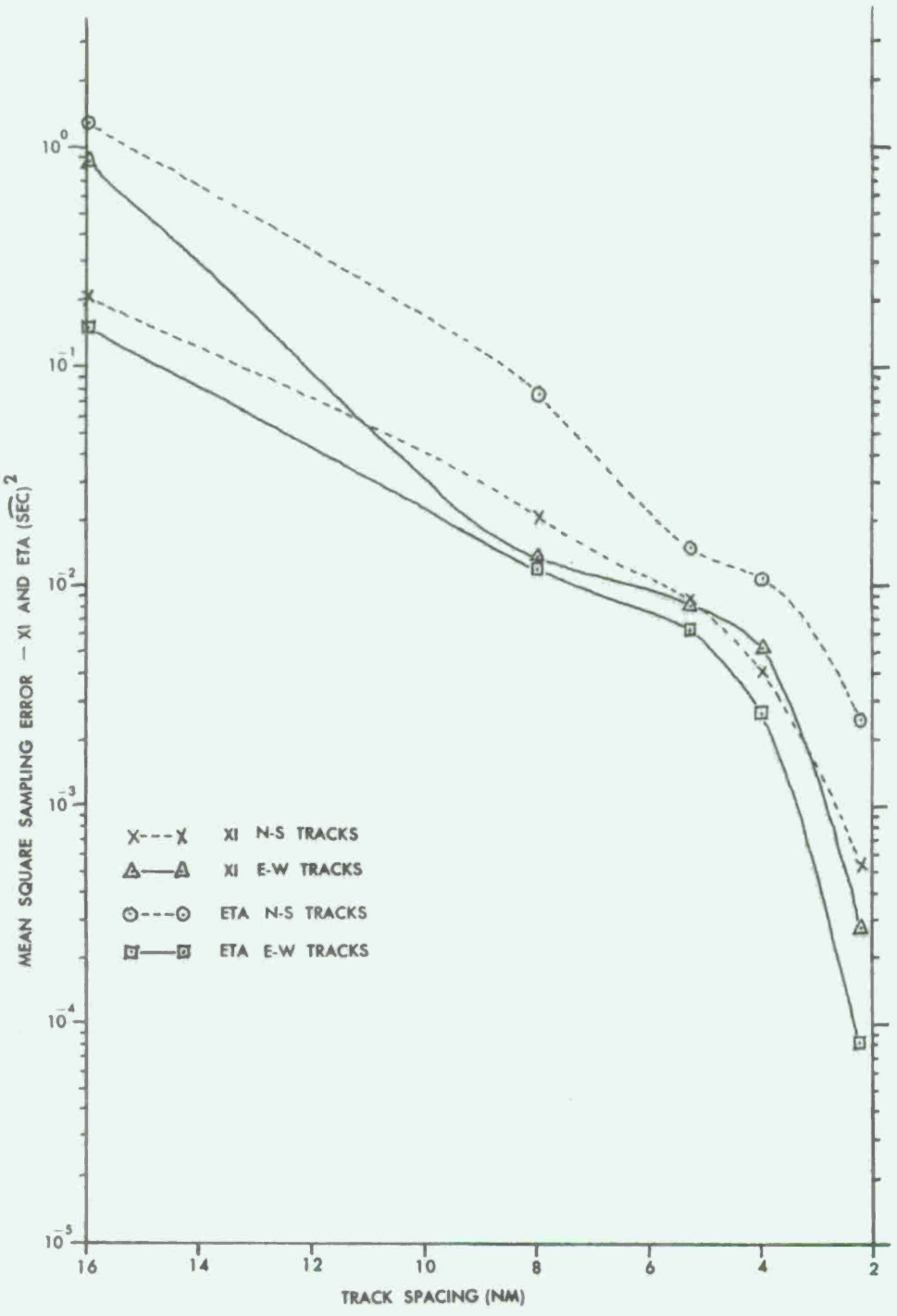

Figure 57. Sampling error vs. track spacing for XI and ETA.

pronounced. In addition, it should be noted that, in general, the along-track component of vertical deflection contains less error than the cross-track component. Reference to Figures 11 and 29 indicates that this numerical result is entirely consistent with that predicted by the theory.

Survey Design for Oceanic Sound Speed

The procedure which has been developed for estimating the boundaries of relatively homogeneous oceanic sound speed provinces from existing historical data is outlined in Figure 23. Although oceanic sound speed is, in reality, a four-dimensional function, ie., a function of latitude, longitude, depth, and time, the distribution of existing data, and the cost of large scale shipboard survey operations precludes the simultaneous consideration of all four variables on anything but a small test basis.

The basic approach to the design of sound speed surveys consists of applying the procedure for the design of track-type surveys to detailed measurements made along a short survey line within each homogeneous province. In this operation, the survey "tracks" are vertical profiles of sound speed as a function of depth. In order to test this survey design procedure, a series of measurements were made within a particular homogeneous winter season province which was expected to exhibit a significant amount of high frequency temporal variability. To obtain the time series test data, 17 vertical profiles of sound speed were collected at approximately the same geographic position in as short a time as the mechanics of the operation would allow. The depth range of the measurements was from 25 meters to 1500 meters covering a time span of approximately 2900 minutes.

Figure 58 is a contour chart of the gridded residual data derived from these measurements. This residual field is constructed by removing the average profile from each observed profile in order to show the time variations in depth ranges in which the sound speed possessed a large vertical gradient. The actual time of each profile or "station" is shown in Figure 58. Immediately following the time series measurements, a spatial series was collected along an east-west line. These data consist of 16 profiles collected at a nominal spacing of 15 nautical miles covering a total distance of 210 nautical miles. Figure 59 is a contour chart of the gridded residual sound speed field derived from this set of measurements. In both of these data sets, the grid interval in depth was 25 meters. For the temporal variation data, the horizontal grid interval was 25 minutes, and for the spatial variation, the grid was 1.45 nautical miles which is roughly equivalent to 25 minutes. Figures 60 and 61 show the two dimensional amplitude spectra of these data.

During the design phase of this experimental survey operation, it was anticipated that the temporal variations would exhibit a sufficiently stationary character over the several days of survey operation so that the temporal variations could be separated from the spatial variation spectrum to produce a relatively uncontaminated space series. As shown in Figures 60 and 61, such was not the case. The spectral content of the time variations for frequencies less than 0.2 cycles/data interval was significantly larger than that obtained for the space series. As a consequence, stationarity could not be assumed and the space series was analyzed in its original form. The result of applying the two-dimensional survey design procedure to each of these data sets is

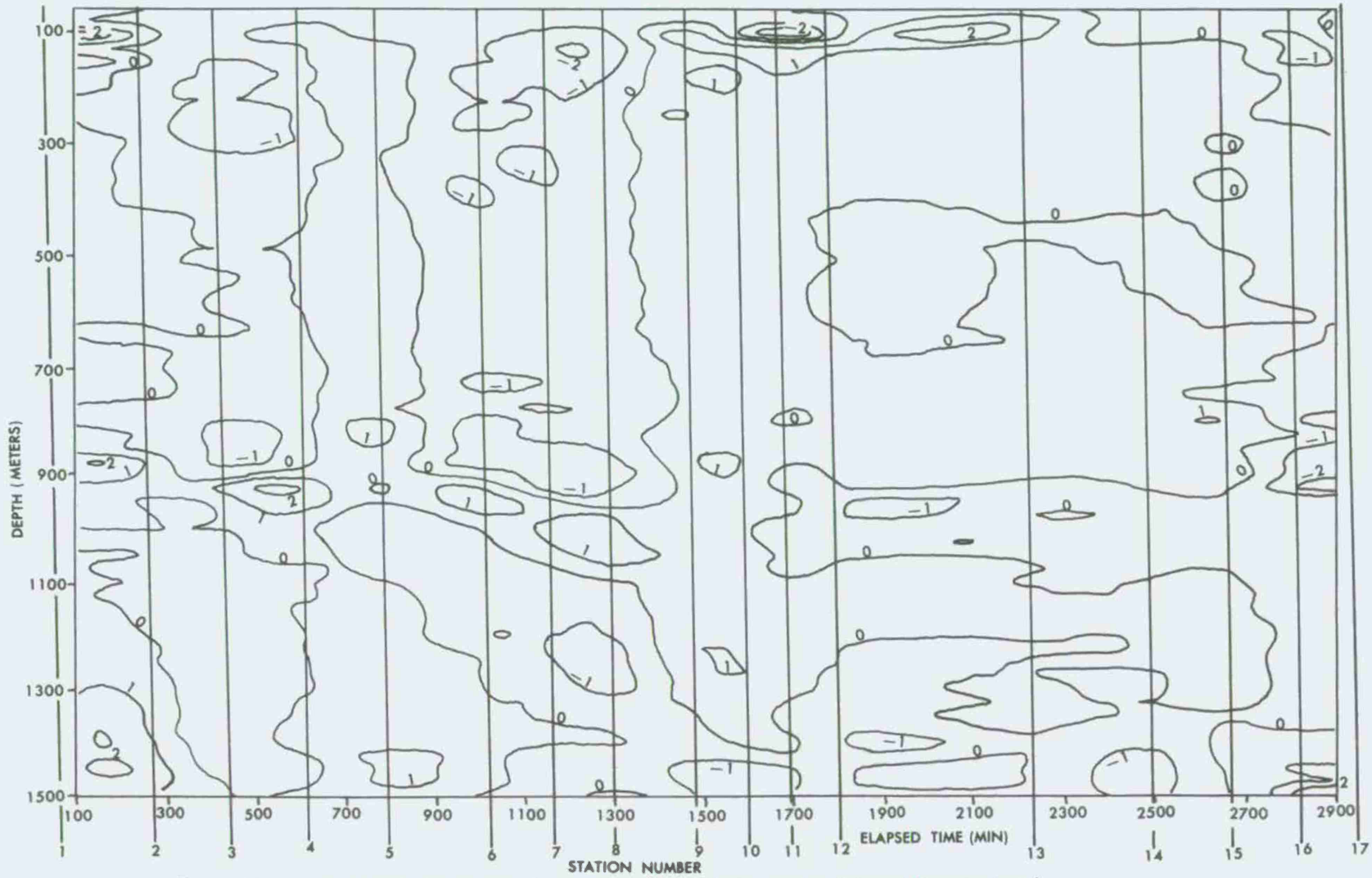

Figure 58. Temporal variation of oceanic sound speed residuals—contour interval (1 meter/sec.).

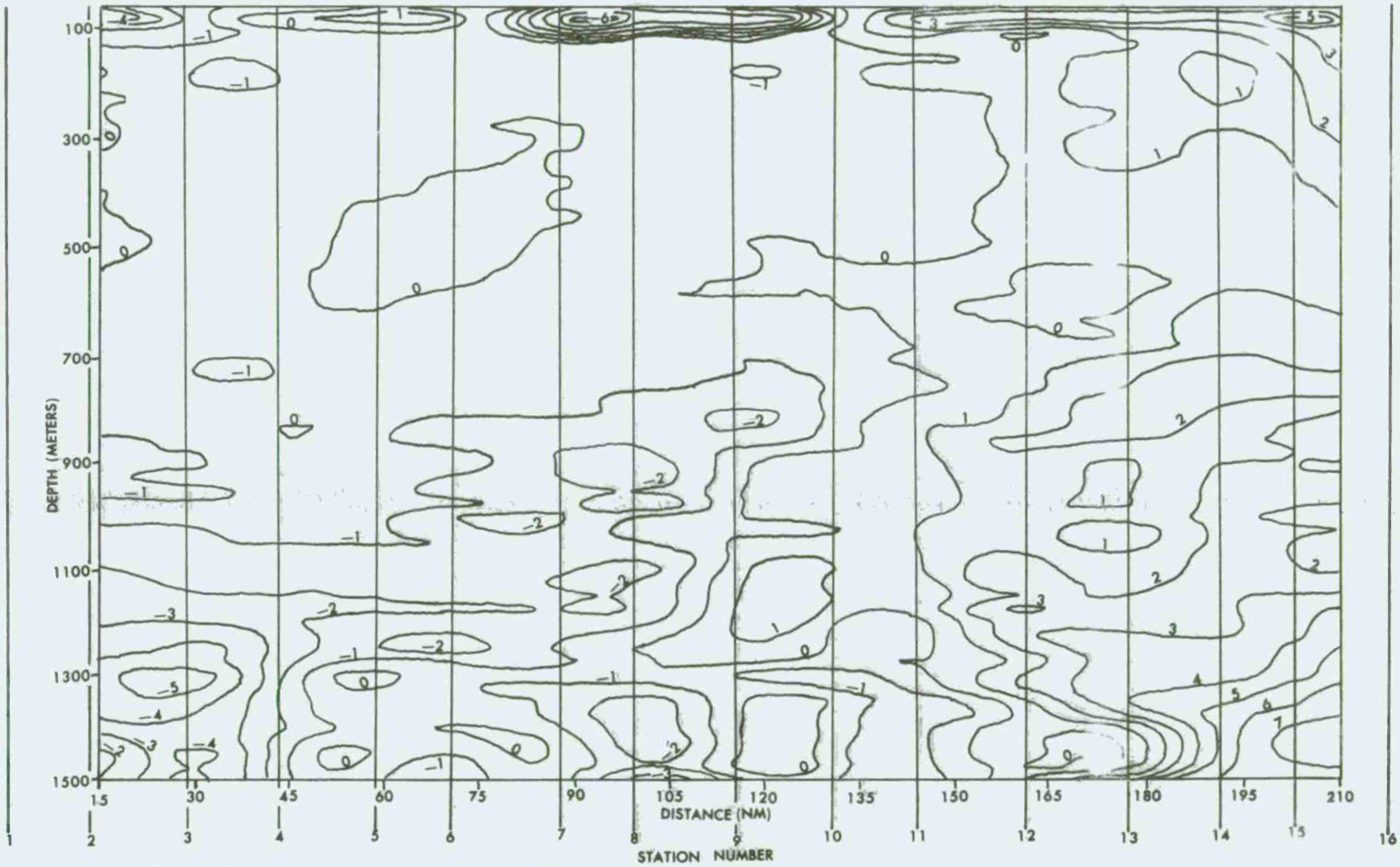

Figure 59. Spatial variation of oceanic sound speed residuals—contour interval (1 meter/sec.).

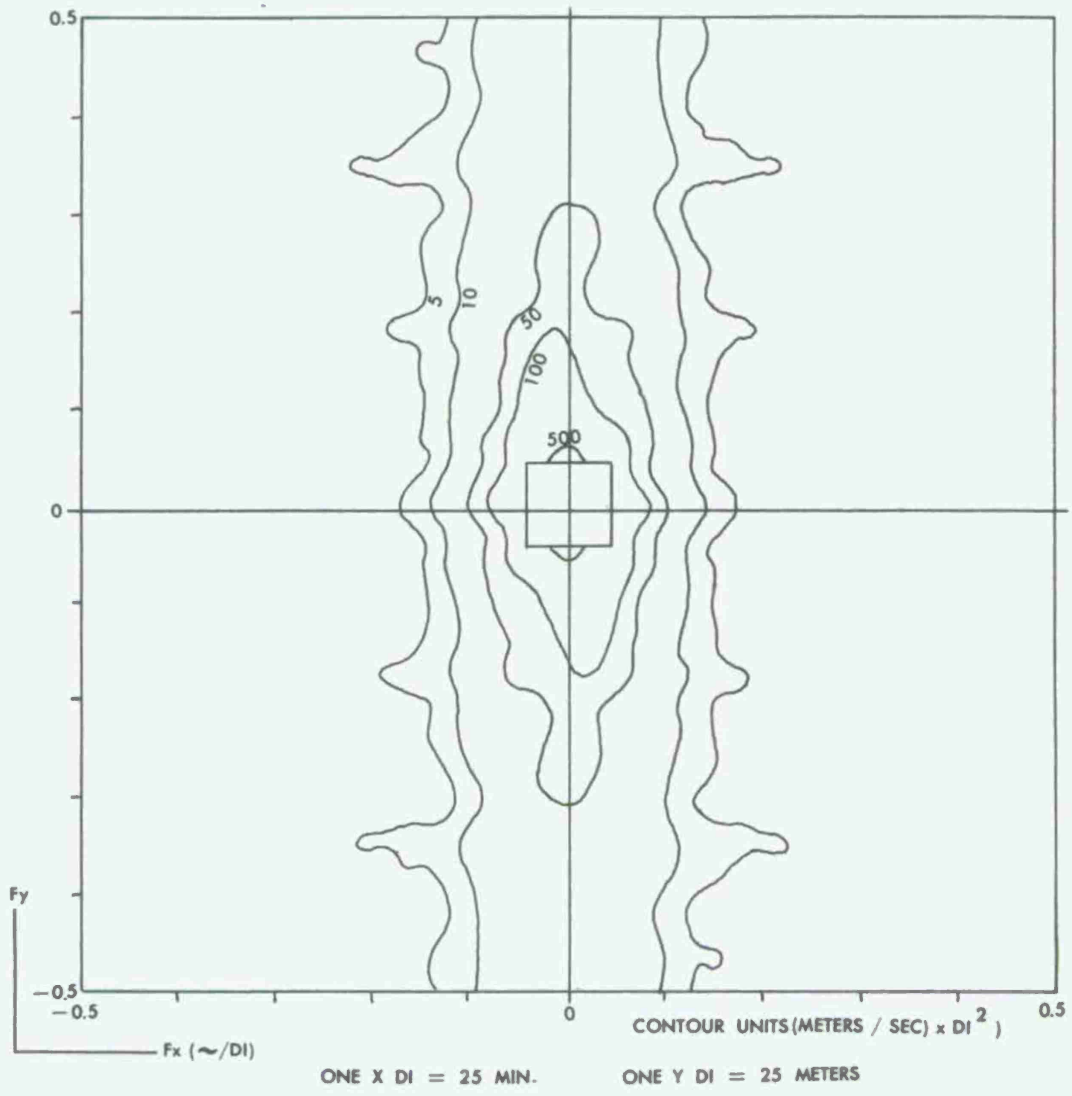

Figure 60. Spectrum of sound speed temporal variations.

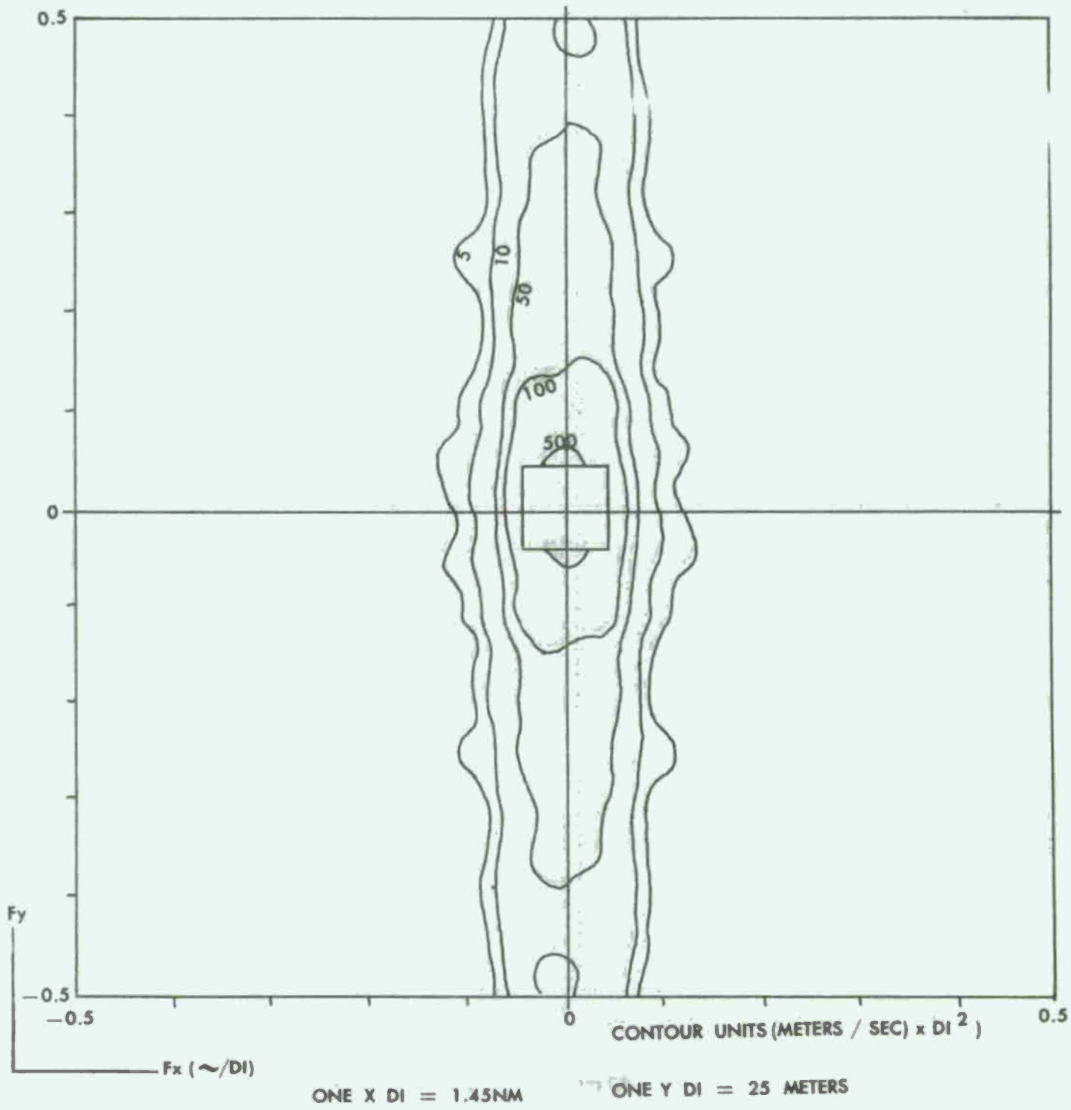

Figure 61. Spectrum of sound speed spatial variations.

shown in Figure 62. This figure shows the estimated sampling error over the depth range 25-1500 meters as a function of profile spacing in both time and space.

These data may also be utilized to illustrate the facility with which this sampling theory may be adapted to many different situations. In this example, if the one-dimensional Fourier transform is computed using data at each grid point occurring at a common depth, contours of the amplitude spectrum as a function of both depth and normalized frequency in the horizontal dimension may be obtained. Figures 63 and 64 illustrate the resulting spectra. A straightforward application of equations (3) and (4) to these one-dimensional transforms results in a contour chart of estimated sampling error as a function of both depth and horizontal spacing as shown in Figures 65 and 66.

By comparing the average sampling error shown in Figure 62 with that shown in Figure 65 at various depths, the importance of the additional information obtained by the one-dimensional analysis is readily apparent. For example, assume that a temporal variation survey is to be conducted in this area to a specified accuracy of 1 $(m/sec)^2$. Figure 62 indicates that the required sample spacing to achieve this accuracy is approximately 1050 minutes. However, Figure 65 indicates that this sample spacing will be expected to produce almost four times the allowable error at depthsless than 200 meters. Thus, the appropriate survey design for this accuracy specification would consist of stations extending to 200 meters and spaced 300 minutes apart with every fourth station extending to a depth of 1500 meters.

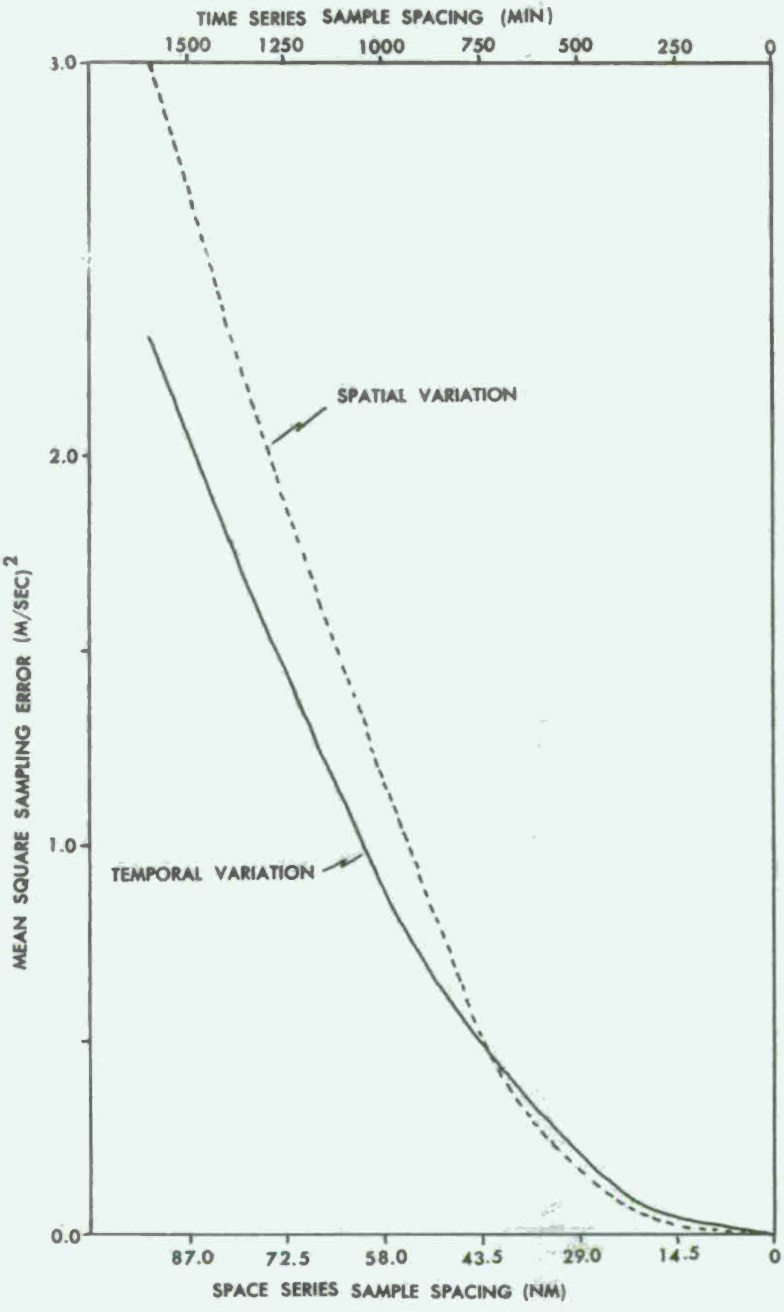

Figure 62. Sampling error vs. station spacing for oceanic sound speed.

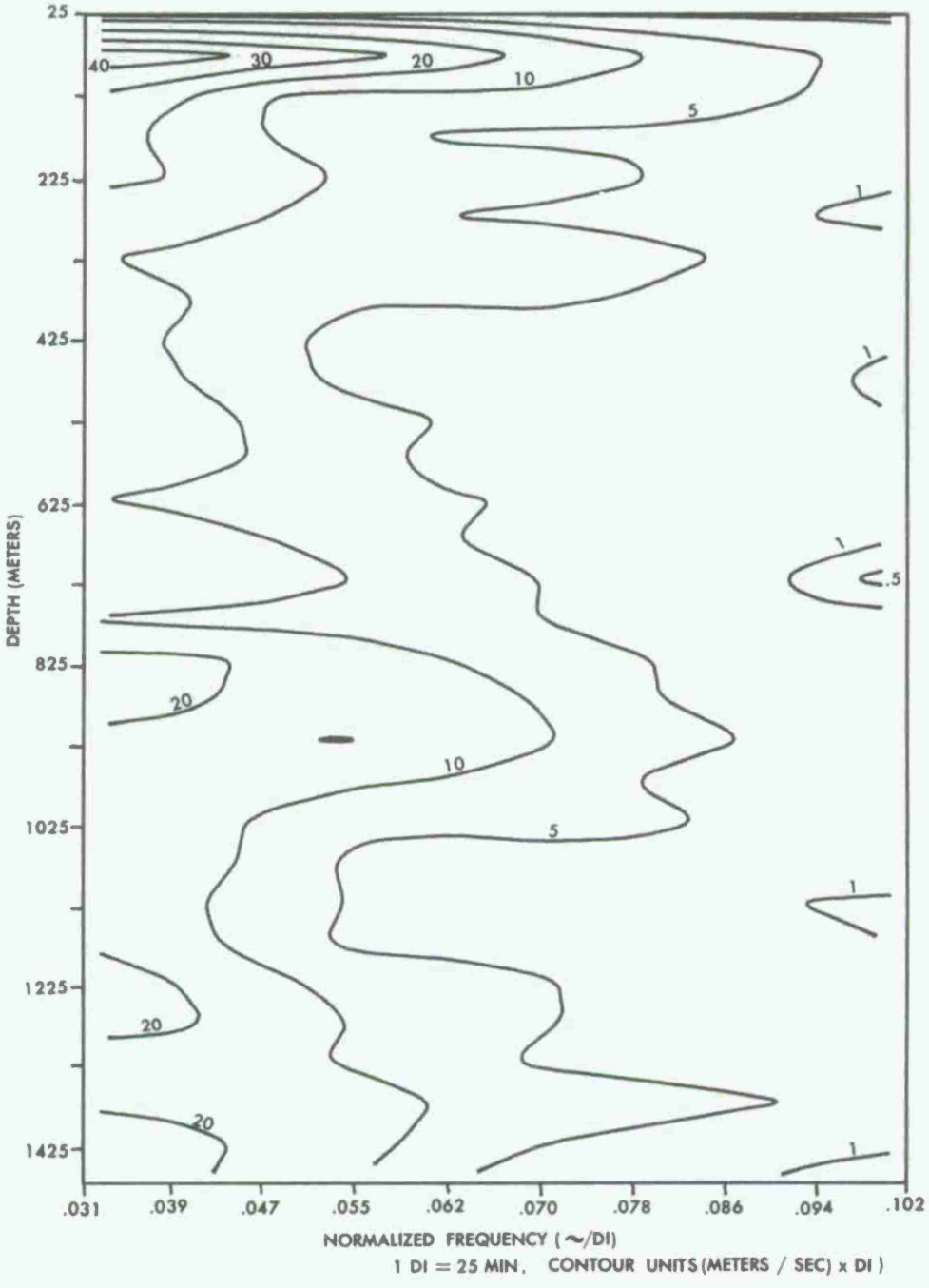

Figure 63. Spectrum of sound speed temporal variations vs. depth.

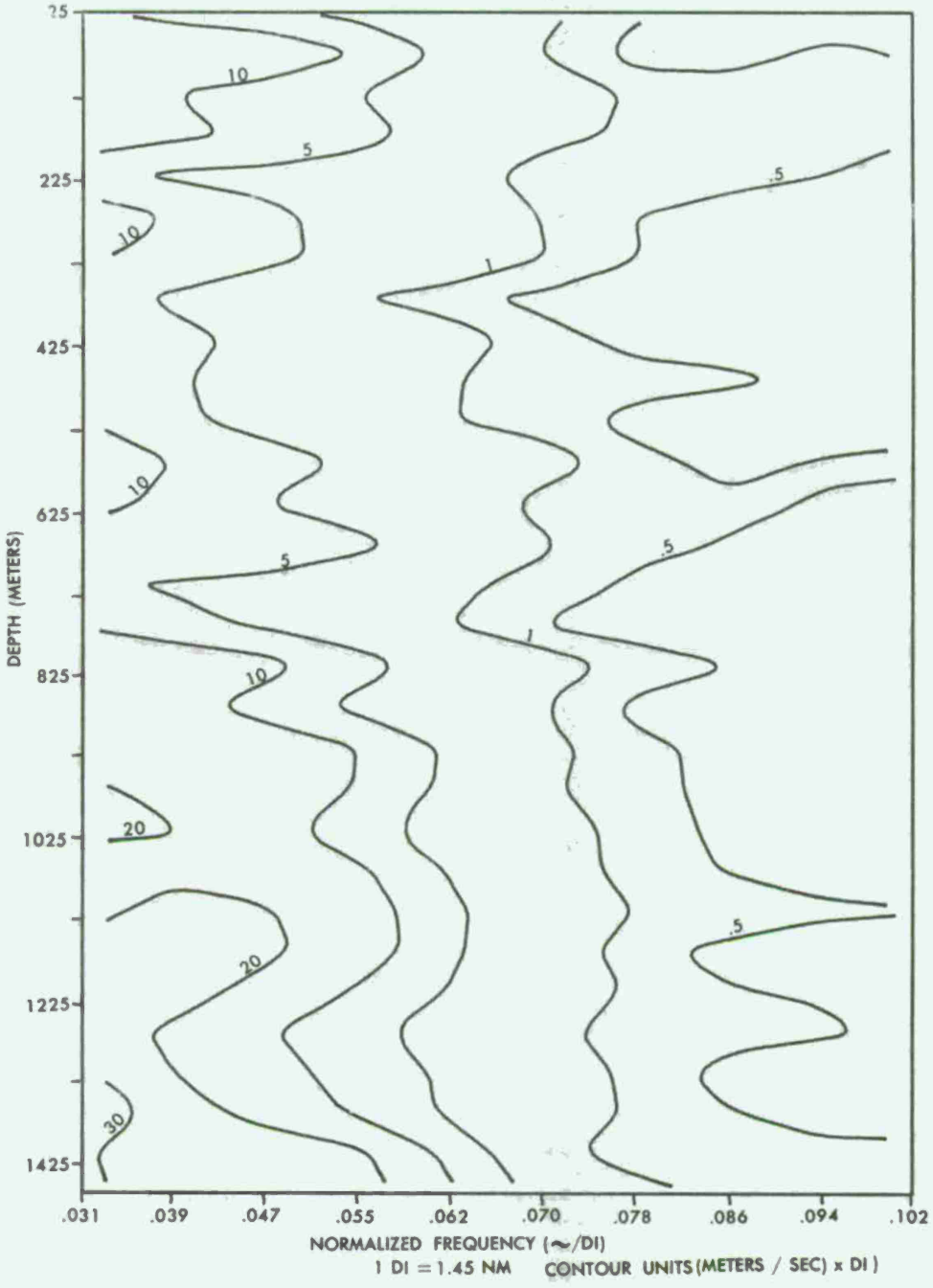

Figure 64. Spectrum of sound speed spatial variations vs. depth.

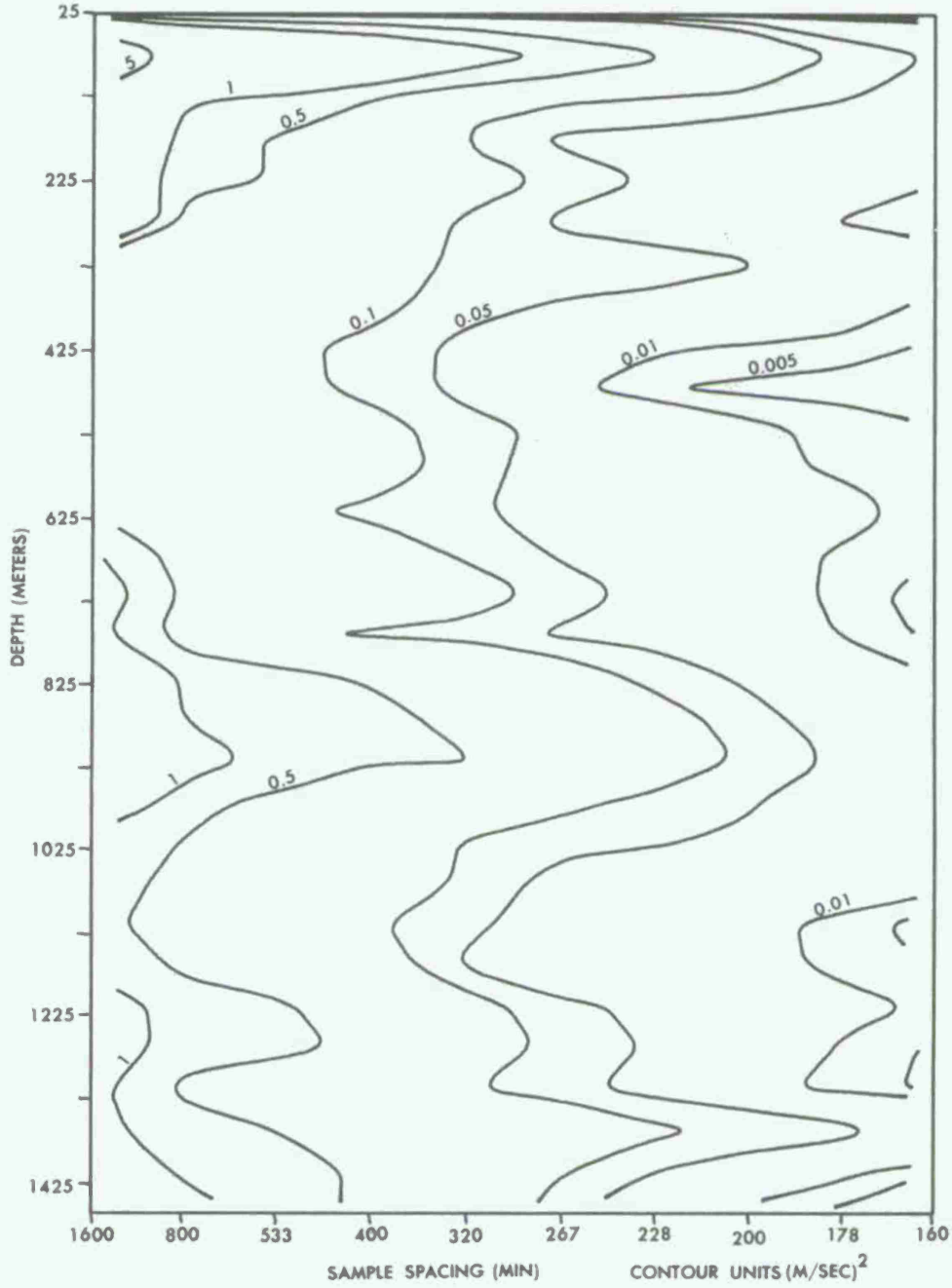

Figure 65. Sampling error vs. depth for sound speed temporal variations.

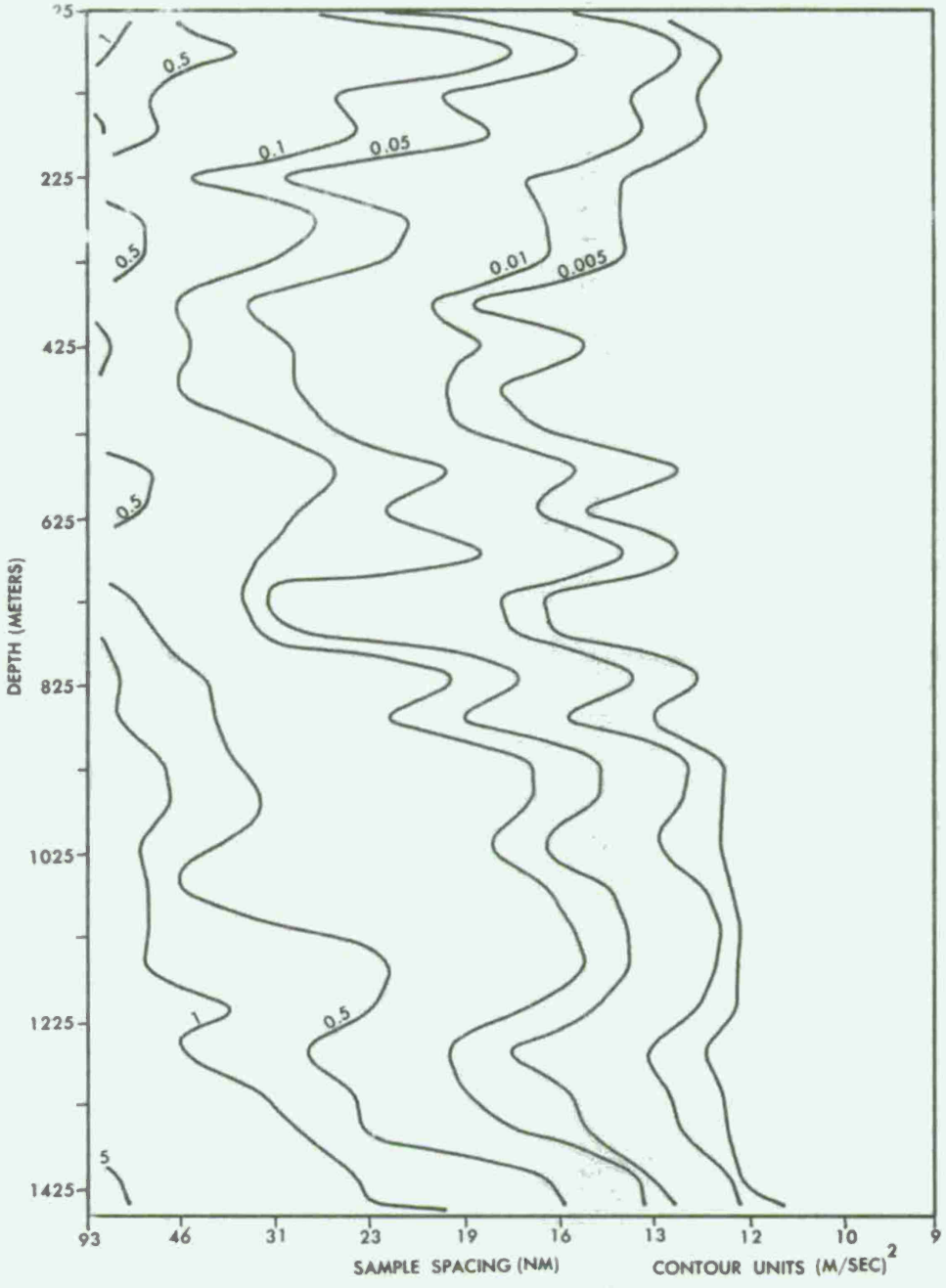

Figure 66. Sampling error vs. depth for sound speed spatial variations.

An Example of the Effect of Sampling Error on Geophysical Interpretation

In some cases, the magnitude of the sampling error generated by a particular survey pattern may be quite small and yet have a significant effect upon operations performed on the survey data. This example was designed to illustrate the effect of a very small sampling error upon the interpretation of the gravity anomaly associated with a two-dimensional fault. The interpretation technique which was applied to equally spaced digital data computed along a profile normal to the strike of the fault model was developed by Davis (1971). This technique is based on the use of characteristic curves derived through two digital band-pass filters. The amplitude responses of these filters were selected to produce an efficient regional-residual separation by minimizing the effect of the overlap of anomaly spectrum and regional spectrum by retaining only enough short wavelength anomaly information to allow a quantitative interpretation.

The parameters of the fault model (Figure 2) selected for this example are as follows: depth = 5 km, thickness = 6 km, density contrast = 0.5 g/cc, dip = 60° SE, and strike = 20°. The gravity anomaly generated by this model was computed for an 80x80 km area at a grid spacing of 1 km utilizing the formulation given in Davis (1971). Figure 67 is a contour chart of this model anomaly. The two-dimensional amplitude spectrum of this field computed via the FFT and appropriate prewhitening is shown in Figure 68. The strong lineation of the anomaly field from this model is reflected as a lineation of the two-dimensional spectrum rotated by 90°. The low-amplitude lineations parallel to the frequency axes are a consequence of a small roundoff error in computing the original gridded data.

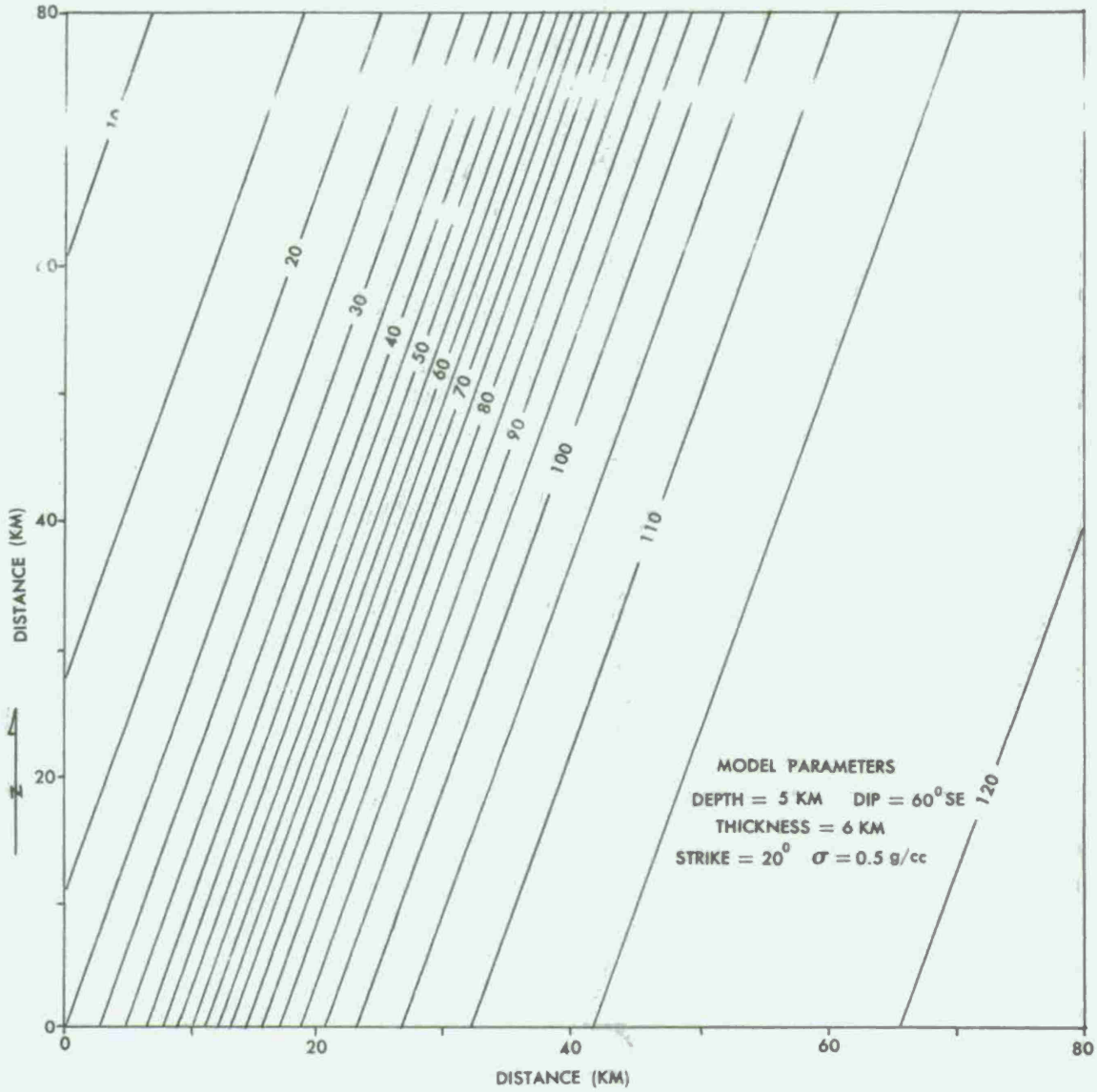

Figure 67. Gravity field generated by a two-dimensional fault model -contour interval (5 mgals).

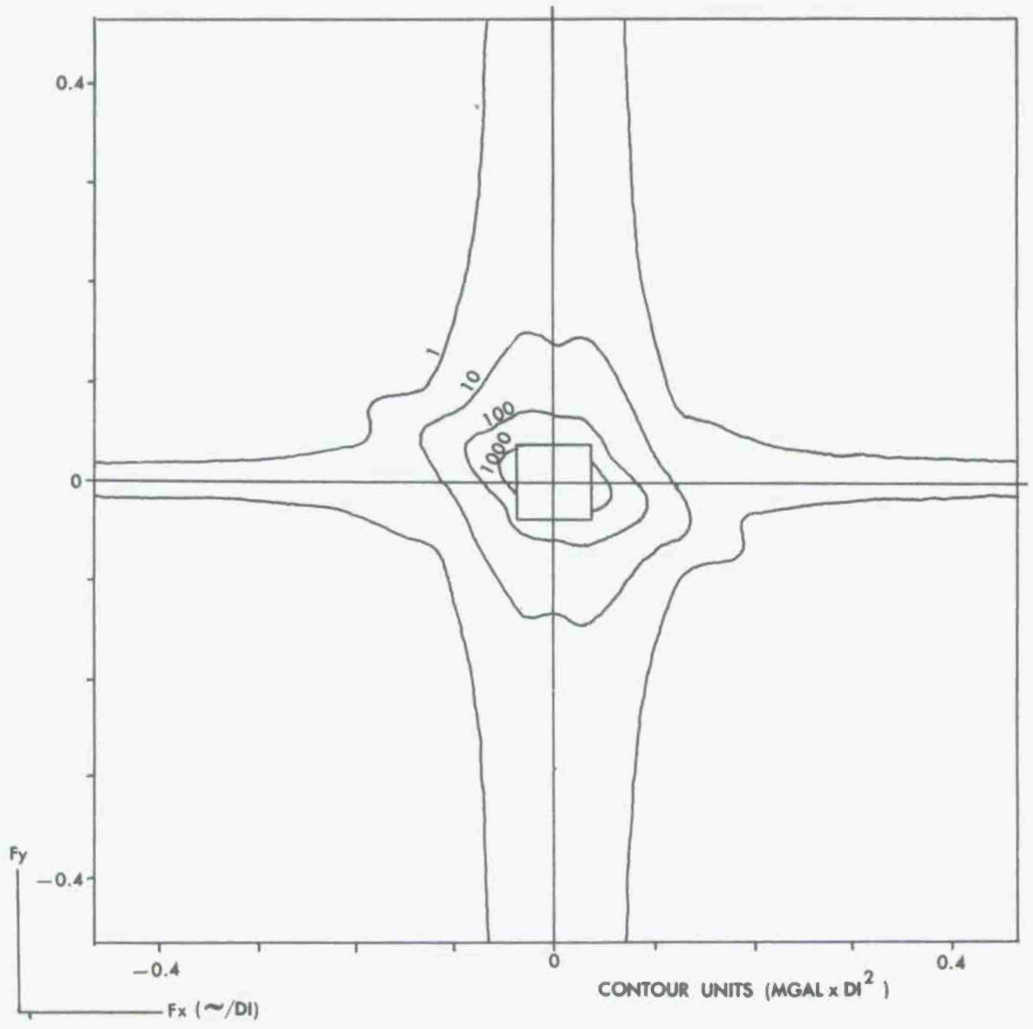

Figure 68. Two-dimensional spectrum of gravity fault model.

In order to illustrate the effect of sampling error on the interpretation of this anomaly, equations (6)-(8) were applied to the real and imaginary parts of this two-dimensional spectrum, with $S_T(x,y)$ on two model north-south survey tracks at various spacings. Figure 69 shows the resulting estimates of mean square sampling error as a function of north-south track spacing. Note particularly the low level of sampling error associated with a track spacing of between 8 and 6.4 km. Figure 70 is a contour chart of the predicted two-dimensional amplitude spectrum of the sampling error for a north-south track spacing of 5.3 km. In this case, the cross track replication of the transform resulted in a slight clockwise rotation of the main lineation of the error spectrum with respect to the direction of the lineation of the anomalous field. This rotation indicates that the lineation of the sampling error in the two-dimensional space domain will be at a slight angle to the strike of the model.

In order to determine the effect of this sampling error on interpretation, a track-type survey was simulated by selecting every sixth column of data from the model field shown in Figure 67 and utilizing a spline interpolation (Davis and Kontis, 1970) to produce data on a one km grid. A cubic spline interpolation algorithm which was specifically designed to extract a profile from a set of gridded data (Vanwyckhouse, 1973) was then utilized with this interpolated grid to obtain a sample profile normal to the strike of the model. Figure 71 is a comparison of the true one-dimensional amplitude spectrum of a profile normal to the strike of the body with the spectrum of the profile generated from the simulated survey data. The 70 percent response points of the two digital band-pass filters utilized in the interpretation are also shown

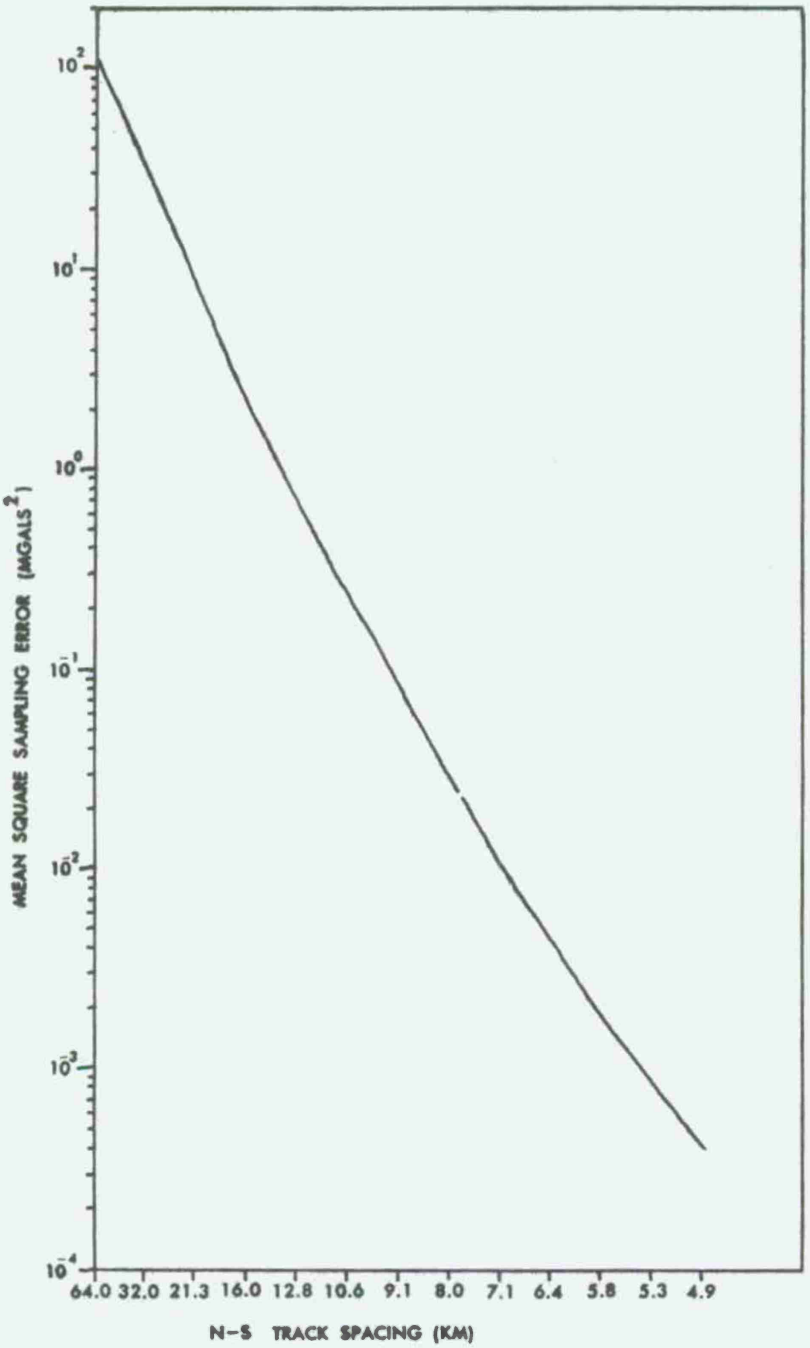

Figure 69. Mean square sampling error vs. N-S track spacing for fault model.

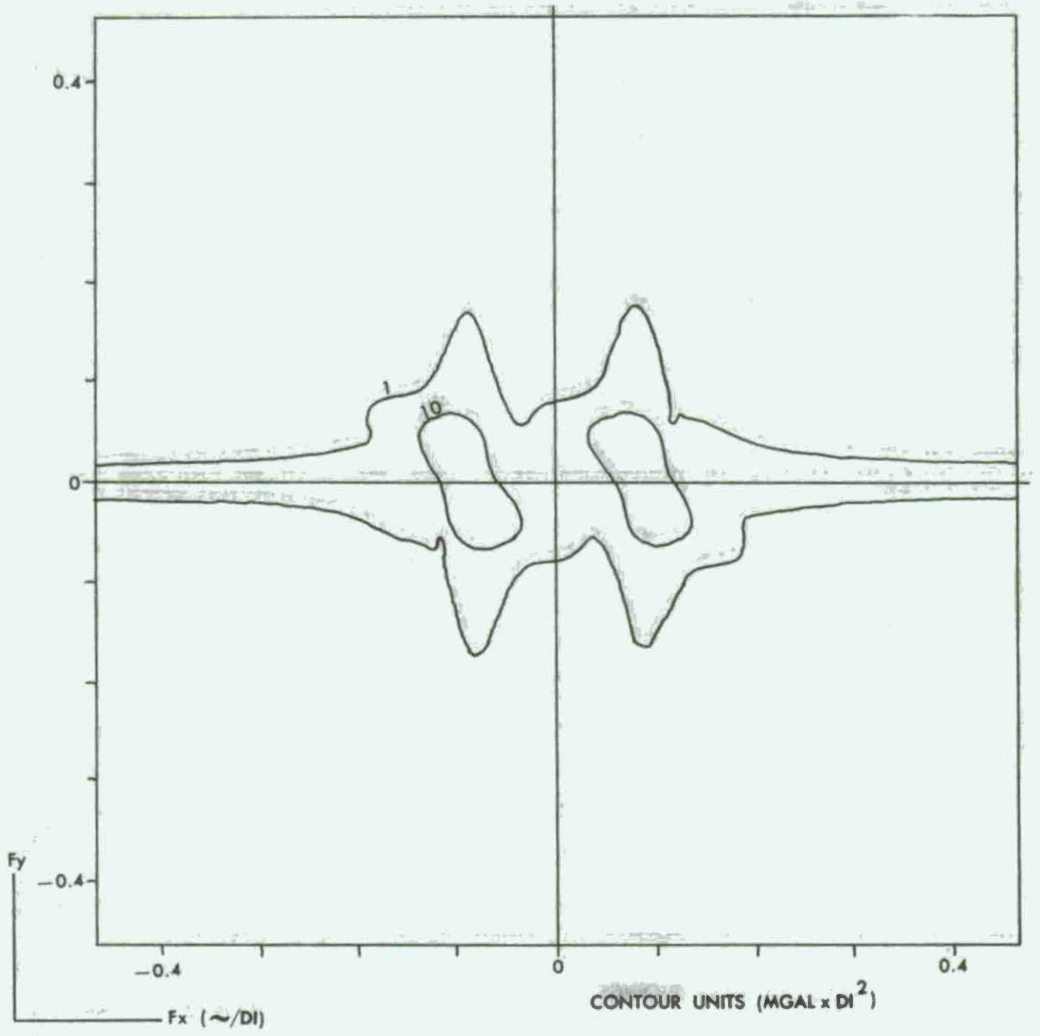

Figure 70. Sampling error spectrum for N-S track spacing of 5.8 km.

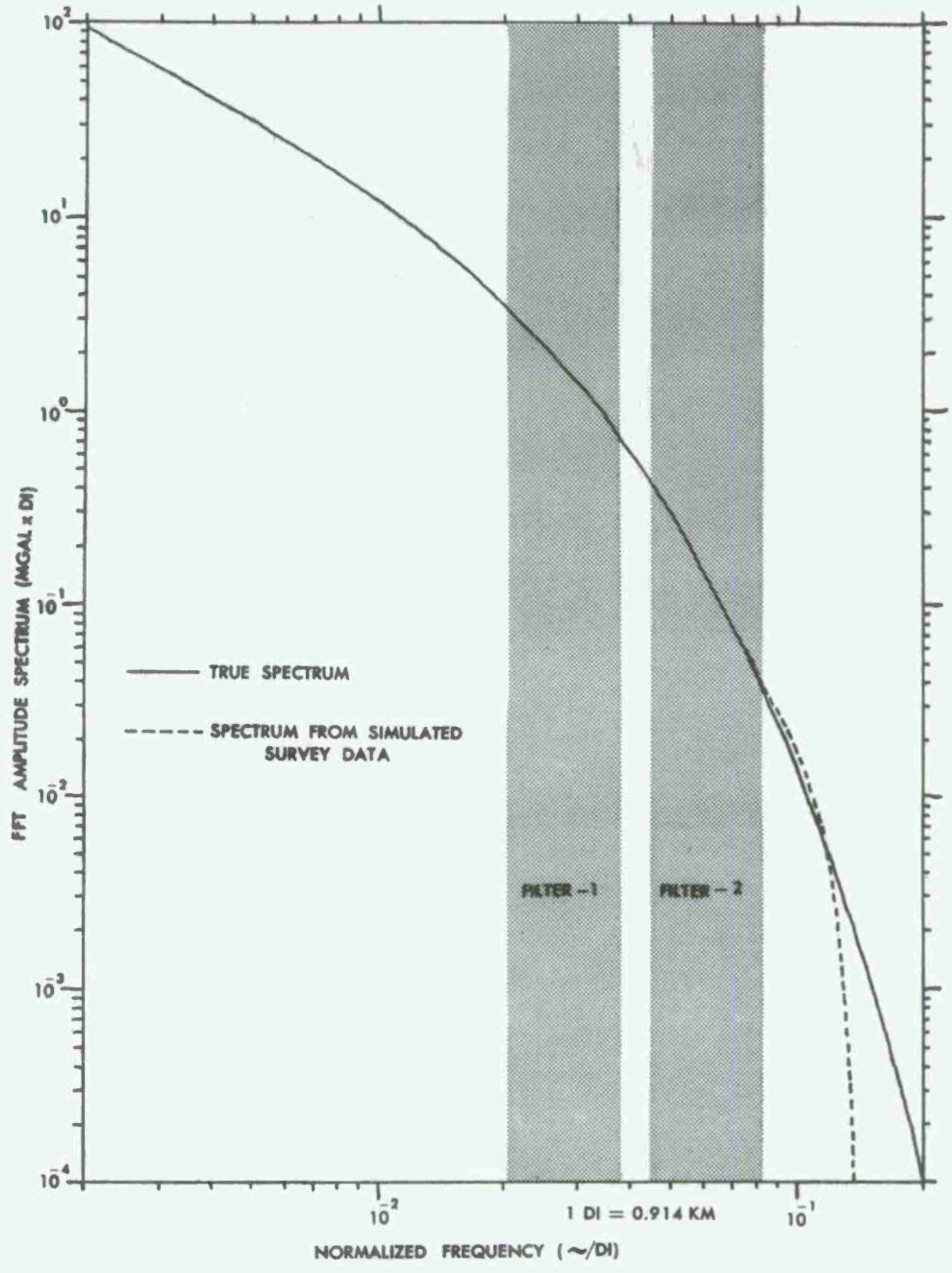

Figure 71. Comparison of true spectrum of a profile normal to strike of model vs. spectrum of profile constructed from N-S tracks spaced at 6.0 km.

in this figure. Note particularly the rather small magnitude of the sampling error falling within the pass band of the filters. Applying the interpretation technique (Davis, 1971) to the model profile which was uncontaminated by sampling error resulted in the following estimates: depth = 4.9 km, thickness = 6.1 km, dip = 61°, and density contrast = 0.45 g/cc. The interpreted quantities derived from the profile recovered from the simulated survey data were as follows: depth = 6.3 km, thickness = 2.3 km, dip = 30°, and density contrast = 1.10 g/cc. This result clearly indicates the advisability of estimating sampling error, especially in cases where the short wavelength components of the survey data are of primary importance.

SUMMARY AND CONCLUSIONS

The requirement for designing geophysical surveys in such a way that the true continuous field may be derived to a predetermined accuracy from digital samples is basic to any data collection operation. The time required in the collection and analysis of reconnaissance data, as well as the detailed surveys of the small type areas, may be justified not only from a purely scientific standpoint but, with the present cost of shipboard operations exceeding $2000 a day, from an economic standpoint as well.

Detailed tests of the mathematical procedures applicable to the design of geophysical surveys which have been presented indicate the accuracy and efficiency with which the appropriate estimates of sampling error may be derived by operating in the two-dimensional frequency domain. The importance of some form of prewhitening or window modification for computing accurate spectral estimates from a finite length of data obtained from a "red noise" process has been clearly demonstrated. The raster sampling model consisting of a set of parallel delta function ridges has been shown to be an appropriate mathematical model for defining two-dimensional track-type surveys.

Several practical applications have been presented to demonstrate the adaptability of the theory to a wide variety of survey operations and the relative ease with which estimates of mean square error and the two-dimensional spectral content of this sampling error may be computed. The use of a so-called power fold approximation, combined with a priori knowledge of the orientation of major lineations, has been developed for survey design in near real-time using small scale

computers. The practical procedures which are presented for designing surveys to produce products of a specified accuracy in which the accuracy requirement is placed not on the survey data but upon quantities computed from the data by two-dimensional cross correlation or convolution operations is of particular importance from the standpoint of systems analysis. Finally, an example of the effect of sampling error on a problem of geophysical interpretation clearly illustrates the fact that, although the magnitude of the sampling error may be quite small, it may have a significant effect upon operations performed on the survey data.

No attempt has been made to specify an allowable sampling error for any of the survey designs which have been presented here. This decision can only be made on a case by case basis and will depend upon the ultimate use of the survey data. The test results which have been presented indicate clearly that this theory will, for the first time, provide the individual investigator with an accurate and efficient technique for designing track-type geophysical surveys to meet a predetermined accuracy specification.

Future work in this area will be directed toward modifying the procedure for designing surveys for vertical deflections in order to remove the requirement for detailed type area surveys. This modification should provide a basis for real-time survey design through the use of reconnaissance tracks normal to the survey pattern combined with an assumption of short wavelength isotropy to produce an estimate of the two-dimensional spectrum which will be accurate in the cross-track direction.

APPENDIX A

THE DESIGN OF PREWHITENING FILTERS

An excellent technique for the practical computation of the digital weight function required for one-dimensional prewhitening filters has been developed by Martin (1957) and evaluated by Linnette (1961). For general low-pass filters, the 2N+1 filter weights, symmetric about K = 0 to insure no phase shift, are computed from

$$L_K = \left[\frac{\text{Cos } (2\pi KH)}{1-16H^2K^2}\right]\left[\frac{\text{Sin } 2\pi K\ (V_c+H)}{\pi K}\right], \quad K = -N....0....N, \qquad \text{(A-1)}$$

where K is the weight number, H is a parameter controlling the shape of the amplitude response, and V_c is the normalized cutoff frequency in cycles/data interval. The parameter H is usually assigned a value between 0.01 and 0.20. In general, for a specified value of N, the slope of the frequency response of the filter and the magnitude of the first side lobe decrease as H is increased. The cutoff frequency is defined as that point where the amplitude response leaves 100 percent in the case of a low-pass filter or reaches zero in the case of a high-pass filter. In order for the filter to have unity gain, a correction must be applied to the weights generated by equation (A-1) to insure that their sum is unity. This correction is

$$\Delta = 1 - \left[L_o + 2\sum_{K=1}^{N} L_K\right] \qquad \text{(A-2)}$$

At values of K = 0 and K = ± H/4, equation (A-1) is of indeterminate form. Application of L'Hospital's rule to evaluate the limit as K approaches these values yields

$$L_o = 2(V_c+H) \text{ for } K = 0$$

and

$$L_K = \frac{\text{Sin}[2\pi K(V_c+H)]}{4K} \quad \text{for } K = \pm H/4.$$

The final corrected filter weights for the general low-pass digital filter are given by $W_K = L_K + \frac{\Delta}{2N+1}$.

The weights for the high-pass prewhitening filter (P_K) are simply constructed by subtracting W_K from an all-pass filter defined as

$$A_K = \begin{cases} 1, & K=0 \\ 0, & K=\pm 1 \ldots . \pm N \end{cases} \quad \text{Thus, } P_K = \begin{cases} 1-W_K, & K=0 \\ -W_K, & K=\pm 1 \ldots . \pm N \end{cases}$$

Experience has shown that, for one-dimensional prewhitening of a gravity or magnetic profile containing T digital values, the filter control parameters given by $V_c = \frac{1}{T+0.1T}$, H = 0.2, N = 3 produced a reasonably white spectrum.

A computational procedure for generating the two-dimensional digital weight function for prewhitening gridded data has been developed by Lavin and Devane (1970). The digital filter weights possess circular symmetry to insure circular symmetry in the two-dimensional spatial frequency domain, and are given by

$$W(r) = \frac{aJ_1(2\pi ar)}{r} \frac{J_o(\pi r\Delta k)}{1-(\frac{2\pi r\Delta K}{\alpha})^2} , \qquad \text{(A-3)}$$

where $r = (x^2+y^2)^{1/2}$, $a = (K_C+K_T)/2$ with K_C defined as the normalized cutoff frequency and K_T the normalized termination frequency in cycles per data interval, $\alpha = 4.80965\ldots$, and $\Delta K = K_T-K_C$.

Equation (A-3) is undefined at $r = 0$ and $r = \frac{\alpha}{2\pi\Delta K}$. Application of L'Hospital's rule at these points yields $W(o) = \pi a^2$ and $W(\frac{\alpha}{2\pi\Delta K}) = \frac{\pi a \Delta K}{2} J_1(\frac{\alpha a}{\Delta K}) J_1(\frac{\alpha}{2})$. As in the one-dimensional case, a correction equivalent to equation (A-2) is applied to insure unity gain, and the high-pass prewhitening weights are derived by subtracting equation (A-3) from the two-dimensional all-pass filter. In general, an acceptable prewhitening filter for gridded "red noise" type processes, such as gravity or magnetic data, may be generated by setting $K_c = \frac{1}{T+0.1T}$, $\Delta K = 0.3$, and terminating equation (A-3) by setting the maximum value of x and y equal to four data intervals, ie., $x,y = -4....0....4$.

APPENDIX B

THE SHANNON SAMPLING THEOREM

Shannon (1949) states that, given equally spaced digital values f(mT) of a continuous function f(t) which is band-limited to the normalized frequency range $-\pi \leq \omega \leq \pi$, and such that $\int_{-\pi}^{\pi} |F(\omega)| d\omega$ exists, f(t) may be represented by

$$f(t) = \sum_{m=-\infty}^{\infty} f(mT) \frac{\text{Sin } \pi(t-mT)}{\pi(t-mT)} \quad \text{for all } t.$$

The proof of this theorem consists of showing that

$$\lim_{N\to\infty} \left| f(t) - \sum_{-N}^{N} f(mT) \frac{\text{Sin } \pi(t-mT)}{\pi(t-mT)} \right| = 0 \quad \text{for all } t.$$

To begin with, the inverse Fourier transform of the so-called boxcar function, defined as

$$B(\omega) = \begin{cases} 1, & |\omega| \leq \pi \\ 0, & \text{elsewhere,} \end{cases}$$

is required. By definition,

$$b(t) = \frac{1}{2\pi} \int_{-\infty}^{\infty} B(\omega) e^{i\omega t} d\omega = \frac{1}{\pi} \int_{0}^{\pi} \cos \omega t d\omega = \frac{\text{Sin}\pi t}{\pi t}.$$

Thus, utilizing the shifting theorem for Fourier transforms (Papoulis, 1962), we have

$$\frac{\text{Sin } \pi(t-mT)}{\pi(t-mT)} = \frac{1}{2\pi} \int_{-\pi}^{\pi} e^{i\omega(t-mT)} d\omega.$$

Then

$$0 \leq \left| f(t) - \sum_{-N}^{N} f(mT) \frac{\text{Sin } \pi(t-mT)}{\pi(t-mT)} \right|$$

$$= \left| \frac{1}{2\pi} \int_{-\pi}^{\pi} F(\omega) e^{i\omega t} d\omega - \frac{1}{2\pi} \sum_{-N}^{N} f(mT) \int_{-\pi}^{\pi} e^{i\omega(t-mT)} d\omega \right|$$

$$= \frac{1}{2\pi} \left| \int_{-\pi}^{\pi} e^{i\omega t} \left[F(\omega) - \sum_{-N}^{N} f(mT) e^{-i\omega mT} \right] d\omega \right| . \qquad \text{(B-1)}$$

Since $F(\omega)$ is defined in the interval $[-\pi,\pi]$, it may be expanded in a Fourier series $F(\omega) \simeq \sum_{-\infty}^{\infty} c_m e^{-i\omega m}$ where $c_m = \frac{1}{2\pi} \int_{-\pi}^{\pi} F(\omega) e^{i\omega m} d\omega$. But, since $f(t)$ is bandlimited,

$$f(t) = \frac{1}{2\pi} \int_{-\pi}^{\pi} F(\omega) e^{i\omega t} d\omega,$$

so

$$c_m = f(mT) = \frac{1}{2\pi} \int_{-\pi}^{\pi} F(\omega) e^{i\omega mT} d\omega,$$

and

$$F(\omega) \simeq \sum_{m=-\infty}^{\infty} f(mT) e^{-i\omega mT} . \qquad \text{(B-2)}$$

Applying the Schwarz inequality (Kaplan, 1952), given by

$$\left| \int f(x) g(x) dx \right| \leq \left(\int |f(x)|^2 dx \right)^{1/2} \left(\int |g(x)|^2 dx \right)^{1/2},$$

to equation (B-1) yields

$$\frac{1}{2\pi} \left| \int_{-\pi}^{\pi} e^{i\omega t} \left[F(\omega) - \sum_{m=-N}^{N} f(mT) e^{-i\omega mT} \right] d\omega \right|$$

$$\leq \frac{1}{2\pi} \left(\int_{-\pi}^{\pi} |e^{i\omega t}|^2 d\omega \right)^{1/2} \left(\int_{-\pi}^{\pi} |F(\omega) - \sum_{m=-N}^{N} f(mT) e^{-i\omega mT}|^2 d\omega \right)^{1/2} = A \cdot B,$$

where

$$A = \frac{1}{2\pi}\left(\int_{-\pi}^{\pi} \left| e^{i\omega t} \right|^2 d\omega\right)^{1/2}$$

and

$$B = \left(\int_{-\pi}^{\pi} \left| F(\omega) - \sum_{m=-N}^{N} f(mT) e^{-i\omega mT} \right|^2 d\omega\right)^{1/2}.$$

Since $\left| e^{i\omega t} \right|^2 = 1$, then $A = 1/\sqrt{2\pi}$, and utilizing equation (2), it is clear that, as $N \to \infty$, $B \to 0$, thus

$$f(t) = \lim_{N\to\infty} \sum_{m=-N}^{N} f(mT) \frac{\text{Sin } \pi(t-mT)}{\pi(t-mT)} \text{ for all } t.$$

REFERENCES

Alldredge, L. R., G. D. Van Voorhis, and T. M. Davis, 1963, A magnetic profile around the world: J. Geophys. Res., v. 68, no. 12, pp. 3679-3692.

Blackman, R. B., and J. W. Tukey, 1958, The Measurement of Power Spectra: Dover Pub., Inc. New York, 190 pp.

Bracewell, R., 1965, The Fourier Transform and its Applications: McGraw-Hill Book Co., New York, 381 pp.

Burg, J. P., 1967, Maximum entropy spectral analysis: paper presented at 37th Annual International S.E.G. Meeting, Oklahoma City, Oklahoma, October 31.

Capon, J., 1969, High-resolution frequency-wave number spectrum analysis: Proc. IEEE, v. 57, pp. 1408-1418.

Cooley, J. W., and J. W. Tukey, 1965, An algorithm for the machine calculation of complex Fourier series: Math of Comput., v. 19, pp. 297-301.

Davis, T. M., and A. L. Kontis, 1970, Spline interpolation algorithms for track-type survey data with application to the computation of mean gravity anomalies: NAVOCEANO TR-226, Wash. D. C., 82 pp.

Davis, T. M., 1971, A filtering technique for interpreting the gravity anomaly generated by a two-dimensional fault: Gphys., v. 36, no. 3, pp. 554-570.

Gilman, D. L., F. J. Fuglister, and J. M. Mitchell, Jr., 1963, On the power spectrum of "red noise": J. Acous. Soc. Am., v. 20, no. 2, pp. 182-184.

Glicken, M., 1962, Eotvos corrections for a moving gravity meter: Gphys., v. 27, no. 4, pp. 531-533.

Gradshteyn, I. S., and I. M. Ryzhik, 1965, Table of Integrals, Series and Products: Academic Press, New York, 1086 pp.

Grant, F. S., and G. F. West, 1965, Interpretation Theory in Applied Geophysics: McGraw-Hill Book Co., New York, 583 pp.

Hamming, R. W., 1962, Numerical Methods for Scientists and Engineers: McGraw-Hill Book Co., New York, 411 pp.

Heiskanen, W. A., and H. Moritz, 1967, Physical Geodesy: W. H. Freeman Co., New York, 364 pp.

Kaplan, W., 1952, Advanced Calculus: Addison-Wesley, New York, 679 pp.

Kontis, A. L., R. R. Michlik, and T. M. Davis, 1974, Analysis of deflection of the vertical inner-zone methods: NAVOCEANO SP-260, Wash. D. C., 75 pp

Lacoss, R. T., 1971, Data adaptive spectral analysis methods: Gphys., v. 36, no. 4, pp. 661-675.

Lavin, P. M., and J. F. Devane, 1970, Direct design of two-dimensional digital wave number filters: Gphys., v. 35, no. 6, pp. 1073-1078.

Linnette, H. M., 1961, Statistical filters for smoothing and filtering equally spaced data: NEL Research Report No. 1049, 36 pp.

Martin, M. A., 1957, Frequency domain applications in data processing: General Electric Co. Document No. 57SD340, 128 pp.

Michlik, R. R., 1973, Fast algorithm utilizing cubic spline interpolation for computing vertical deflections and geoid undulations - Program VERDNT: NAVOCEANO Tech. Note No. 6D-2-73, (UNPUBLISHED), 117 pp.

National Oceanographic Data Center, 1964, Processing physical and chemical data from oceanographic stations: NODC Pub. M-2 (REVISED), 113 pp.

Papoulis, A., 1962, The Fourier Integral and Its Applications: McGraw-Hill Book Co., New York, 318 pp.

Pickett, R. L., 1972, Precision of sound speed estimated from BT's: Marine Tech. Soc. J., v. 6, no. 6, pp. 37-38.

Rankin, W. E., 1974, Program SPLNTR: An algorithm for interpolating irregularly-spaced data: NAVOCEANO Tech. Note No. 6004-1-74, (IN PRESS).

Rapp, R. H., 1964, The prediction of point and mean gravity anomalies through the use of a digital computer: Inst. of Geodesy, Photogrammetry, and cartography, Report No. 43, Ohio State Univ., 177 pp.

Shannon, C. E., 1949, Communication in the presence of noise: Proc. IRE., Pp. 10-21.

Shapiro, R., and F. Ward, 1960, The time-space spectrum of the geostrophic meridional kinetic energy: J. Meteor., no. 17, pp. 621-626.

Shaw, L., I. Paul, and P. Hendrickson, 1969, Statistical models for the vertical deflection from gravity-anomaly models: J. Gphys. Res., vol. 74, no. 17, pp. 4259-4265.

Shepard, D., 1968, A two-dimensional interpolation function for computer mapping of irregularly-spaced data: Harvard Papers in Theoretical Geography: Harvard U., Cambridge, Mass., 19 pp.

Sverdrup, H. U., M. W. Johnson, and R. H. Fleming, 1942, The Ocean, Their Physics, Chemistry and General Biology: Prentice-Hall, Inc., 1087 pp.

Tukey, J. W., 1967, An introduction to the calculations of numerical spectrum analysis, Proceedings of advanced seminar on spectral analysis of time series: Wiley, New York, pp. 25-46.

Van Voorhis, G. D., and T. M. Davis, 1964, Magnetic anomalies north of Puerto Rico: Trend removal with orthogonal polynomials: J. Gphys. Res., v. 69, pp. 5363-5371.

VanWyckhouse, R. J., 1973, Synthetic bathymetric profiling system (SYNBAPS): NAVOCEANO TR-233, Wash. D. C., 138 pp.

Vening Meinesz, F. A., 1928, A formula expressing the deflection of the plumbline in the gravity anomalies and some formulae for the gravity-field and the gravity potential outside the geoid: Proc. Koninkl-Ned. Akad. Wetenschap, v. 31, pp. 315-331.

Wilson, W. D., 1960, Speed of sound in sea water as a function of temperature, pressure, and salinity: J. Acous. Soc. Am., v. 32, no. 6. pp. 641-644.

Wilson, W. D., 1960, Equation for the speed of sound in sea water: J. Acous. Soc. Am., v. 32, no. 10, p. 1357.

Wylie, C. R., 1960, Advanced Engineering Mathematics: McGraw-Hill Book Co., New York, 696 pp.

UNCLASSIFIED

SECURITY CLASSIFICATION OF THIS PAGE *(When Data Entered)*

REPORT DOCUMENTATION PAGE		READ INSTRUCTIONS BEFORE COMPLETING FORM
1. REPORT NUMBER NOO RP-13	2. GOVT ACCESSION NO.	3. RECIPIENT'S CATALOG NUMBER
4. TITLE *(and Subtitle)* Theory and Practice of Geophysical Survey Design		5. TYPE OF REPORT & PERIOD COVERED Final 6. PERFORMING ORG. REPORT NUMBER
7. AUTHOR(s) Thomas M. Davis		8. CONTRACT OR GRANT NUMBER(s)
9. PERFORMING ORGANIZATION NAME AND ADDRESS Naval Oceanographic Office Washington, D.C. 20373		10. PROGRAM ELEMENT, PROJECT, TASK AREA & WORK UNIT NUMBERS 62759N HF-52-552-320
11. CONTROLLING OFFICE NAME AND ADDRESS Naval Oceanographic Office Washington, D.C. 20373		12. REPORT DATE October 1974 13. NUMBER OF PAGES 137
14. MONITORING AGENCY NAME & ADDRESS*(if different from Controlling Office)*		15. SECURITY CLASS. *(of this report)* UNCLASSIFIED 15a. DECLASSIFICATION/DOWNGRADING SCHEDULE

16. DISTRIBUTION STATEMENT *(of this Report)*

Approved for public release; distribution unlimited

17. DISTRIBUTION STATEMENT *(of the abstract entered in Block 20, if different from Report)*

18. SUPPLEMENTARY NOTES

19. KEY WORDS *(Continue on reverse side if necessary and identify by block number)*

Survey Design
Sampling Theory
Ocean Surveys
Gravity
Deflection of the Vertical

20. ABSTRACT *(Continue on reverse side if necessary and identify by block number)*

A theory for designing parallel track-type geophysical surveys, as well as the necessary numerical algorithms for implementing this theory, has been developed which is easily applied to many different sampling problems. Within this context, survey design consists of defining the appropriate track spacing, track direction, and down-track sampling rate which will produce a set of discrete digital measurements describing the environment to a predetermined accuracy.

(Continued)

DD FORM 1 JAN 73 1473 EDITION OF 1 NOV 65 IS OBSOLETE
S/N 0102-014-6601

UNCLASSIFIED

SECURITY CLASSIFICATION OF THIS PAGE *(When Data Entered)*

These procedures are based primarily upon the use of one- and two-dimensional Fourier transforms applied to appropriate numerical models of the sampling process in order to estimate the variance or mean square error as well as the spectral content of the sampling error. Since these error estimates are computed in the spatial frequency domain, application of the convolution theorem is shown to produce a particularly efficient process for propagating the error estimates through a variety of linear operations performed upon the survey data.

Several practical applications are presented to illustrate the adaptability of the theory. These applications include the near real-time design of hydrographic surveys utilizing a small-scale computer, the design of gravity surveys from which estimates of vertical deflection and geoid undulation may be derived to a specified accuracy, and the design of oceanic sound speed surveys which illustrates the application of the theory to three-dimensional fields.